NOSC TR 1121

Technical Report 1121
July 1986

MINIMUF—85: An Improved HF MUF Prediction Algorithm

D. B. Sailors
R. A. Sprague
W. H. Rix

NAVAL OCEAN SYSTEMS CENTER

San Diego, California 92152-5000

F. M. PESTORIUS, CAPT, USN
Commander

R. M. HILLYER
Technical Director

ADMINISTRATION INFORMATION

The work discussed in this report was completed by Code 542 of the Naval Ocean Systems Center.

Released by
D. B. Sailors, Head
Inonospheric Branch

Under authority of
J. H. Richter, Head
Ocean and Atmospheric
Sciences Division

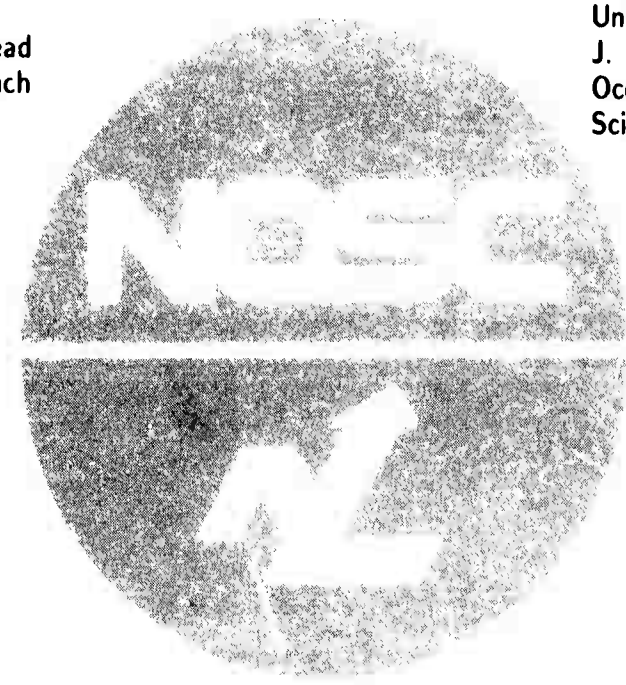

UNCLASSIFIED

SECURITY CLASSIFICATION OF THIS PAGE

AD-A178305

REPORT DOCUMENTATION PAGE

1a. REPORT SECURITY CLASSIFICATION UNCLASSIFIED	1b. RESTRICTIVE MARKINGS
2a. SECURITY CLASSIFICATION AUTHORITY	3. DISTRIBUTION/AVAILABILITY OF REPORT Approved for public release; distribution is unlimited.
2b. DECLASSIFICATION/DOWNGRADING SCHEDULE	
4. PERFORMING ORGANIZATION REPORT NUMBER(S) NOSC TR 1121	5. MONITORING ORGANIZATION REPORT NUMBER(S)
6a. NAME OF PERFORMING ORGANIZATION Naval Ocean Systems Center 6b. OFFICE SYMBOL (if applicable) NAVOCEANSYSCEN	7a. NAME OF MONITORING ORGANIZATION
6c. ADDRESS (City, State and ZIP Code) Code 542 San Diego, CA 92152-5000	7b. ADDRESS (City, State and ZIP Code)
8a. NAME OF FUNDING/SPONSORING ORGANIZATION U.S. Army 8b. OFFICE SYMBOL (if applicable)	9. PROCUREMENT INSTRUMENT IDENTIFICATION NUMBER
8c. ADDRESS (City, State and ZIP Code) AMSEL-COM-RY Ft. Monmouth, NJ 07703	10. SOURCE OF FUNDING NUMBERS PROGRAM ELEMENT NO.: RDA PROJECT NO.: MP48 TASK NO.: AGENCY ACCESSION NO.: DNO88607

11. TITLE (Include Security Classification)

MINIMUF-85: An Improved HF MUF Prediction Algorithm

12. PERSONAL AUTHOR(S)

D.B. Sailors, R.A. Sprague, W.H. Rix

13a. TYPE OF REPORT	13b. TIME COVERED	14. DATE OF REPORT (Year, Month, Day)	15. PAGE COUNT
Interim	FROM _____ TO _____	July 1986	112

16. SUPPLEMENTARY NOTATION

17. COSATI CODES			18. SUBJECT TERMS (Continue on reverse if necessary and identify by block number)
FIELD	GROUP	SUB-GROUP	Maximum usable frequencies, solar index Sunspot numbers raytracing

19. ABSTRACT (Continue on reverse if necessary and identify by block number)

An improved version of MINIMUF-3.5, called MINIMUF-85, was developed to predict accurate maximum usable frequencies (MUFs) under conditions of anomalously high sunspot numbers; also, to predict values of f_0F2 suitable for raytracing applications, to predict M3000 factor vaiues usable for determining the mirror height of reflection for oblique incidence propagation, and to predict accurate MUFs for paths having a portion of the path in the polar region. This version includes sunspot number dependence in both the f_0F2 and the M-factor calculations and provides a natural saturation in the MUF versus sunspot number curve, reducing the error in predicted MUF values under very high sunspot number conditions. The polar and nonpolar f_0F2 models are welded together by means of a folding function. MINIMUF-85 predicts 0.14 MHz low on average and has an rms error of 4.08 MHz; whereas, MINIMUF-3.5 had a bias of 0.51 MHz low and an 4.33 rms error when compared on the same 39 paths.

The subjects of the choice of solar index for forecasting purposes, of sounder updating, of the effects of the underlying layers on both M-factor estimation and determination of the mirror height of reflection, and of future improvements in MINIMUF are discussed.

20. DISTRIBUTION/AVAILABILITY OF ABSTRACT	21. ABSTRACT SECURITY CLASSIFICATION
☐ UNCLASSIFIED/UNLIMITED ☒ SAME AS RPT ☐ DTIC USERS	UNCLASSIFIED

22a. NAME OF RESPONSIBLE INDIVIDUAL	22b. TELEPHONE (Include Area Code)	22c. OFFICE SYMBOL
D.B.Sailors	(619) 225-7706	Code 542

DD FORM 1473, 84 JAN

83 APR EDITION MAY BE USED UNTIL EXHAUSTED
ALL OTHER EDITIONS ARE OBSOLETE

UNCLASSIFIED

SECURITY CLASSIFICATION OF THIS PAGE

CONTENTS

TABLES

ILLUSTRATIONS

SUMMARY

OBJECTIVE

To improve MINIMUF-3.5.

RESULTS

1. The model was improved by comparing the predicted data to f_oF2 values measured at 30 sites.

2. The sunspot number variation in MINIMUF-3.5 was deleted and the constant 58.0 called A_1 in MINIMUF-3.5 was replaced by a linear equation in sunspot number.

3. The M-factor portion of the algorithm was modified to include sunspot number, seasonal, and diurnal variations using over 7200 observed oblique sounder median MOFs on 39 paths in the fitting process.

4. A special f_oF2 model was added for use in the polar regions.

RECOMMENDATIONS

1. Use MINIMUF-85 in all applications now using MINIMUF-3.5.

2. Use the f_oF2 model in MINIMUF-85 in ray-tracing applications where f_oF2 from MINIMUF-3.5 is now used.

3. Use the M-factor model in MINIMUF-85 to determine a M3000 factor for obtaining mirror reflection heights for oblique incidence propagation rather than a fixed F2-region height.

4. Use the resultant value of mirror reflection height to determine take-off angles for use in determining antenna gains and path loss in applications where now a fixed value of take-off angle at a given range is used.

5. Use the f_oF2 data base to improve the f_oF2 representation of MINIMUF-85 by determining the sunspot number, seasonal, and geographic dependencies of the parameters A_o, A_1, and $\cos^{\eta}\chi_{eff}$.

6. Introduce the effects of underlying layers on M-factor estimation.

7. Continue to improve the polar representation.

INTRODUCTION

The effective operation of long distance high frequency (HF) systems is increased in proportion to its ability to predict variations in the ionosphere, since such ability permits the selection of optimum frequencies, antennas, and other circuit parameters. Most variations in HF system performance are directly related to changes in the ionosphere, which in turn are affected in a complex manner by solar activity, seasonal and diurnal variations as well as latitude and longitude.

Originally, manual methods were developed for analyzing these effects on HF circuits of short, intermediate, and long distances (reference 1). Because the manual methods are laborious and time consuming, various organizations developed computer programs to analyze HF circuit performance. A commonly predicted parameter in these programs is the maximum usable frequency (MUF). The MUF is the highest frequency that can be propagated by ionospheric refraction between given points at a given time.

However, these computer programs depended on the use of main frame computers. In the day-to-day management of frequency assets of a communication system, the usual procedure was to rely on a set of so-called "propagation charts" produced by these programs. To meet publication deadlines, these charts had to be produced months in advance. Hence, any possibility of real-time prediction was not possible.

In 1978 a simple semiempirical algorithm, called MINIMUF-3.5, was developed for predicting the MUF on small mobile propagation forecast (PROPHET) terminals (references 2, 3). With this tool it was possible to develop a variety of new forecast applications where the use of the large-scale propagation programs in the operational environment was not practical.

In its initial development, verification of MINIMUF-3.5 was done by comparing the predictions with oblique-incidence sounder data. The data base used encompassed 196 path months (4704 test points) of observed maximum observed frequencies (MOF) over 23 different HF sounder paths. MINIMUF-3.5 was found to have an rms error of 3.8 MHz.

Subsequent to this comparison, a more complete verification of MINIMUF-3.5 was made (reference 4). In this test, 4668 MOFs measured on 25 paths are compared against the predicted values from ITSA-1 (reference 5) and HFMUFES 4 (references 6, 7). The data were divided into subsets to see the effect of particular paths, path length and orientation, season, month, sunspot number, diurnal trends, geographic region and sounder type. MINIMUF-3.5 had a bias of 0.08 MHz low (0.6 percent low) and an rms error of 3.7 MHz (3.6 percent). It was least accurate during the sunrise and sunset transition hours and for path lengths 5000 to 7000 km than it was for other times of the day and path lengths. Linear regression analysis showed that its errors in predicted MUF at sunrise and for path length lengths 5000 to 7000 km are nonlinear and could probably be attributed to the M factor part of the calculation.

During July and August 1982, a field test was conducted from Ft. Lewis, WA; Ft. Leavenworth, KS; and Ft. Knox, KY; to Ft. Bragg, NC, using oblique-incidence sounders. One of the models used in the test for operational frequency selection included MINIMUF-3.5. A comparison was made between the predicted MUFs for those paths and the observed MOFs. When the F-region MOFs are compared against the predicted MUFs from MINIMUF-3.5, it was found that MINIMUF-3.5 consistently predicted high. This experiment was conducted during a period in the solar cycle for which solar activity was unusually high and variable. The mean sunspot number was 113, its standard deviation was 88, and the peak value was 272.

This report describes the development of an improved version of MINIMUF-3.5, called MINIMUF-85. The version developed to predict accurate maximum useable frequencies (MUFs) under conditions of anomalously high sunspot numbers, to predict f_oF2 values suitable for ray-tracing applications, to predict M factor values useable for determining the mirror height of reflection for oblique incidence propagation, and to improve its accuracy for paths into or crossing the polar regions. This version includes sunspot number dependence in both the f_oF2 and the M factor calculations. The M factor portion of the algorithm also was modified to include seasonal and diurnal variations. Appendices A and B give listings of MINIMUF-85 in the BASIC and FORTRAN languages, respectively.

BACKGROUND

MINIMUF 3.5 is a semi-empirical model developed in 1978 (the initial algorithm was called MINIMUF-3) to provide a maximum-usable-frequency (MUF) prediction capability suitable for use on small (micro) computers where time and storage limitations exist. The theory and method used in the development of the MINIMUF 3.5 algorithm has been documented in several earlier reports and will not be presented here (references 2 and 3).

The expression for the MUF used in a MINIMUF 3.5 is given by

$$MUF = M \cdot f_oF2 \tag{1}$$

where M is the obliquity, or M-, factor which reflects the dependence of the MUF on transmission path length. The parameter f_oF2 is the critical or penetration frequency at vertical incidence for the F2 layer.

In particular, we have

$$M = \{1 + 2.5[\sin(2.54\Psi)]^{3/2}\} \cdot G_1 \cdot G_2 \cdot G_3 \tag{2}$$

where Ψ is the minimum great circle distance between transmitter and receiver. The various constants in the bracketed term in equation 2 are determined by fitting this expression, without the G_i, i =1,2,3,to an exact transmission curve for a parabolic layer height of 290 km and a ratio of height of maximum of electron density to half-width of the F2 layer of 0.4 (reference 2). The multipliers G_i provide small corrections to the MUF for known systematic departures from the median behavior under certain conditions of path geography or season (reference 2).

The expression for the critical frequency used in MINIMUF 3.5 is

$$f_oF2 = \left(1 + \frac{R}{R_o}\right)\left[A_o + A_1\sqrt{\cos \chi_{eff}}\right]^{1/2} \tag{3}$$

where R_o A_o, A_1 are constants and R is the 12 month running mean sunspot number. The constants in equation 3 were determined by iteratively adjusting

the model in a "real-time" mode, to 36 path months of data chosen to represent a range of transmission path types (reference 2).

In equation 3, χ_{eff} is an "effective" solar zenith angle. $Cos\chi_{eff}$ is modeled as the logged response of a dynamic linear system, "driven" by the instantaneous value of cos χ. By using an effective value of the zenith angle, recognition is given to the fact that the F2 layer, unlike the E and D layers, does not show a relatively simple cos $^{\eta}\chi$ diurnal dependence on χ. The dynamical behavior of the F2 layer is more complicated because various other dependencies make simple, accurate modeling difficult. In keeping with the simplistic nature of the model, defining an effective χ allows relatively accurate modeling without explicitly including these other dependencies (reference 2).

DEVELOPMENT PROCEDURE

This section will present how MINIMUF-85 is developed from MINIMUF-3.5 using both vertical incidence and oblique incidence sounder data. Measurements of f_oF2 data at 30 selected sites were used to improve the f_oF2 model. Measurements on 39 paths were collected to form a data base of over 7200 observed oblique sounder median MOFs. These data were used to determine the optimum location of control points to be used to introduce a geomagnetic latitude dependence, to improve the M-factor model, and to verify the polar region model. To compare the model against the measured data sets a data screening program is used.

VERTICAL INCIDENCE SOUNDER DATA BASE (f_oF2)

The derivation of the critical frequency expression used in the new model to be described in this report required the construction of an f_oF2 data base. For this purpose we were fortunate to have access to the complete collection of hourly monthly media f_oF2 data, collected since 1930 at many vertical incidence sounder sites and reported to the World Data Center in Boulder, CO. With access to this large amount of data we were able to be selective in determining which sites and time periods to include in our data base. The selection criteria used are based on geographic distribution of the sites and availability of data covering the range of sunspot numbers we wish to include.

Figure 1 shows the geographic distribution of the 30 selected sites. Table 1 gives the name and location included for each site in the f_oF2 data base. With the available data we attempted to obtain maximum distribution over all the continents in order to include all known geographical effects on the f_oF2 in the data. The fact that most of the longer operating stations reporting data are in mid-latitudes (~20° to 60°) means that this region of the world is usually over-represented in comparison with other regions, i.e., polar and equatorial regions. This is perhaps the case in our f_oF2 data base since the second selection criterion, data covering a wide range of sunspot numbers, forced the inclusion of many of these sites.

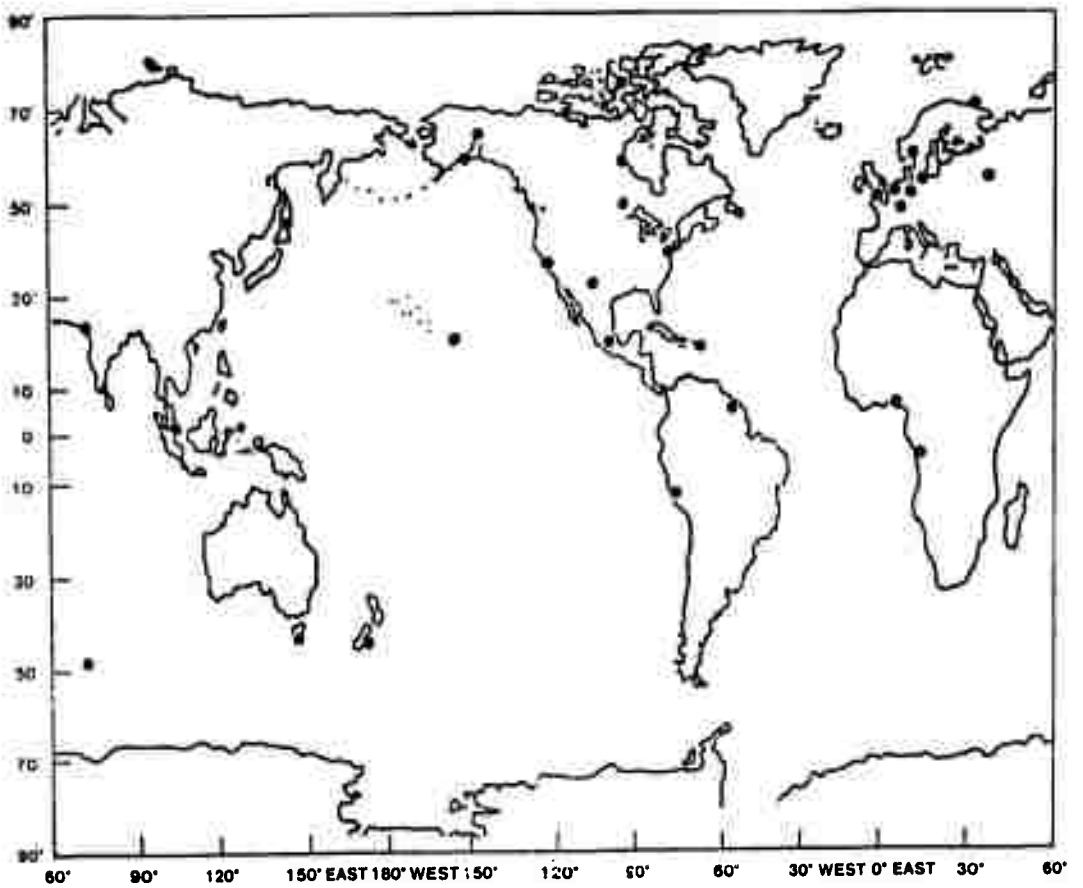

Figure 1. Geographic distribution of sites in f_oF2 data base.

Table 1. Name and geographic location of sites in f_oF2 data base.

SITE	Latitude	Longitude	SITE	Latitude	Longitude
Resolute Bay	74.7N	265.1E	Washington, DC	37.4N	237.8E
Murmansk	69.0	33.0	San Francisco	37.4	237.8
College	64.9	212.2	White Sands	32.3	253.5
Anchorage	61.2	210.1	Ahmedabad	23.	72.6
Kjeller	60.0	11.1	Maui	20.8	203.5
Churchill	58.8	265.8	Mexico City	19.4	260.3
Moscow	55.5	37.3	Puerto Rico	18.5	292.8
Juliusruh/Rugen	54.6	13.4	Ibadan	7.4	3.9
Lindau	51.6	10.1	Paramaribo	5.8	304.8
Slough	51.5	359.4	Singapore	1.3	103.8
Dourbes	50.1	4.6	Kinshasa-Binza	4.5S	15.2
Winnipeg	49.8	265.6	Huncayo	12.0S	284.7
Freiburg	48.1	7.6	Hobart	42.9S	147.3
St. Johns	47.6	307.3	Godley Head	43.6S	172.8
Wakkanai	45.4	141.7	Kerguellen	49.4S	70.3

For each site in table 1, the data base contains a winter month, a summer month, and a spring and fall equinox month in each of four sunspot number ranges, low (0 - 30), medium (31 - 100), high (101 - 150) and very high (>150). This gives a total of 16 months, each with 24 hourly median data values, at each site. In total then, there are 11,520 data points in the data base. The months and years for each site are given in table 2.

We feel that this represents a reasonably complete and inclusive description of the geographical and solar dependencies of the f_0F2 parameter.

OBLIQUE INCIDENCE SOUNDER DATA BASE (MOF)

The oblique sounder data base that was assembled was derived from a variety of sources and spans the period between 1958 and 1976. This data base represents over one complete solar sunspot cycle of propagation data. Attempts were made to make the data base as diverse as possible, including a variety of different path lengths, orientations, geographical locations, and sunspot numbers.

The oblique sounder data set consists of 304 path-months of median hourly MOF values derived from 39 different HF transmission paths. In addition to the original oblique sounder data base reported by Sailors et al. (reference 4), this data base included 14 additional paths. Table 3 summarizes the additional HF oblique sounder data base. The locations of all the paths are shown in figure 2 except for paths for which the scale is too small to illustrate. Of the 39 paths, the longest path was 7808 km and the shortest path was 192 km. Table 4 shows the percentage of the sample in each path length range. Table 5 shows the percentage of the sample in different path orientation categories. The north-south paths are those which lie nominally within ±15° of 0° or 180° bearing. The east-west paths are those which fall nominally within ±15° of a 90° or 273° bearing. The paths which did not meet either criterion were put in the "other" category. Table 6 shows the percentage of the sample categorized according to the geomagnetic latitude location of control points. Table 7 shows the percentage of the sample in each sunspot number (SSN) category.

Table 2. f_oF2 data at each site.

Site	Summer		Fall		Winter		Spring	
Resolute Bay	6/54	6/60	9/54	9/70	12/53	12/59	4/54	4/60
	6/66	6/57	4/62	4/58	12/61	12/57	4/62	4/58
Murmansk	6/64	6/68	9/64	9/68	12/63	12/68	4/65	4/69
	6/66	6/59	9/66	9/58	12/61	12/58	4/62	4/59
College	6/54	6/60	9/54	9/46	12/53	12/59	4/54	4/60
	6/52	6/57	9/50	9/58	12/50	12/57	4/42	4/58
Anchorage	6/54	6/60	9/54	9/60	12/53	12/59	4/54	4/60
	6/62	6/57	9/62	9/58	12/61	12/57	4/62	4/58
Kjeller	6/54	6/56	9/54	9/49	12/54	12/49	4/54	4/53
	6/55	6/57	9/55	9/57	12/55	12/57	4/50	4/58
Churchill	6/54	6/60	9/54	9/70	12/53	12/59	4/54	4/60
	6/66	6/57	9/62	9/58	12/61	12/57	4/62	4/58
Moscow	6/54	6/60	9/54	9/70	12/53	12/59	4/54	4/60
	6/66	6/57	9/62	9/58	12/61	12/57	4/62	4/58
Juliusruh/Rugen	6/64	6/68	9/64	9/68	12/63	12/68	4/65	4/69
	6/66	6/59	9/66	9/58	12/61	12/58	4/62	4/59
Lindau	6/54	6/60	9/54	9/68	12/53	12/59	4/54	4/60
	6/66	6/57	9/62	9/58	12/61	12/57	4/62	4/58
Slough	6/54	6/60	9/54	9/70	12/53	12/59	4/54	4/60
	6/66	6/57	9/62	9/58	12/61	12/57	4/62	4/58
Dourbes	6/64	6/68	9/64	9/68	12/63	12/68	4/65	4/69
	6/66	6/59	9/66	9/58	12/61	12/58	4/62	4/59
Winnipeg	6/54	6/60	9/54	9/70	12/53	12/59	4/54	4/60
	6/66	6/57	9/62	9/58	12/72	12/57	4/62	4/58
Freiburg	6/54	6/60	9/54	9/70	12/53	12/59	4/54	4/60
	6/66	6/57	9/62	9/58	12/61	12/57	4/62	4/58
St. Johns	6/54	6/60	9/64	9/70	12/53	12/59	4/54	4/60
	6/66	6/57	9/62	9/58	12/61	12/57	4/62	4/58
Wakkanhi	6/54	6/60	9/54	9/70	12/54	12/59	4/54	4/60
	6/66	6/57	9/62	9/58	12/61	12/57	4/62	4/58
Washington, DC	6/54	6/60	9/54	9/60	12/53	12/59	4/54	4/60
	6/66	6/57	9/62	9/58	12/61	12/57	4/62	4/58

Table 2 (continued).

Site	Summer		Fall		Winter		Spring	
	6/52	6/57	9/55	9/57	12/50	12/578	4/45	4/48
San Francisco	6/52	6/57	9/55	9/57	12/50	12/57	4/45	4/48
	6/54	6/60	9/54	9/70	12/53	12/59	4/54	4/60
White Sands	6/66	6/57	9/62	9/58	12/61	12/57	4/62	4/58
	6/64	6/68	9/64	9/68	12/63	12/68	4/65	4/69
Ahmedabad	6/66	6/59	9/66	9/58	12/61	12/58	4/62	4/59
	6/54	6/60	9/54	9/70	12/53	12/59	4/54	4/60
Maui	6/66	6/57	9/62	9/58	12/61	12/57	4/62	4/58
	6/64	6/68	9/64	9/68	12/63	12/68	4/65	4/69
Mexico City	6/66	6/59	9/66	9/59	12/61	12/58	4/62	4/59
	6/44	6/51	9/54	9/46	12/53	12/49	4/44	4/50
Puerto Rico	6/45	6/57	9/50	9/57	12/51	12/57	4/45	4/48
	6/54	6/60	9/54	9/70	12/54	12/59	4/54	4/60
Ibadan	6/66	6/57	9/62	9/58	12/61	12/57	4/62	4/58
	6/64	6/60	9/64	9/60	12/64	12/60	4/65	4/60
Paramaribo	6/62	6/58	9/61	9/52	12/61	12/57	4/62	4/58
	6/54	6/60	9/54	9/60	12/53	12/59	4/54	4/60
Singapore	6/62	6/57	9/62	9/58	12/61	12/57	4/62	4/58
	6/543	6/60	9/54	9/60	12/53	12/59	4/54	4/60
Kinshasa-Binza	6/55	6/57	9/55	9/58	12/61	12/57	4/61	4/58
	6/54	6/60	9/54	9/70	12/53	12/59	4/54	4/60
Huncayo	6/66	6/57	9/62	9/58	12/61	12/57	4/62	4/58
	6/54	6/51	9/54	9/46	12/53	12/47	4/54	4/50
Hobart	6/52	6/57	9/50	9/58	12/50	12/57	4/52	4/58
	6/54	6/60	9/54	9/70	12/53	12/59	4/54	4/60
Godley Head	6/66	6/57	9/62	9/58	12/61	12/57	4/62	4/58
	6/64	6/68	9/64	9/68	12/63	12/68	4/65	4/69
Kerguellen	6/66	6/59	9/66	9/58	12/61	12/58	4/62	4/58

Table 3. Additional HF propagation oblique sounder data

Path Number	Transmission Path	Latitude	Longitude	Path Length km	SSN Range	Year	Number of Path Months	Data Source
26	Puerto Rico to Maynard, MS	18.25°N 42.41°N	67.16°W 71.45°W	2715	27-71	1966	8	Ref. 8
27	Thule, Greenland to Stockbridge, NY	76.50°N 43.00°N	68.80°W 75.50°W	3736	72-79	1966-67	3	Ref. 9
28	Andoya, Norway to Maynard, MS	69.00°N 42.41°N	15.00°E 71.45°W	5530	14-20	1965	3	Ref. 8
29	Bangkok, Thailand to Chantaburi, Thailand	12.50°N 13.70°N	102.10°E 100.50°E	219	37	1966	1	Ref. 10
30	Ottawa, Canada to The Hague, Netherlands	45.40°N 52.10°N	75.90°W 4.40°E	5640	52-141	1959-61	17	NOSC file
31	Winnipeg, Canada to Resolute Bay, Canada	49.90°N 74.70°N	97.40°W 94.90°W	2760	122-146	1959-60	6	NOSC file
32	Ottawa, Canada to Resolute Bay, Canada	45.40°N 74.70°N	75.90°W 94.90°W	3400	52-88	1960-61	11	NOSC file
33	Okinawa to St. Kilda, Australia	26.30°N 34.70°S	127.80°E 138.50°E	6872	44-90	1966-67 1970-71	15	NOSC file
34	Okinawa to Townsville, Australia	26.30°N 19.16°S	127.80°E 146.49°	5440	58-90	1966-67 1970-71	9	NOSC file
35	Yamagawa, Japán to St. Kilda, Australia	31.12°N 34.70°S	130.38°E 138.50°E	7364	52-90	1970-72	16	NOSC file
36	Hamagawa, Japan to Townsville, Australia	31.12°N 19.16°S	130.38°E 146.49°E	5846	51-90	1970-72	14	NOSC file
37	Monrovia, Liberia to Rota, Spain	6.23°N 36.62°N	10.75°W 6.35°W	3409	24	1963	1	Ref. 11
38	Monrovia, Liberia to Fort Lamy, Chad	6.23°N 12.17°N	10.75°W 14.98°E	2899	24	1963	1	Ref. 11
39	Tripoli, Libya Accra, Ghana	32.92°N 5.75°N	13.42°E .13°W	3331	51	1961	1	Ref. 12

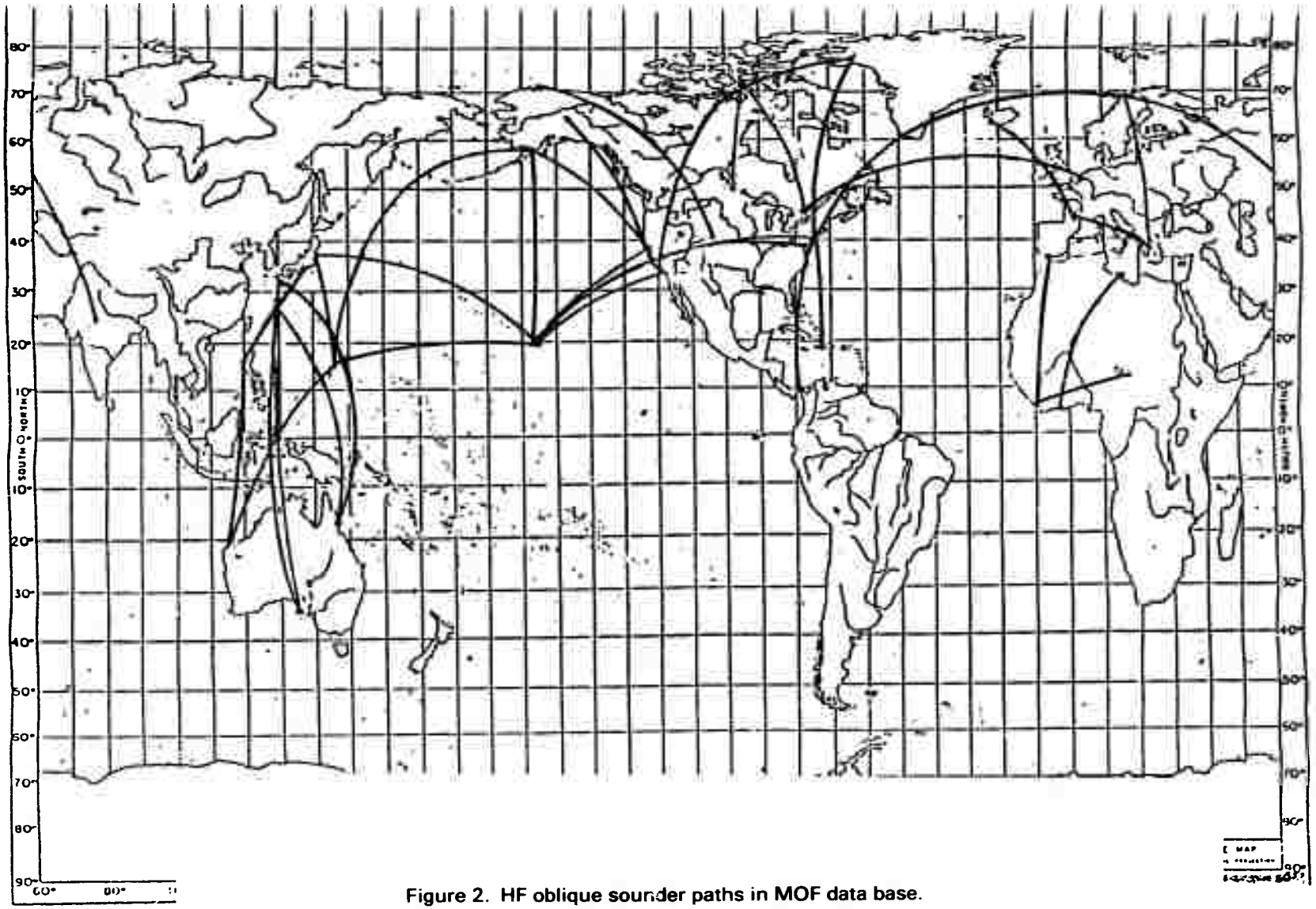

Figure 2. HF oblique sounder paths in MOF data base.

Table 4. Percentage of sample oblique data in each path length range.

Length	Number of Hours	Percentage of Sample
$L \leq 1000$	216	3.0
$1000 < L \leq 2000$	96	1.3
$2000 < L \leq 3000$	1000	13.7
$3000 < L \leq 4000$	1057	14.5
$4000 < L \leq 5000$	1608	22.1
$5000 < L \leq 6000$	1567	21.5
$6000 < L \leq 7000$	1110	15.3
$7000 < L \leq 8000$	622	8.5
Total	7276	100.0

Table 5. Percentage of sample oblique data in path orientation categories.

Path Orientation	Number of Hours	Percentage of Sample
North/South	2629	36.1
East/West	1107	15.2
Other	3516	48.3

Table 6. Percentage of sample oblique data in geomagnetic latitude categories.

Path Type	Number of Hours	Percentage of Sample
Transequatorial	2031	27.9
Low Latitude	984	13.5
Mid-latitude	2712	37.3
High Latitude	977	13.4
Transauroral	572	7.9

Table 7. Percentage of sample in each sunspot number category.

Sunspot Number (Cycle Phase)	Number of Hours	Percentage of Sample
10-30 (minimum)	1865	25.6
31-60 (rise and decline)	1121	15.4
61-90 (near maximum)	1860	25.6
91-120 (maximum)	2101	28.9
121-150 (high maximum)	257	3.5

DATA SCREENING

In the comparison of a program against data, it is desirable to subdivide the data base into subsets according to variables influencing the predicted and observed results (e.g., path length, season, month, geomagnetic latitude, sunspot number, local time at path midpoint, etc.). To accomplish this, a computer program called DASCR3 (acronym for data screening 3) is used. Each of the prediction programs is run for each of the paths or sites in the data bases. The results along with auxiliary information about the propagation situation (e.g., path length, local time of day, sunspot number, etc.) are stored in a data file to be used later by DASCR3.

DASCR3

DASCR3 is a program designed to perform data screening and statistical comparison on two large matrices of observations. For each set of matrices, up to 10 sets of information are read in on propositions to be satisfied and limits on a selected variable. A portion of each matrix is read in and tested for each set of propositions in turn. For each subset satisfying a given set of conditions, the variable to be analyzed is stored temporarily on disc. The next portion of each matrix is then read in and screened and the good observations are added to those already on disc. When the entire matrix has been screened, the screened data are then read into core and the difference (or residual) between the two matrices is taken. These arrays are then sorted to ensure maximum computer efficiency for the statistical evaluation. Finally, a statistical evaluation is then performed of the screened data and their residuals.

An example of the output from DASCR3 is given in figure 3. In this example, MINIMUF 3.5(I) is compared to the observed data. The proposition to be satisfied is all circuits in the data base are to be used. The variables being compared are the observed MOF and predicted MUF. In the printout the observed data are represented by column A and the predicted values are represented by column B. The residual (the observed data minus the predicted value) is given by column D. The relative residual is given by column D/A,

DATA SCREENING PROBLEM 1 MINMUF 3.5 (I) (ALL CIRCUITS)

CONDITIONS TO BE SATISFIED

CIRCUIT NUMBER	GE	1.000000
CIRCUIT NUMBER	LE	40.00000

SUMMARY STATISTICS FOR VARIABLE 15 OBSERVED MUF PREDICTED MUF

STATISTIC	A	B	D	D/A	ABS(D)/A
TOTAL	147758.	144082.	3675.59	179.491	1459.14
POPULATION SIZE	7276.00	7276.00	7276.00	7276.00	7276.00
AVERAGE	20.3076	19.8024	.505166	.246688-001	.200542
R.M.S. VALUE	21.7874	21.2213	4.27785	.391527-001	.329094
MEAN ABSOLUTE ERROR	6.64421	6.31411	3.22360	.236824-001	.158794
STANDARD DEVIATION	7.89221	7.62925	4.24791	.304034-001	.260931
3RD MOMENT ABOUT MEAN	182.687	137.508	26.0065	.301246-004	.622801-001
4TH MOMENT ABOUT MEAN	9482.84	7566.96	1530.41	.725245-005	.933797-001
5TH MOMENT ABOUT MEAN	69068.0	45832.3	12295.0	.108387-005	.163099
6TH MOMENT ABOUT MEAN	.265735+007	.146297+007	359698.	.201030-006	.324241
LOWER DECILE	10.3010	10.0020	-4.69676	-.136777-001	.254631-001
LOWER QUARTILE	14.0001	13.8007	-2.09988	.171481-005	.635577-001
MEDIAN QUARTILE	19.6044	19.2022	.403694	.252694-001	.120109
UPPER QUARTILE	26.6065	25.2005	3.00399	.466954-001	.218998
UPPER DECILE	30.9018	31.0002	5.49845	.583154-001	.455172
.00TH PERCENTILE	.000000	.000000	.000000	.000000	.000000
.00TH PERCENTILE	.000000	.000000	.000000	.000000	.000000
SEMI-INTERQUARTILE RANGE	6.30317	5.69989	2.55193	.233469-001	.776703-001
COEFFICIENT OF VARIATION	.388634	.385269	8.40892	1.23246	1.30113
MINIMUM	4.60000	3.80000	-13.4000	-.343750-001	.000000
MAXIMUM	52.8000	39.4000	28.0000	.253788	2.91304
COEFFICIENT OF SKEWNESS	.371630	.309659	.339279	1.07190	3.50569
COEFFICIENT OF EXCESS	-.555758	-.677903	1.70012	5.48779	17.1443
INTERVAL SIZE	5.00000	5.00000	4.14000	.285163-001	.291304
GIVEN LOWER BOUND	.000000	.000000	.000000	.000000	.000000
GIVEN UPPER BOUND	50.0000	50.0000	.000000	.000000	.000000
CORRELATION COEFFICIENT	.850767				

A MATRIX = OBSERVED

LINEAR REGRESSION ESTIMATE OF Y=AX+B

MEAN SQUARE ERROR	17.203782
STANDARD ERROR OF ESTIMATE	4.147696
EST. OF THE STANDARD ERR. OF THE MEAN	.048625
MEASURE OF ERR. IN REGRES COEF. B	.079834
SLOPE	.880091
INTERCEPT	2.879674

MEAN-SQUARE ESTIMATE OF Y=AX

MEAN SQUARE ESTIMATE	.555971
STANDARD ERROR OF THE ESTIMATE	.745635
SLOPE	1.025512

Figure 3. Example of output from DASCR3.

and the absolute relative residual by column ABS(D)/A. The left hand side of the page shows the statistics calculated for each of these columns. In addition, the correlation coefficient between the observed and predicted data are given. Included also are the slope, intercept and mean square error of linear regression. The standard error of the estimate of Y = AX, where Y_i is the measured data point and X_i the predicted point, is given as well as the slope A. In this example, 7276 data points were selected by DASCR3 from 7276 data points. Note that the average absolute relative residual for this case is 20.0 percent.

SCREENING DATA BASE

Each version of the computer program being tested is run to produce a data base corresponding to the observed data base. Auxiliary information outputted to be screened included universal time of propagation, month, year, sunspot number, path length in kilometers, geographic latitude and longitude of the path midpoint, the local time at the path midpoint, the path orientation with respect to north, the geomagnetic latitude at each of the control points, the predicted MUF, path identification number, and sounder type.

Before the actual data screening has begun, data points in both observed and predicted bases corresponding to observed values at the extremes of the particular measuring sounder are removed from the data base. The final number of hourly values in the data base was 7276 points.

ANALYSIS OF RESIDUALS BETWEEN PREDICTIONS AND OBSERVED DATA

An indication of the accuracy of the numerical predictions of MUF can be obtained from a study of the residuals between observed data and predicted values. The terms residual, relative residual, and absolute relative residual are used with the following standard meaning:

$$\text{residual} = (\text{observed datum}) - (\text{predicted value}) \qquad (4)$$

$$\text{relative residual} = \frac{\text{residual}}{\text{observed datum}} \tag{5}$$

$$\text{absolute relative residual} = \frac{\text{absolute residual}}{\text{observed datum}} . \tag{6}$$

Certain statistical measures of these terms have proved useful in past ionospheric studies in comparing predicted and observed data (reference 4). These include

(1) The average residual (av. res.)
(2) Root mean square residual (rms res.)
(3) The mean absolute error of the residual (mae res.)
(4) The average relative residual (av. rel. res.)
(5) The root mean square relative residual (rms rel. res.)
(6) The mean absolute error of the relative residual (mae rel. res.)
(7) The average absolute relative residual (ave. abs. rel. res.)
(8) Correlation coefficient between observed and predicted values
(9) The standard error of the estimate of linear regression

Values of each of these parameters are produced by DASCR3 as can be seen by examining figure 3. The average residual and the average relative residual locate the center of the distributions of error and are sometimes referred to as the bias in the estimate. The mean absolute errors of the residual and relative residual are a measure range of the error and are the first moments about the average residual and average relative residual, respectively. They provide information about the range of variation. The average absolute relative residual is a measure of the average magnitude of the error.

The root mean square residual and relative residuals are measures of the dispersion in the error. In fact, the rms residual and rms relative residual are the standard deviations of the error about the origin (zero bias) and are related to the standard deviation about the mean according to

$$\sigma^2 = \nu_2 - \nu_1^2 \tag{8}$$

where ν_2 is the mean square error (the square of the rms error) and ν_1 is the bias. When the bias is small or nearly zero, then the standard deviation and

the rms error are nearly the same. Otherwise, the rms error is larger than the standard deviation.

A measure of the degree of association or the closeness of fit between variables is given by the correlation coefficient. The degree indicates the strength of the tendency for high (or low) values of one variable to be associated with high (or low) values of the other variable.

A description of the nature of the relationship between variables is called regression analysis (reference 13). Regression analysis is concerned with the problem of describing or estimating the value of one variable, called the dependent variable, on the basis of one or more other variables, called independent variables. In other cases regression may be used merely to describe the relationship between known values of two or more variables.

Regression analysis that involves the determination of a linear relationship between two variables is referred to as simple linear regression. Here, the variable y is given as $y = a + bx$ where x is the independent variable and y is the dependent variable. The coefficients a and b are determined in the regression analysis. A measure of the success of linear regression analysis is the standard error of the estimate given by

$$S_{y.x} = \left[\sigma_y^2\left(1 - \gamma^2\right)\right]^{1/2} \tag{9}$$

where σ_y is the standard deviation in the observed datum and γ is the correlation coefficient between the observed data in predicted values. If the relationship is truly linear, then the bias of the estimate should be removed (or made nearly zero). An estimate of the standard error of mean is given by

$$S_{\bar{y}.x} = \frac{S_{y.x}}{\sqrt{n}} \tag{10}$$

A measure of the error in the regression coefficient is given by

$$S_b = \left[\frac{S_{\bar{y}.x}}{\sigma_x}\right]^{1/2} \tag{11}$$

SUNSPOT REPRESENTATION

In 1984, an improved version of MINIMUF-3.5 was presented, which improved the accuracy of the algorithm for sunspot numbers greater than 100 by limiting the growth of the f_oF2 portion of the calculation as the sunspot number became high (reference 14). It retained the simplicity of MINIMUF-3.5 and is as accurate as MINIMUF-3.5 at sunspot numbers less than 100.

For years of high solar activity, the literature indicates that an algorithm with a limitation on the increase of MUF at high solar activity is desirable (references 15, 16, and 17). Vasil'yeva and Kerblay indicate that there are three types of dependencies of f_oF2, a factor in the MUF computation, on solar activity. Type I includes the kinds of dependencies that can be considered as linear over the entire range of sunspot number R. Type II behavior is characterized by f_oF2 increasing with R to 100-140 and remaining constant or changing insignificantly with further increase in R. In type III behavior, the dependence is characterized by a more intense increase of f_oF2 for high values of R. The geographic location of these types of solar variation of f_oF2 with R are dependent on local time and season. Vasil'yeva examined the percentage distribution of the various types of dependencies of f_oF2 on R. He subdivided type II into two additional categories. Type IIa were cases where f_oF2 continued to grow at large values, but more slowly than at low and medium solar activity. Type IIb includes dependencies where not only the growth of f_oF2 is limited, but also where the critical frequencies decrease somewhat with increasing solar activity. The percentage of cases of each type of dependence of f_oF2 on R were given as follows: (I) 20.7%, (II) 64.8%, (IIa) 4.2%, (IIb) 3.2%, and (III) 7.3%.

This improved version of MINIMUF-3.5, MINIMUF-B, was developed by altering MINIMUF-3.5 so that a version called MINIMUF-A was developed for which the predicted MUFs were not dependent on sunspot number. The equation for f_oF2 in MINIMUF-A became

$$f_oF2 = \left(A_o + A_1 \sqrt{\cos \chi_{eff}}\right)^{1/2} \qquad (12)$$

MINIMUF-B was similar to MINIMUF-3.5 except that the expression for f_oF2 was given by

$$f_oF2 = f(R)\left(A_o + A_1 \sqrt{\cos \chi_{eff}}\right)^{1/2} \qquad (13)$$

where f(R) was a function dependent on the sunspot number R.

The function f(R) was found by calculating the residuals between the predicted MUFs from MINIMUF-A and the corresponding MOFs from the oblique sounder data base. The residuals were subdivided into subsets according to sunspot variation. The first subset was for data for which the sunspot number used for the calculation of the MUF varied from 10 to 20. In each subsequent subset the sunspot number was incremented by 10. The average residual (the bias) is calculated in each subset to help determine the needed sunspot variation. In particular, a multiplying constant A is determined in each sunspot interval that made the bias zero.

A polynomial equation was fit in a least square sense to these constants. For this purpose a standard subroutine for a Hewlett-Packard hand held programmable calculator was used. The program approximated the function f(R) by a polynomial of degree m, where $2<m<4$. The special Chebyshev polynomials for discrete intervals were used. Figure 4 shows the results of fitting both a second order polynomial and a fourth order polynomial. It also shows the multiplier used by MINIMUF-3.5 and the multiplier determined by calculating the residuals between MUFs predicted by MINIMUF-A and MOFs from the observed data base. First note the oscillatory nature of the multiplying constants A, particularly at sunspot numbers greater than 100. The fourth order fit has an oscillatory nature too. The second order fit and MINIMUF-3.5 gives the best fit below sunspot number 100. The second order fit also has the ability to limit the growth of f_oF2 at sunspot numbers above 100.

A further investigation was made to determine the cause of the large peak in the observed multiplying constants A. The multiplying constants are determined as a function of sunspot number for individual paths. It is found that, for two paths in the oblique sounder data base, the f_oF2 decreases with increasing R for R > (120-140). This type of dependence on sunspot number only occurred 3.2 percent of the time (reference 16). Hence, the data for

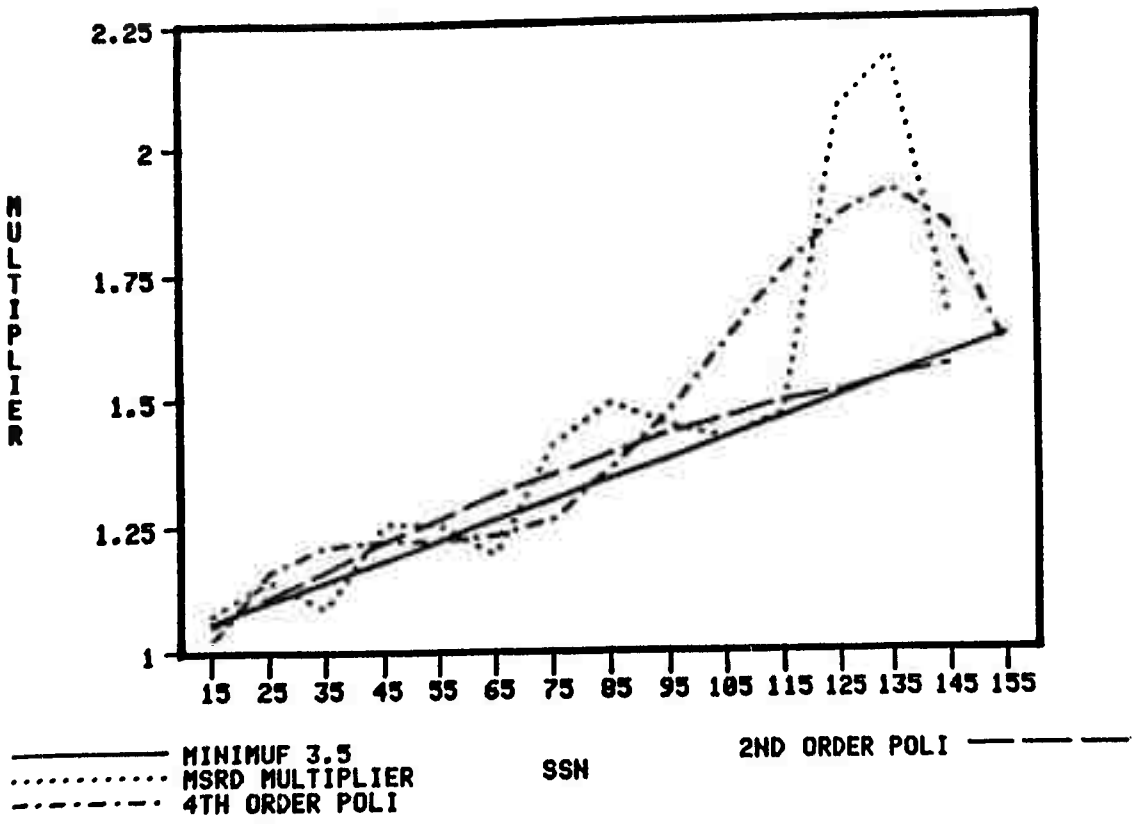

Figure 4. Initial sunspot number multiplier fit.

these two paths, Winnipeg to Resolute Bay and Ottawa to The Hague, were dropped from the oblique sounder data base used to determine f(R). Subsequent work on improving MINIMUF in the polar region showed these two paths to be particularly illustrative of the weakness of MINIMUF in the polar regions.

A new second order fit was made to the multipliers using the adjusted oblique sounder data base. The multiplier for MINIMUF-3.5, the new second order fit, and the data points are shown in figure 5. As can be seen in figure 5, below a sunspot number of about 125 the second order fit and MINIMUF-3.5 differ only by a small amount. But at high sunspot levels, as occurred during July and August 1982, the second order fit would provide a limit on the growth of the f_0F2 part of the MUF computation. Table 8 gives the coefficients for the second order fit.

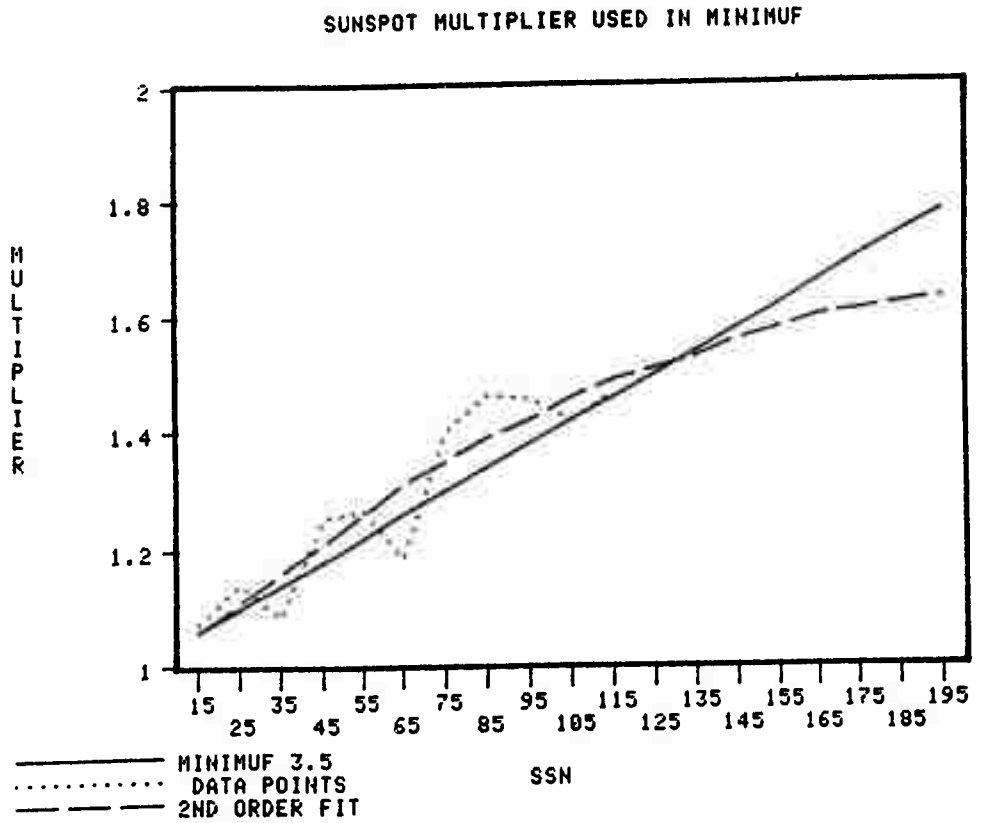

Figure 5. Second order sunspot number multiplier fit.

To further improve the fit, the multiplying constants A were smoothed by averaging each pair of data points starting at the lowest sunspot interval. The resulting fit along with the multiplier from MINIMUF-3.5 is presented in figure 6. Table 8 gives the coefficients for the smoothed second order fit.

The accuracy of both MINIMUF-3.5 and the smoothed version of MINIMUF-B was determined by comparing the bias and the rms error of the residuals from both programs as a function of the sunspot number. Overall the bias and rms error for MINIMUF-3.5 were 0.52 MHz low and 4.33 MHz, respectively. For MINIMUF-B, the bias and rms error were 0.14 MHz low and 4.33 MHz, respectively. To determine the accuracy of the program as a function of sunspot number, the data were divided into sunspot number categories. Table 9 gives the bias and rms error for each model. A negative number means that the model predicted high. As can be seen, the most notable differences in accuracy as a function of the sunspot number are in the bias. In the sunspot number range 10-120, the bias is always less than 1.0 MHz. However, at the sunspot numbers greater than 120, much higher biases are shown.

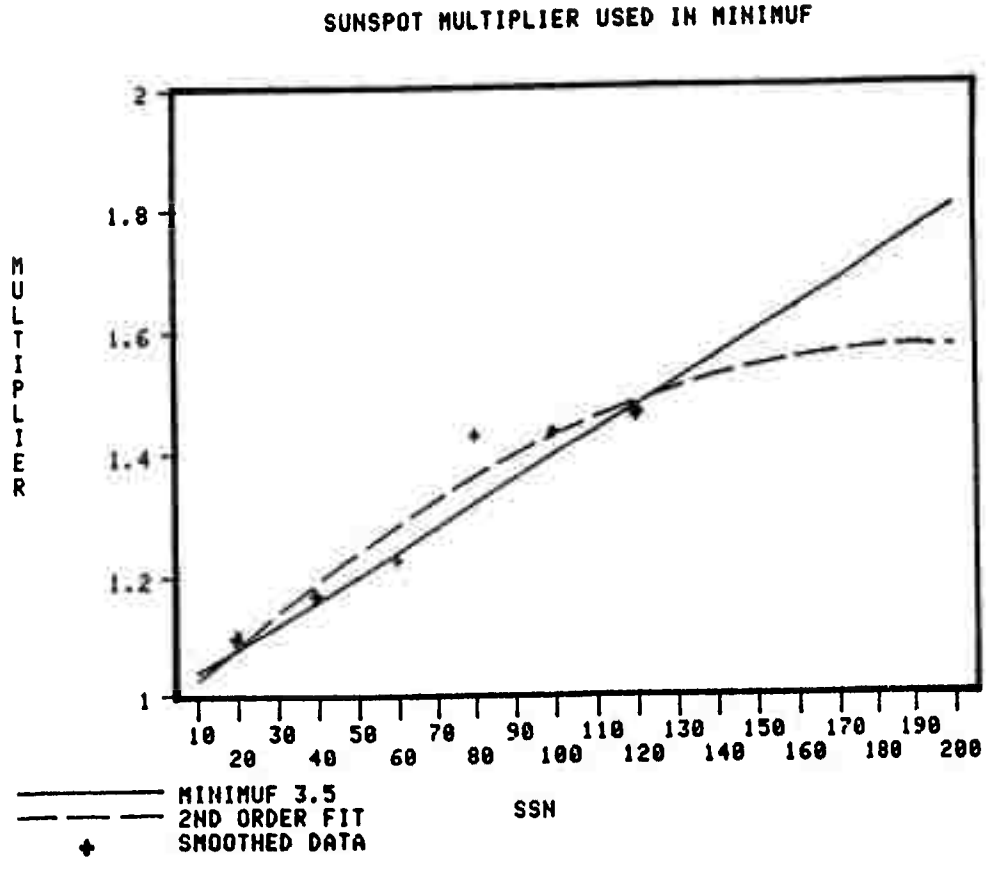

Figure 6. Second order sunspot number multiplier fit to smoothed data.

Table 8. Coefficients for $f(R) = d_o + d_1 R + d_2 R^2$.

Version	d_o	d_1	d_2
unsmoothed	0.966184943	0.006147659	-0.000014123
smoothed	0.965142201	0.006288535	-0.000016288

Table 9. Accuracy of MINIMUF-3.5 and the smoothed version of MINIMUF-B as a function sunspot number.

Sunspot number	Range Bias (MHz)	MINIMUF-3.5 RMS Error (MHz)	MINIMUF-B Bias (MHz)	MINIMUF-B RMS Error (MHz)
10 - 30	0.40	3.63	0.42	3.61
31 - 60	0.22	4.45	-0.41	4.46
61 - 90	0.87	4.70	0.13	4.72
91 - 129	-0.94	4.14	-0.41	4.20
120 - 150	4.49	6.68	4.70	6.76

In the development of MINIMUF-B, two paths, Winnipeg to Resolute Bay and Ottawa to The Hague, were deleted from the data set to obtain f(R). With these paths deleted, the overall accuracy of MINIMUF-3.5 was 0.34 MHz low with an rms error of 4.23. For MINIMUF-B, the overall accuracy was 0.05 MHz high with an rms error of 4.26 MHz.

CHOICE OF CONTROL POINTS

In MINIMUF-3.5 the calculated MUF is the minimum value evaluated at specific "control points" along the great circle propagation path. In the original version of MINIMUF-3.5, the control point locations for path lengths greater than 4000 km were located 2000 km from either terminus (reference 2). However, in the next versions (references 3 and 18), the control points for path lengths greater than 4000 km were located at one quarter, one half, and three quarters of the path length along the great circle path. In a version published in the United Kingdom (reference 19), the control points were located one quarter and three quarters of the path length along the great circle path. For all versions, the control point for path lengths less than 4000 km is located at the path mid-point. The version of MINIMUF-3.5 used to determine the solar variation presented earlier in this report was the original version with control points located 2000 km from either terminus for path lengths greater than 4000 km.

This section examines these three choices of control points. The original version of MINIMUF-3.5 was modified so that it calculated control points at 1/4, 1/2, and 3/4 of the great circle path length; this version was called MINIMUF-D. Another version was created that calculated control points at 1/4 and 3/4 of the great circle path length only; this version was called MINIMUF-E. These two versions are compared to the original MINIMUF-3.5 as a function of path length in tables 10 and 11. Table 10 gives the bias, and table 11 gives the rms error of the models. From 0-4000 km only the midpoint is used as a control point so there is no difference between the models. From 4000 - 6000 km, the original MINIMUF-3.5 had the smallest bias and lowest rms error. However, from 6000 - 8000 km, MINIMUF-D had the lowest bias of the three versions and a lower rms error than MINIMUF-3.5. The difference in rms error between MINIMUF-D and MINIMUF-E is insignificant.

Table 10. Bias of MINIMUF models with range (MHz).

Range (km)	MINIMUF-3.5	MINIMUF-D	MINIMUF-E	MINIMUF-F	MINIMUF-I
0-1000	0.91	0.91	0.91	0.91	0.91
1000-2000	-2.99	-2.99	2.99	-2.99	-2.99
2000-3000	0.97	0.97	0.97	0.97	0.75
3000-4000	0.20	0.20	0.20	0.20	0.00
4000-5000	0.76	1.89	1.87	0.76	0.74
5000-6000	1.75	2.34	2.29	1.75	1.58
6000-7000	-0.92	-0.51	-0.56	-0.51	-0.51
7000-8000	-0.41	-0.16	-0.24	-0.16	-0.16

Table 11. RMS error of MINIMUF models with range (MHz).

Range (km)	MINIMUF-3.5	MINIMUF-D	MINIMUF-E	MINIMUF-F	MINIMUF-I
0-1000	2.34	2.34	2.34	2.34	2.34
1000-2000	4.05	4.05	4.05	4.05	4.05
2000-3000	4.08	4.08	4.08	4.08	3.99
3000-4000	5.14	5.14	5.14	5.14	5.10
4000-5000	3.53	3.97	3.96	3.53	3.53
5000-6000	5.18	5.41	5.40	5.18	5.07
6000-7000	3.83	3.76	3.77	3.76	3.76
7000-8000	4.24	4.18	4.17	4.18	4.18

A fourth version of MINIMUF was created called MINIMUF-F that had control points at the path midpoint for path lengths less than or equal 4000 km, control points located 2000 km from either terminus for path lengths greater than 4000 km, but less than or equal 6000 km, and control points located at 1/4, 1/2, and 3/4 of the great circle path length for path lengths greater than 6000 km. The results for this version are presented in tables 10 and 11. Obviously it has the lowest bias and rms error of the four versions.

GEOMAGNETIC LATITUDE DEPENDENCE

To account for critical frequency separation between ordinary and extraordinary traces, it is common in prediction methods to add one-half the gyrofrequency to the f_oF2 in determination of the MUF. However, in the use of

MINIMUF-3.5, the determination of the constants in the fitting process includes implicitly the gyrofrequency for the paths for which the constants were determined. For the northern most path used in the fitting process, the gyrofrequency at path midpoint is approximately 1.2 MHz. On the average, the gyrofrequency is approximately 1.0 MHz in the MINIMUF fitting process. At high latitudes the gyrofrequency can get as high as 1.8. Hence, a bias can exist in the f_oF2 as large as 0.4 MHz. For an M factor of 3.2, this causes a bias in the MUF of 1.28 MHz low.

Because of this potential bias in MINIMUF-3.5 at high latitudes, the effect of adding one-half the gyrofrequency to the f_oF2 was investigated. Two versions of MINIMUF were produced. The first, MINIMUF-G, added one-half the gyrofrequency to the f_oF2 at all latitudes. The second, MINIMUF-H, added one half the gyrofrequency to the f_oF2 at latitudes greater than 55°N geomagnetic. In each version 0.5 MHz was subtracted off to remove the implicit fitting of the gyrofrequency in MINIMUF-3.5.

From Davies (reference 20), the gyrofrequency for an earth centered dipole field is given by

$$f_H = 0.870 \left(\frac{R_e}{R_e + R_F}\right)\left(1 + 3 \sin^2\theta\right)^{1/2} \text{ (MHz)} \qquad (14)$$

where R_e = earth radius (6371 km)

H_F = height of the maximum ionization of the F-layer at the midpoint of the propagation path

θ = latitude of the midpoint of the propagation path in magnetic coordinates (radians).

Substituting the approximate value for R_e and 300 km for R_F, equation (14) becomes

$$f_H = 0.7578\left(1 + 3 \sin^2\theta\right)^{1/2} \text{ (MHz)} \qquad (15)$$

From Davies (reference 20) the geomagnetic latitude θ is given by

$$\sin\theta = \sin\phi\sin\phi_o + \cos\phi\cos\phi_o\cos(\lambda - \lambda_o) \quad (16)$$

where ϕ = latitude of the midpoint of the propagation path (radians)

λ = longitude of the midpoint of the propagation path (radians)

ϕ_o = latitude of the North magnetic pole (1.3666 radians, North or 78.3°N)

λ_o = longitude of the North magnetic pole (1.2043 radians, West or 69°W).

Substituting the values of ϕ_o and λ_o into equation (17) provides

$$\sin\theta = 0.9792\ \sin\phi + 0.2028\ \cos\phi\ \cos(\lambda - 1.2043)\ . \quad (17)$$

The accuracy of MINIMUF-G, MINIMUF-H, and MINIMUF-3.5 are compared to observed MOFs on the 39 paths. The latitude of the control points are divided into five latitude regions: transequatorial (TE), low latitude (LO), mid-latitude (M), high latitude (H), and transauroral (TA). Table 12 shows the path categories for the additional paths added to the data base since the 1981 comparison (reference 4). The path characteristics for the first 25 paths are given in Table 10 of reference 4. Tables 13 and 14 show the bias and rms error of these models, respectively. Only at high and transauroral latitudes is there an improvement in predicted MUF by using one-half of the gyrofrequency added to the f_oF2.

MINIMUF-I included in tables 10, 11, 13, and 14 is a combination MINIMUF-F, optimum control point version, with MINIMUF-H, half the gyrofrequency added to f_oF2 at high latitudes. Note that MINIMUF-I is less accurate in transequatorial and low latitude regions even though MINIMUF-H is better there. This occurs because on three very long paths the additional control point at path midpoint causes an additional bias in the result. The accuracy of the prediction at the control points at path midpoint is probably less accurate than those control points at higher latitudes nearer the path terminals.

Table 12. Additional path characteristics.

No.	Transmission Path	Orientation	Latitude of Control Points	Region
26	Puerto Rico to Maynard, MS	N-S	M	B
27	Thule, Greenland to Stockbridge, NY	N-S	TA	C
28	Andoya, Norway to Maynard, MS	E-W	TA	C
29	Bangkok, Thailand to Chantaburi, Thailand	Other	LO	A
30	Ottawa, Canada to The Hague, Netherlands	Other	H	C
31	Winnipeg, Canada to Resolute Bay, Canada	N-S	TA	A
32	Ottawa, Canada to Resolute Bay, Canada	N-S	TA	A
33	Okinawa to St. Kilda, Australia	N-S	TE	C
34	Okinawa to Townsville, Australia	Other	TE	C
35	Yamagawa, Japan to St. Kilda, Australia	N-S	TE	C
36	Yamagawa, Japan to Townsville, Australia	Other	TE	B
37	Monrovia, Liberia to Rota, Spain	N-S	LO	A
38	Monrovia, Liberia to Fort Lamy, Chad	Other	LO	A
39	Tripoli, Libya to Accra, Ghana	Other	LO	A

TE = Transequatorial
LO = Low latitude
M = Mid-latitude
H = High latitude
TA = Transauroral

E-W = East/West
N-S = North/South
A = Continental
B = Ocean
C = Combined land/ocean

Table 13. Bias of MINIMUF models with geomagnetic latitude region (MHz).

Latitude Region	MINIMUF-3.5	MINIMUF-G	MINIMUF-H	MINIMUF-I
TE	0.31	0.63	0.31	0.43
LO	0.87	1.13	0.87	1.12
M	-0.24	-0.38	-0.24	-0.19
H	1.98	1.54	1.60	1.60
TA	1.73	1.14	1.14	1.14

Table 14. RMS error of MINIMUF models with geomagnetic latitude region (MHz).

Latitude Region	MINIMUF-3.5	MINIMUF-G	MINIMUF-H	MINIMUF-I
TE	4.85	4.91	4.85	4.80
LO	4.79	4.83	4.79	4.83
M	3.47	3.48	3.47	3.44
H	4.12	3.93	3.96	3.96
TA	5.41	5.25	5.25	5.25

Table 15 shows the progression of improvement in the models with each succeeding change. MINIMUF-I is the version of MINIMUF for which further development was done.

Table 15. Overall comparison of MINIMUF models.

Program	Biaz MHz	rms error MHz
MINIMUF-D	0.98	4.46
MINIMUF-E	0.95	4.46
MINIMUF-F	0.60	4.32
MINIMUF-G	0.48	4.32
MINIMUF-H	0.42	4.29
MINIMUF-I	0.51	4.28
MINIMUF-3.5	0.51	4.33

CRITICAL FREQUENCY MODEL

In this section the development of an improved f_oF2 portion of MINIMUF is presented. This involves the fitting of the expression for f_oF2 portion to vertical incidence f_oF2 data.

Equation (3) presented earlier shows that the only sunspot number dependence in the MINIMUF 3.5 model is through the linear multiplying factor $1 + R/R_o$. The value of $R_o = 250$ is chosen based on the limited data set used to determine the contents in the model as described above. This data set had a maximum sunspot number of 85. Hence, it is perhaps not surprising that

the model proved less than adequate for the range of sunspot numbers encountered during July/August 1982 test.

The original MINIMUF 3.5 algorithm is derived using the 12 month running mean sunspot number. In practice however, all types of sunspot numbers have been used as input to MINIMUF-3.5 for prediction purposes. During the July/August 1982 test, for example, daily observed values of sunspot numbers were input to MINIMUF with much less than satisfactory results. Since this procedure is followed in many instances, especially when MINIMUF is used as a real-time frequency selection aid, we have changed the sunspot representation from the smoothed 12 month running mean sunspot number to the monthly median values. This more closely agrees with what is used in practice. However, one can still expect significant errors when daily sunspot number values are input. This is especially true during times of very active and disturbed solar conditions.

In the development that follows, the basic functional form of equation (3) is retained with the attempt to develop a new model altogether. The predictive capability of the current model is quite good for low to mid-range values of sunspot number, and our intent is to improve the accuracy for the high and very high sunspot range without compromising its success in these other ranges. With this criterion established, we began an investigation of the values of A_0 and A_1 as they existed in MINIMUF-3.5.

We began by graphically comparing the diurnal predictions of equation (3) to vertical incidence f_oF2 data gathered at several representative sites described earlier for various sunspot number values. These results showed that, in general, the bias value, A_0, in equation (3) is not a strong function of sunspot number. The value of A_1, however, allowed too much diurnal amplitude variation at very high sunspot number values. Figure 7 illustrates the effect of the value of A_1 being too large. In the case presented (Moscow, August 1970, SSN = 194), the maximum predicted value is about 2.5 MHz high. An obvious approach then is to remove the linear function of sunspot number in equation (3), and let A_1 become the only function of sunspot number in the new f_oF2 expressions. This function of sunspot number replaced that derived for

MINIMUF-B presented earlier. The f_oF2 data set was then partitioned into 24 segments, each containing a range of 10 in sunspot number, from the lowest value in the data base, approximately 1, to the highest of approximately 245. For each of these segments, values of $[(f_oF2_d)^2 - A_o]$ are compared to values of $\sqrt{\cos \chi_{eff}}$, where $\cos \chi_{eff}$ is the value returned from MINIMUF 3.5 for the particular time and location corresponding to each data point f_oF2_d.

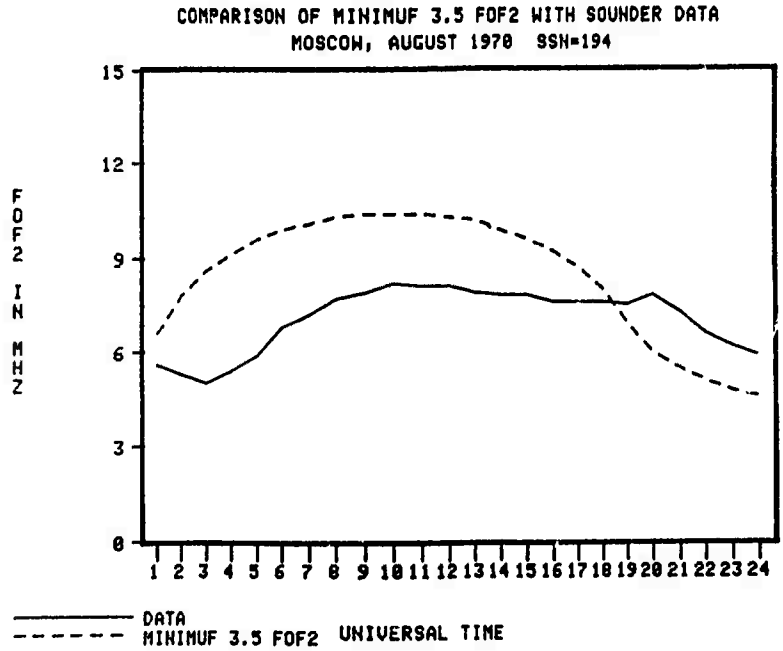

Figure 7. Example of the comparison of MINIMUF-3.5 f_oF2 with vertical ionosonde data.

The result of the comparison, using the DASCR3 statistical data comparison program, is a set of 24 mean square estimated values, one for sunspot number segment, of the multiplier A_1, where

$$(f_oF2_d)^2 - A_o = A_1 \sqrt{\cos \chi_{eff}}. \tag{18}$$

A linear least squares fit is then derived for this set of 24 data points, resulting in the equation

$$A_1(SSN) = 0.814R + 22.23 . \tag{19}$$

Because A_1 appears under the square root sign in equation (3), the resulting expression for f_oF2 is nonlinear with sunspot number. Figure 8 shows the results using the new expression versus that obtained from MINIMUF-3.5(I) for

a cos χ_{eff} = 0.5. Note that the new expression provides a saturation effect, albeit a slow one, in the behavior of the critical frequency as a function of sunspot number.

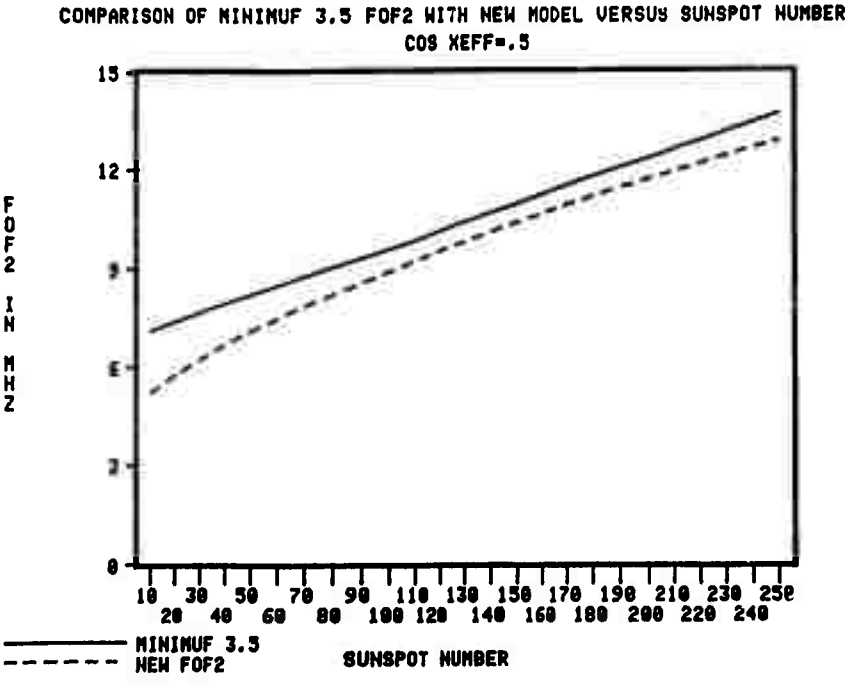

Figure 8. Comparison of MINIMUF-3.5 f_oF2 with new model versus sunspot number for cos χ_{eff} = 0.5.

A comparison of the predictions of this improved f_oF2 expression versus data, for each of the four ranges of sunspot number and for the entire data base is given in table 16. In this table the first value shows the results of a comparison of the MINIMUF-3.5(I) f_oF2 expression, equation (3), in each of these sunspot number ranges. The average difference (the bias), the rms error, and the correlation coefficient between the models and the observed data are given.

The results of the comparison show that the changes to the critical frequency portion of the MINIMUF-3.5 algorithm significantly improves the overall accuracy of the prediction. Note particularly the change in the correlation coefficient between the models and the f_oF2 values. This shows

clearly that the new expression is a much better representation of f_oF2. The correlation, however, does drop somewhat with increasing sunspot number.

Table 16. Statistical Comparison of Accuracy of f_oF2 Predictions of MINIMUF-3.5 and MINIMUF-85.

MINIMUF-3.5 / MINIMUF-85

SSN RANGE	AVERAGE DIFF (OBS-PRED)	RMS VALUE, DIFF (MHZ)	CORR. COEFF.
Low (<30)	-0.97/0.44	2.51/1.56	0.24/0.65
Med (31-100)	-0.71/0.15	2.92/1.86	0.21/0.63
High (101-150)	-0.43/0.33	3.66/2.55	0.14/0.58
Very high (>150)	-0.94/0.15	4.29/3.25	0.05/0.50
Entire data base	-0.77/0.26	3.37/2.35	0.39/0.69

These improvements in the f_oF2 model will be reflected most dramatically in the short path length MUF prediction of the new model where the f_oF2 dominates over the M-factor. We will also see improvements in ray trace applications where accurate critical frequencies are important in predicting mode structure when operating close to the MUF.

M-FACTOR MODEL

In the previous section, a new f_oF2 representation for MINIMUF is determined by fitting equation (3) against f_oF2 vertical incidence sounder data. Having done this, it was necessary to make adjustments to the M-factor model so that the resulting predicted MUF is in fact a MUF. This is done by comparing the resulting predicted MUF to the observed MOF data base. In so doing, sunspot number, seasonal, and diurnal dependencies are incorporated into the M-factor model.

SUNSPOT NUMBER DEPENDENCE

As shown in figure 8, the changes in the f_oF2 algorithm described above provide a "saturation" effect, albeit a slow one, in the behavior of the

critical frequency as a function of the sunspot number. This is a frequently observed effect in the dynamics of the critical frequency (references 15, 16, 17). It is also known that the obliquity factor, hereafter called the M-factor, shows an inverse dependence on sunspot number (references 21 and 22). The combination of these two behaviors, combined in the product of equation 1, produces a natural and relatively fast cut-off in the use of the MUF as a function of the sunspot number. It is felt that the poor performance of MINIMUF-3.5 during periods of very high sunspot number can, at least partially, be attributed to the lack of sunspot number dependence in the M-factor.

In order to determine the sunspot number dependence of the M-factor, we followed a similar procedure to that described above for the critical frequency. That is, the MOF data base described earlier, which consisted of hourly median values of MOF scaled from oblique ionograms part of which represented a maximum monthly median sunspot number of approximately 145, was subdivided into 15 segments, each defined by a range of 10 in sunspot number. Using the DASCR3 statistical program, we compared prediction using equation 1, using the improved f_oF2 described above instead of the original f_oF2, with actual data values. This resulted in a set of 15 multipliers, A_2, defined by

$$MOF_d = A_2(SSN) \times M \times \sqrt{A_o + A_1(SSN) * \sqrt{\cos \chi_{eff}}}. \qquad (20)$$

Again a linear least square fit is made to the A_2 data points. This resulted in the function for A_2,

$$A_2(SSN) = 1.3022 - 0.00156\ R \qquad (21)$$

which, as expected, shows the monotonically decreasing behavior as a function of the sunspot number. Figure 9 shows a comparison of the derived multiplying factors and the linear fit to the factors. Figure 10 shows a comparison of this new MUF expression versus the original as a function of the sunspot number for a 3000 km path with $\cos \chi_{eff} = 0.5$.

It should be noted that figure 10 shows saturation at a MUF value of approximately 11 MHz for this case. This relatively low value is due to a lack of a very high sunspot number data in the MOF data base. It would be

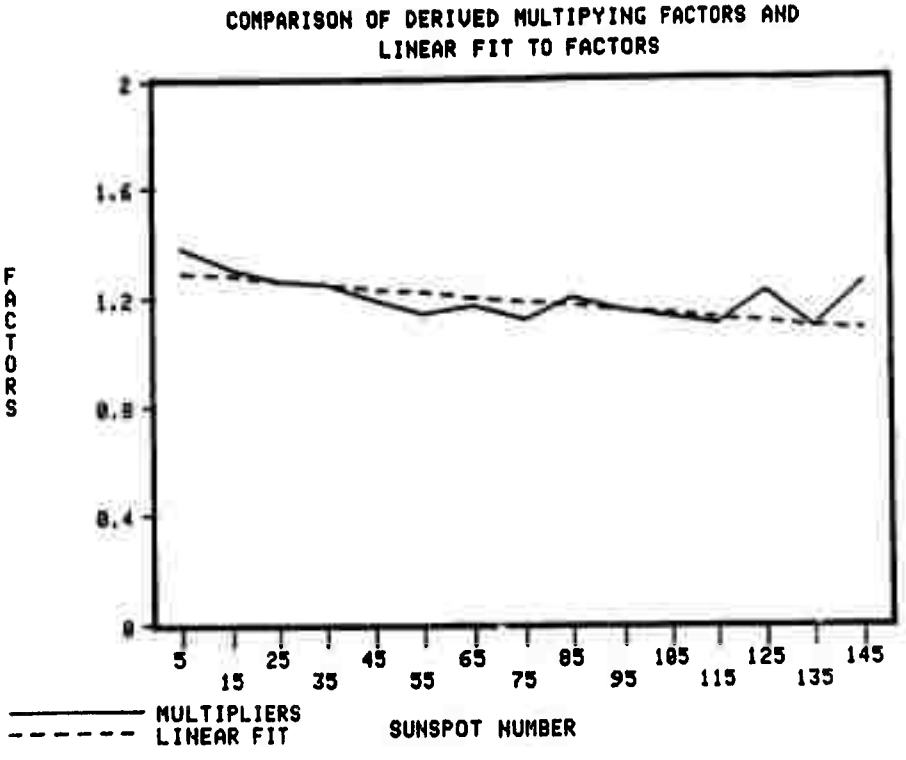

Figure 9. Comparison of derived sunspot multiplying factors and a linear fit to the factors.

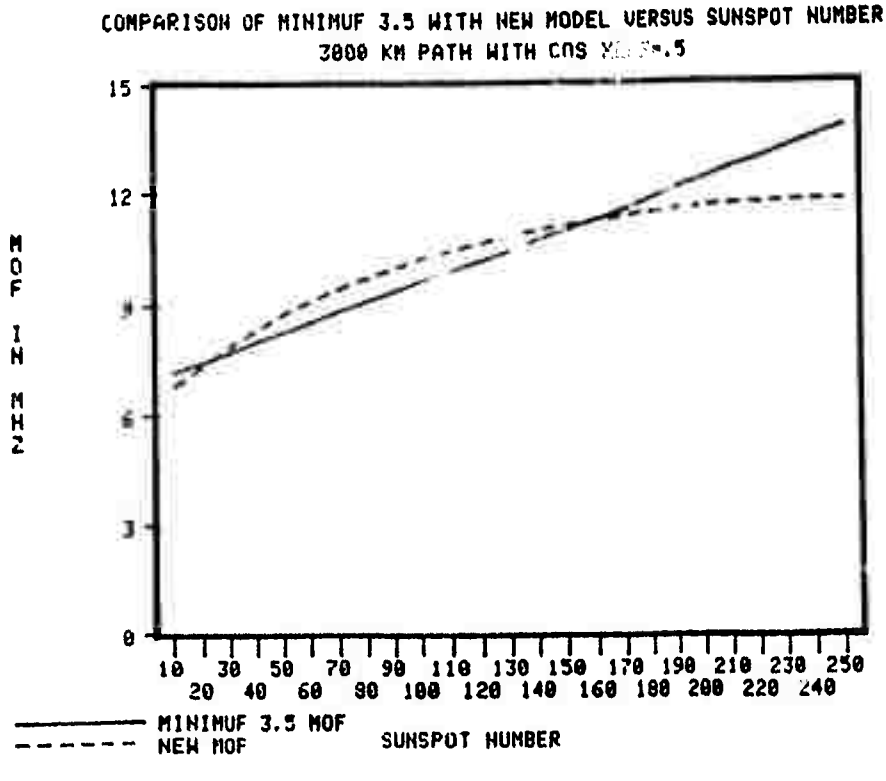

Figure 10. Comparison of MINIMUF-3.5 with new model versus sunspot number, 3000 km path with cos χ_{eff} = 0.5.

desirable to obtain more high sunspot number data (> 150). The inclusion of this data and a repeat of the process described above, should lead to a higher cut-off value for the MUF.

The important point to be stressed is that the technique described does, in fact, lead to a cut-off in the MUF with increasing the sunspot number. This is in line with observation which shows that, unlike the linear behavior described by equation (1), the MUF does saturate at high sunspot number values.

In table 17 we show the effect of these changes, both in the f_0F2 and the M-factor, on the prediction of the MUF for the limited range of sunspot numbers in the MOF data base. Note that these changes have not significantly altered the overall predictive capability of the algorithm for these smaller sunspot number values, as intended. The increase in rms error in the new model might be due to the use of a linear fit to the multiplying factors rather than a second order fit.

Table 17. Comparison of accuracy of MINIMUF-3.5 with intermediate version of new model with SSN dependence in f_0F2 and M-factor.

	Avg. Diff. (MHz)	RMS Diff. (MHz)	Corr. Coef.
MINIMUF-3.5	0.52	4.28	0.85
INTERMEDIATE	-0.11	4.52	0.85

SEASONAL DEPENDENCE

It is well known that the MOF is a seasonally dependent parameter. During the winter months, for example, increased electron density levels in the ionosphere generally cause a lowering of the height of maximum electron density. This "winter anomally" allows higher frequencies to propagate on a given transmission path. Consequently, we normally see larger MOFs in the winter than in the summer or equinox months. To include these effects in the model, we followed a similar procedure to that described above to derive a seasonal (monthly) dependence in the M-factor part of the algorithm.

The MOF data base is again segmented, this time by month, into 12 separate data bases. For each of these data bases, we compare prediction from equation (1), with the above changes incorporated, to the measured data. That is, we compared the predictions of the expression

$$A_3(\text{month}) * A_2(\text{SSN}) * M * f_oF2$$

to corresponding values of MOF_d from the data base using DASCR3. This resulted in 12 values of the multiplier A_3, one for each month. These values were then fit with a 6^{th} order Fourier series given by

$$\begin{aligned} A_3(\text{month}) = {} & 0.9925 + 0.011\sin M + 0.087\cos M \\ & - 0.043\sin 2M + 0.003\cos 2M \\ & - 0.013\sin 3M - 0.022\cos 3M \\ & + 0.003\sin 4M + 0.005\sin 5M \\ & + 0.018\cos 6M \end{aligned} \qquad (22)$$

where $M = \frac{2\pi \text{ month}}{12}$.

In figure 11 we show the derived multiplier and the Fourier fit to the multipliers. Note that there is a small increase, compared to the summer months, evident in these multiplers, thus giving a small increase to the MUF values during the winter period. In table 18 we show a comparison of the predictions of this intermediate algorithm, with seasonal and the sunspot number dependence in the M-factor and improved f_oF2, against those of MINIMUF-3.5 for the entire MOF data base. Again we see that, for the ranges of sunspot number and seasons contained in the MOF data base, the results of the above changes have not significantly altered the predictive capability of the original algorithm. We feel that with the seasonal dependence in the M-factor, we have a more versatile and accurate prediction program which reflects more of the dependencies we see in the MOF parameter. What's more, we also have a more accurate M-factor which can be used for other purposes within the PROPHET program.

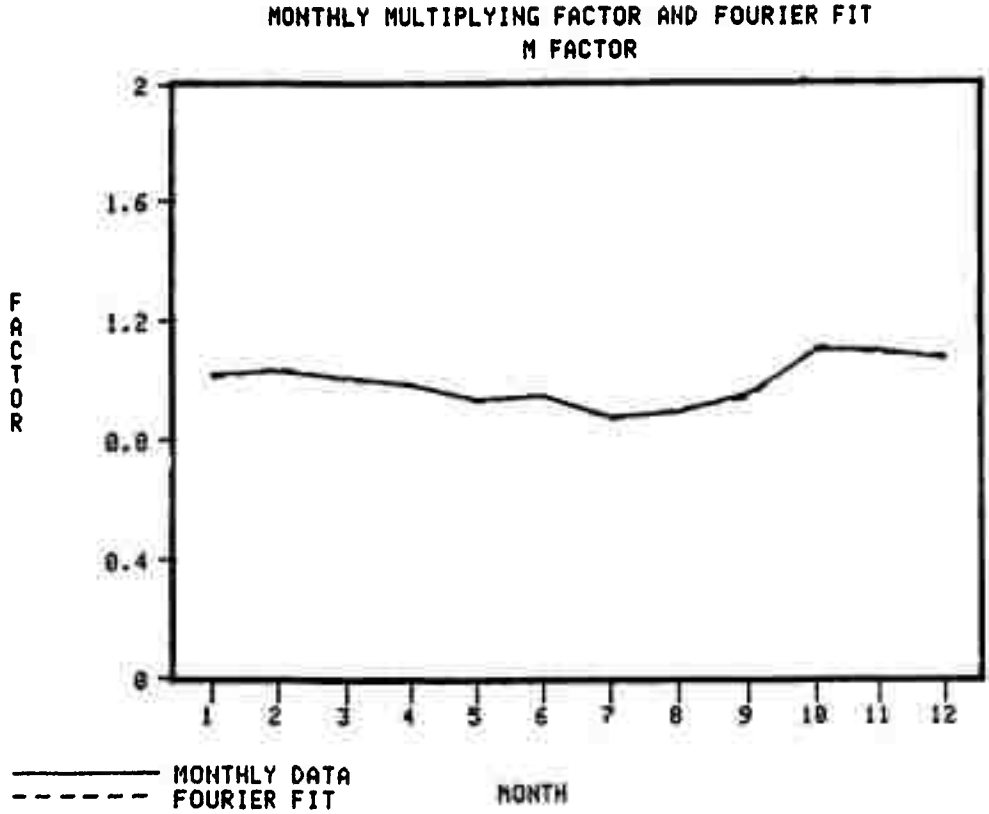

Figure 11. Monthly multiplying factor and Fourier fit to M-factor.

Table 18. Comparison of accuracy of MINIMUF-3.5 with intermediate version with seasonal dependence in M factor.

	Avg. Diff. (MHz)	RMS Diff. (MHz)	Corr. Coef.
MINIMUF-3.5	0.52	4.28	0.85
INTERMEDIATE	0.02	4.15	0.85

TIME DEPENDENCE

Finally, in order to have a diurnally varying M-factor which would reflect diurnal changes in the height of the F2 layer, we used the procedure described above to determine the time dependence of the M-factor.

In order to separate night from day in the paths that make up the MOF data base, it is of course necessary to use local time at the control points for this p: edure. Then, following the method of the other cases described

above, the data base is segmented into two parts, a seven hour "day" and a "night" part. A comparison of the predictions of the expression

$$A_4(\text{time}) * A_3 * A_2 \times M * f_oF2$$

with the day part of the data base led to a set of multipliers, A_4, which could be adequately fit with a linear function of local time.

$$\text{(DAY)} \quad A_4(\text{time}) = 1.11 - 0.01\, t_{local}. \tag{23}$$

For the night part of the procedure, some problems arose. The complication is that length of day (and night) differs greatly among the paths in the data base. This leads to a large amount of fluctuation in the day/night transition time multipliers. It proved necessary to introduce a new time coordinate, hours after sunset, in order to adequately fit the nighttime multipliers. This fit is accomplished with a 6^{th} order Fourier series,

$$\begin{aligned}\text{(NIGHT)} \quad A_4(\text{time}) = {} & 1.0195 \\ & -0.06\sin 2t - 0.037\cos 2t \\ & +0.018\sin 4t - 0.003\cos 4t \\ & +0.025\sin 65 + 0.018\cos 6t \\ & +0.007\sin 8t - 0.005\cos 8t \\ & +0.006\sin 10t + 0.017\cos 10t \\ & -0.009\sin 12t - 0.004\cos 12t\end{aligned}$$

where $t = t_{local} - t_{sunset}$.

Table 19 shows a final comparison of the new version of the MINIMUF algorithm, MINIMUF-85, to the prediction of MINIMUF-3.5 against the MOF data base. We note that there is a significant improvement in the overall bias of the model and a relatively small improvement in the RMS value and correlation coefficient. Overall, then, the predictive capability of the model has improved even over the relatively restricted set of data in the MOF data base.

Table 19. Statistical comparison of MINIMUF-3.5 and MINIMUF-85 predictions of MUF against MOF data base.

	Avg. Diff. (MHz)	RMS Diff. (MHz)	Corr. Coef.
MINIMUF-3.5	0.52	4.28	0.85
MINIMUF-85	0.16	4.19	0.86

POLAR REGION CRITICAL FREQUENCY MODEL

The physical basis for MINIMUF-3.5(I) is that all variations of the free electron density in the ionosphere are driven by solar zenith angle. MINIMUF is developed by starting with this assumption, developing a corresponding mathematical model, and then fitting associated free parameters to a set of oblique sounder data. It is not then surprising that MINIMUF-3.5(I) encounters problems when predicting MUFs at polar latitudes. This weakness is rooted in two factors. First, an important contribution to ionization at high latitudes is made by particle precipitation. Solar photon induced dissociation is not the only significant source of ionospheric free electrons. Second, data from radio circuits with control points in the polar regions are not included in the parameter fitting process in the development of MINIMUF. The control point with the highest geomagnetic latitude included in the determination of MINIMUF parameters is the midpoint between Toulouse, France, and Keflavik, Iceland. The value of the geomagnetic latitude at this control point is 58.1°N, which is too low to include the effects of particle precipitation.

The fact that high latitude ionospheric behavior differs sharply from that at lower latitudes has been recognized for some time. This sharp difference requires the introduction of new routines into MINIMUF specifically tailored to model the behavior of the MOFs at high latitudes. By merging the specific polar model with the model of lower latitude behavior already present in MINIMUF, significant improvements in the prediction of high latitude MOFs can be realized.

THE POLAR MODEL

The Chiu Polar Model (reference 23) for the F2 layer is developed as one component of a global phenomenological model of ionospheric electron density. The basis of the model is an analysis by Arima and Gonezawa (reference 24) of variations of electron density into seasonal, nonseasonal annual, and non-seasonal semiannual categories. The first version of a global model as developed by Ching and Chiu (reference 25) separates the global variations

into polar and nonpolar regimes. The polar and nonpolar functions describing each regime are welded together by means of a folding function.

The folding function determines when polar effects (particle precipitation) become dominant. It is a function of geomagnetic latitude and the sunspot number. The folding function makes a fairly abrupt transition from 0 to 1 between geomagnetic latitudes of 60° to 75°. Figure 12 is a plot of the folding function for a sunspot number of zero. When the folding function is near one, particle precipitation effects are supposed to dominate. When the folding function is near zero, solar zenith angle is the major factor in causing ionization. In between there exists a fairly narrow transition region where both sources of free electrons are significant.

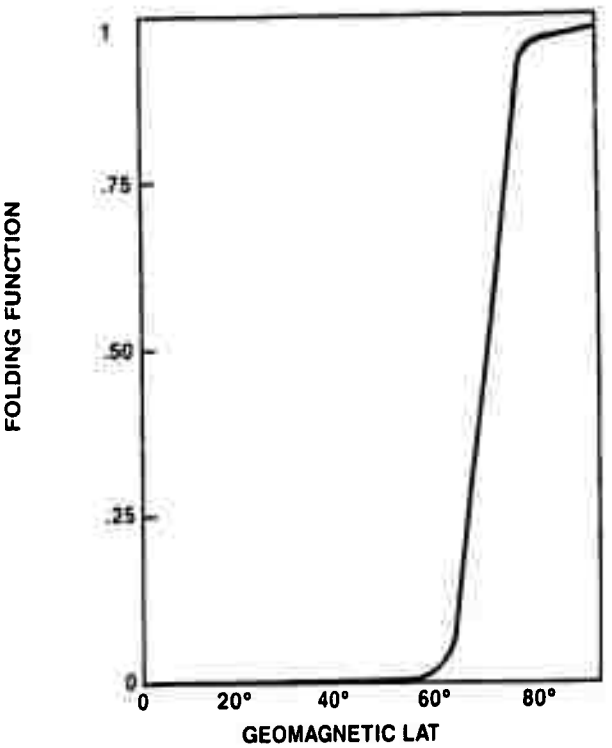

Figure 12. The folding function for monthly smoothed sunspot number = 0.

The Chiu Polar Model represents a refinement of the Ching-Chiu model. Both models include diurnal, seasonal, and nonseasonal annual dependence. The major improvement in the Chiu model involves generating distinct models for the North and South polar regions. This change recognizes some of the peculiar longitudinal dependencies which characterize the South polar region.

The Chiu Polar Model is based on vertical sounder data gathered from 18 different polar stations over an entire solar cycle. The model predicts large scale variations in ionospheric electron density and thus may be directly applied to the task of predicting f_oF2.

PROCEDURE FOR INCORPORATING THE CHIU POLAR MODEL INTO MINIMUF

The Chiu Polar Model predicts the value of electron density. It is the electron densities from the two regimes that the folding function is designed to properly combine. In folding a polar function into MINIMUF, it is necessary to isolate that portion of MINIMUF which calculates f_oF2 and then converts the value of f_oF2 into electron density. MINIMUF's f_oF2 is found by dividing its calculated value for MUF at each control point by the range-dependent portion of the M factor. Note that the G factors which are empiricaly latitude dependent adjustments to MINIMUF remain in the value to f_oF2 produced by MINIMUF. f_oF2 is then converted to electron density by use of the equation (25).

$$f_oF2\ (\text{MHz}) = 2.85\ N^{1/2}(\text{electrons/cm}^3)\ . \tag{25}$$

The electron density from MINIMUF is multiplied by a factor of one minus the folding function and then added to the product of the folding function and the Chiu Polar Model electron density as shown in equation (26).

$$N_{total} = (1-f)N_{MINIMUF} + f\ N_{polar}\ . \tag{26}$$

The total electron density at the control point is then converted back to an f_oF2 at the control point by using equation (25). Finally the MUF is obtained by multiplying the value of f_oF2 by the range-dependent portion of the M-factor.

PROCEDURES USED FOR TESTING MODEL ACCURACY AT POLAR LATITUDES

One of the difficulties associated with building a polar model is the lack of adequate oblique sounder data with control points located where polar

effects are important. The only type of data available from south polar regions is in the form of f_oF2 soundings, the study of which formed the basis of the Chiu Polar Model to begin with. Consequently, no study of the accuracy of the south polar model was attempted.

For checking the effect of introducing the north polar model into the calculation of the MUF, five different paths comprising a total of 52 path months of MOFs formed the data base. In these paths the value of the folding function at the control points varied from 0.20 to 1.0. For paths 1 and 2, monthly average MOFs are taken at four hour intervals when available. For paths 3, 4, and 5 the sampling rate of the monthly average rate is set at two hour intervals. The data on the specific paths sampled and the number of sample points are presented in table 20. The first two paths are additional paths not contained in the 39 path oblique sounder MOF data base. The MOFs are compared with the MUFs predicted by the following three algorithms: (1) MINIMUF-3.5(I); (2) MINIMUF-3.5(I) combined with the Chiu Polar Model via the folding function; and (3) MINIMUF-85 combined with the Chiu Polar Model via the folding function.

The errors are computed using the following formulas:

$$\text{Bias} \equiv \frac{1}{N} \sum_{i=1}^{N} \left(\text{MUF}_{\text{predicted } i} - \text{MOF}_{\text{observed } i} \right) \tag{27}$$

$$\text{RMS error} \equiv \left\{ \frac{1}{N} \sum_{i=1}^{N} \left(\text{MUF}_{\text{predicted } i} - \text{MOF}_{\text{observed } i} \right)^2 \right\}^{1/2} \tag{28}$$

where N = the number of sample points. A positive bias for the polar model error analysis means the model predicts high.

RESULTS OF COMPARISON OF POLAR MODEL

A review of table 20 makes clear the fact that MINIMUF-3.5(I) contains an inadequate model of the polar ionosphere. This inadequacy may be traceable to the fact that at polar latitudes, particle precipitation becomes the dominant

Table 20.
Prediction errors in various versions of MINIMUF over polar paths.

	Path	Latitude	Longitude	Length	Value of folding function @ control points	Sunspot Range	Number of data points in sample	Standard bias	MINIMUF 3.5i RMS error	MINIMUF with polar function folded in bias	MINIMUF with polar function folded in RMS error	MINIMUF with polar function folded in and MINIMUF-85 bias	MINIMUF with polar function folded in and MINIMUF-85 error
1.	Thule	76.4N	68.3W	3952	0.816	10	38	+2.27	2.92	+0.06	1.40	+2.66	3.17
	Pullman	46.7N	117.2W			18							
2.	Andoya	69.0N	15.4E	6571	0.621	10	44	-3.07	4.64	-3.71	4.55	-1.96	3.74
	Pullman	46.7N	117.2W		0.999 0.998	18							
3.	Winnepeg	49.9N	97.4W	2760	0.795	122	72	-12.72	13.38	-2.95	4.71	-1.40	3.86
	Reolute Bay	74.7N	94.9W			146							
4.	Ottawa	45.4N	75.9W	3387	0.806	52	132	-11.60	11.82	-1.51	3.66	+0.44	3.63
	Resolute Bay	74.7N	94.9W			88							
5.	Ottawa	45.4N	75.9W	5628	0.204	52	72	-13.14	14.30	-3.06	5.33	-2.57	5.59
	The Hague	52.1N	4.4E		0.294	141							
Sample Averages								-6.85	10.92	-2.23	3.93	-0.57	4.00

source of ionization while MINIMUF-3.5(I) hypothesizes that ionization is driven solely by solar zenith angle. It would then be expected that MINIMUF-3.5(I) would produce its largest errors during periods when particle precipitation effects are most significant.

This is the case illustrated in the data displays of figures 13 through 18. During polar winter, minimal direct solar illumination is available. MINIMUF-3.5(I) therefore predicts relatively low values for MUFs influenced by high latitude control points. However, particle precipitation effects continue unabated during polar winter. Thus MINIMUF-3.5(I) should consistently underestimate the wintertime MUFs along polar paths to a greater degree than during other seasons. As shown in figure 13, the winter errors are almost double the error produced during the summer. Particle precipitation effect also increase with the sunspot activity. Therefore, the error in MINIMUF 3.5(I) should be positively correlated with the sunspot number. This hypothesis is confirmed by the results displayed in figure 16. The error in MINIMUF-3.5(I) rises dramatically as sunspot number increases above 50.

Figures 14, 15, 17, and 18 illustrate that both MINIMUF-3.5(I) enhanced by the Chiu Polar Model and MINIMUF-85 enhanced by the Chiu Polar Model also produce their largest errors in winter and at a high sunspot number. Part of this error may be traced to the fact that folding function for all sampled paths includes some fraction of MINIMUF-3.5(I) which results in folding in a fractional amount of the error from MINIMUF-3.5(I). Figure 18 indicates that the improved M factor present in MINIMUF-85 improves the performance of MUF prediction with variances in the sunspot number.

MINIMUF-3.5(I)'s estimates of MUF are an overall average of about 7 MHz low over the polar paths sampled. This underestimate is improved to about 2 MHz by adding the Chiu Polar Model. By enhancing MINIMUF-85 with the Polar Model, the overall average bias is reduced to about 0.5 MHz. These results again support the contention that the particle precipitation effects ignored in MINIMUF-3.5(I) are significant.

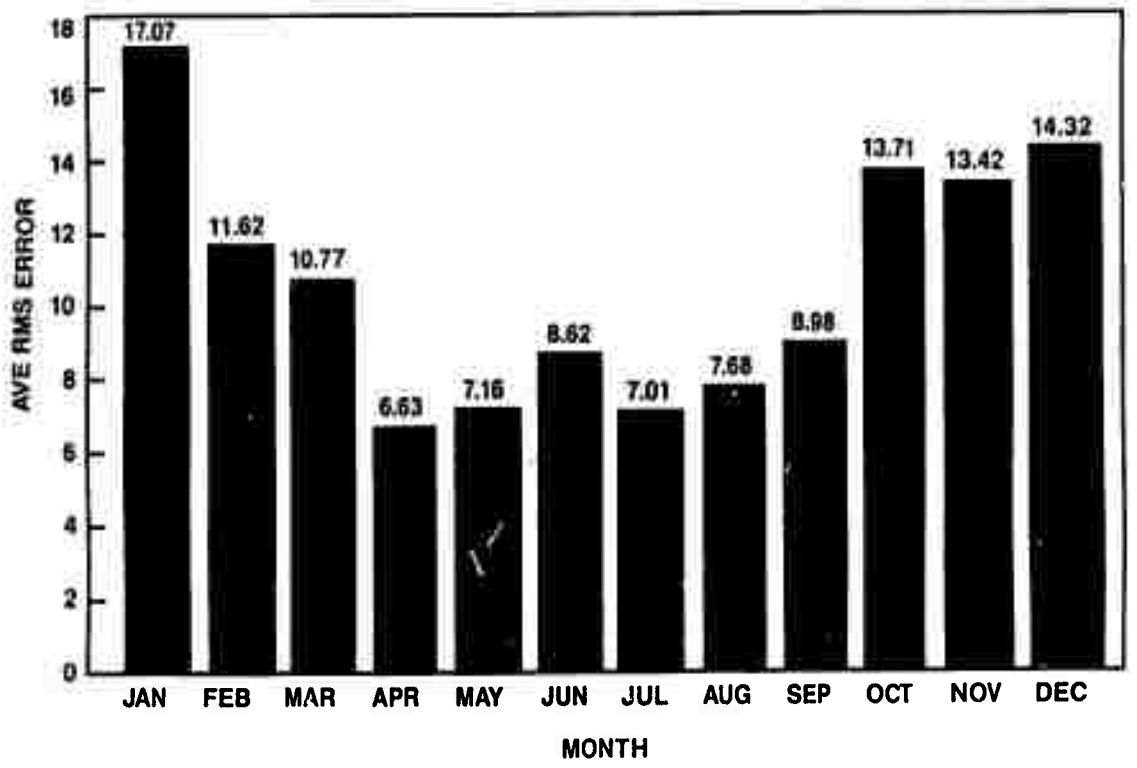

Figure 13. MINIMUF-3.5(I) rms error as a function of month for five selected polar paths.

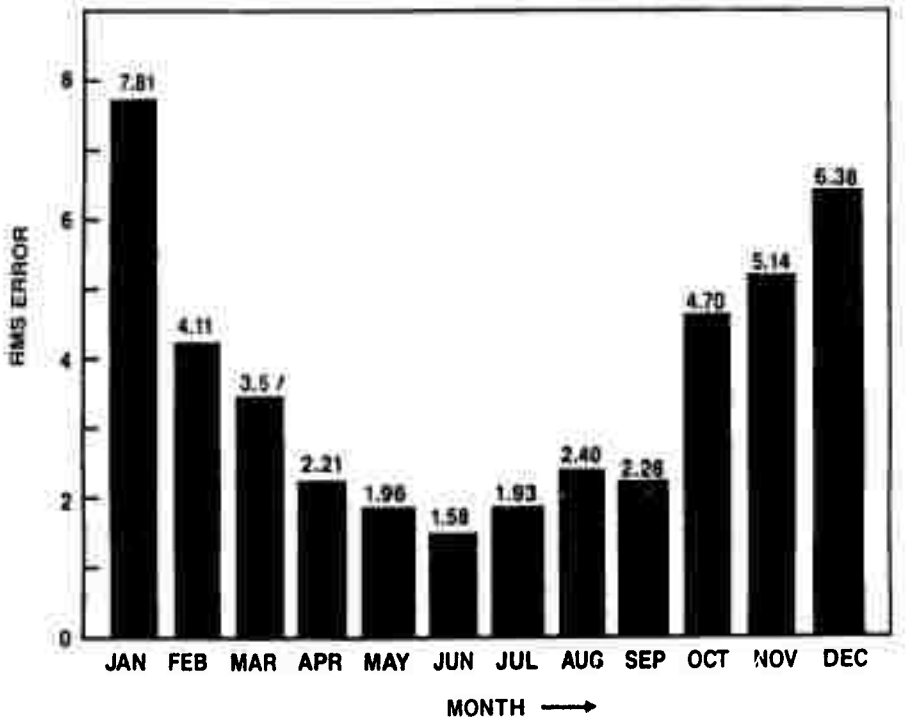

Figure 14. MINIMUF-3.5(I) folded with polar model rms error as a function of month for five selected polar paths.

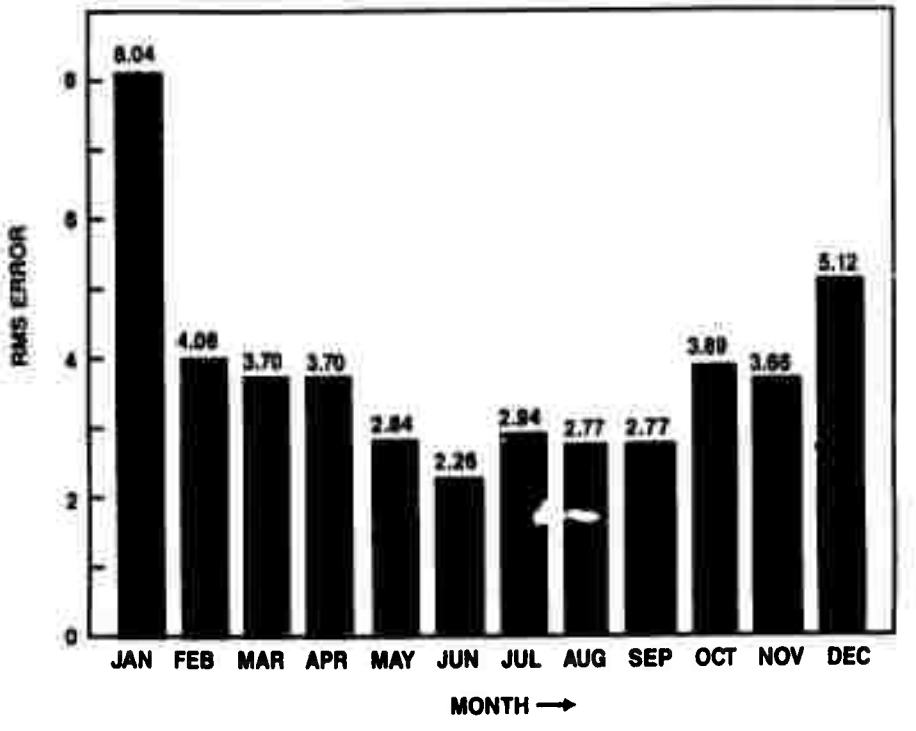

Figure 15. MINIMUF-85 folded with polar model rms error as a function of month for five selected polar paths.

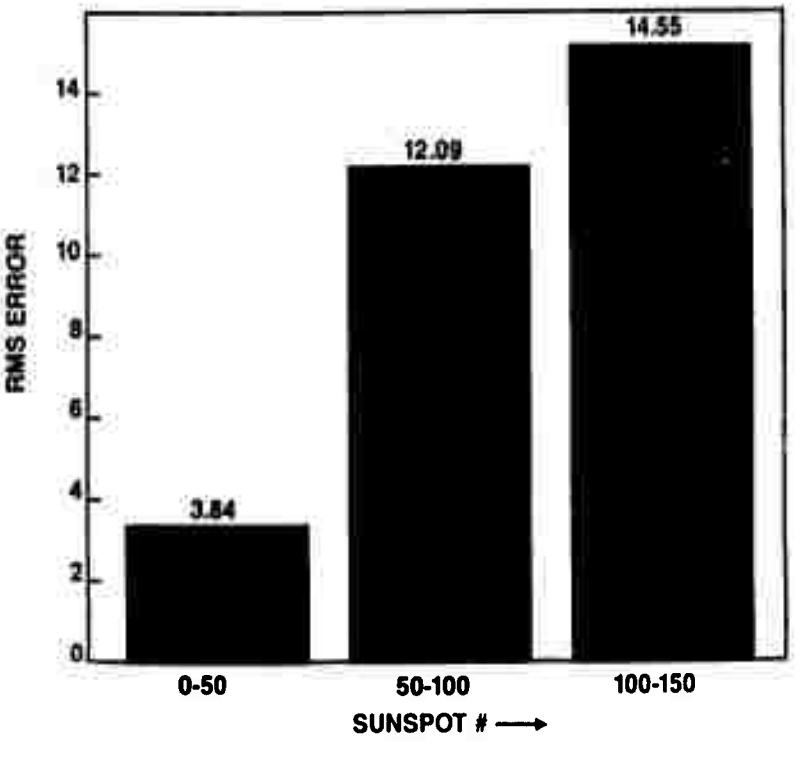

Figure 16. MINIMUF-3.5(I) rms error as a function of sunspot number for five selected polar paths.

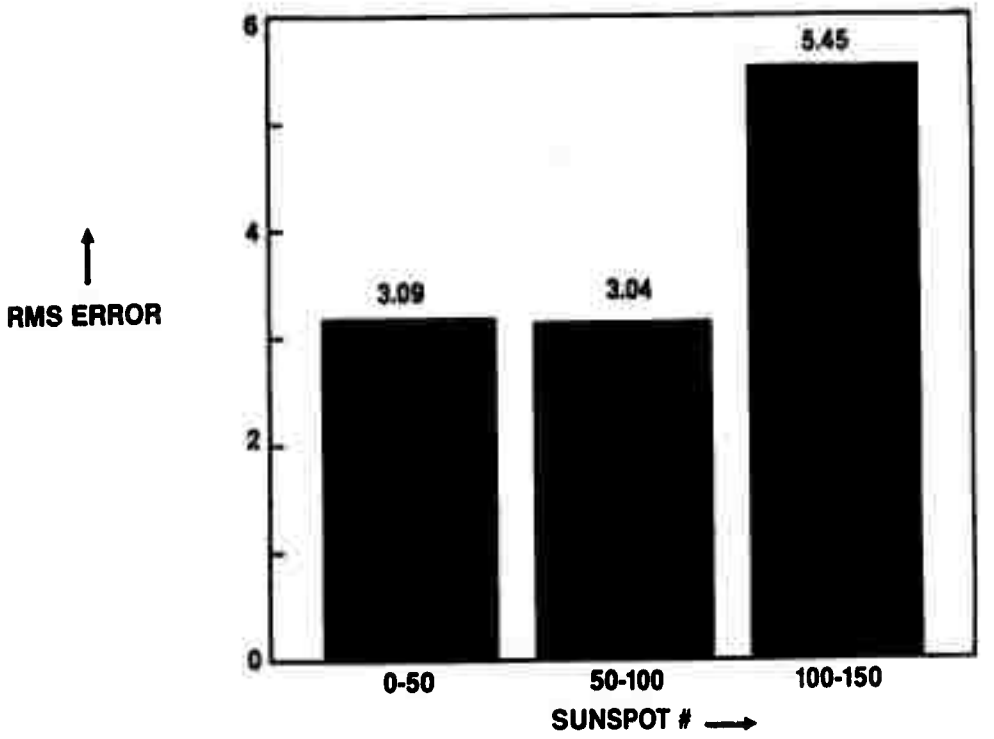

Figure 17. MINIMUF-3.5(I) with polar model folded in rms error as a function of sunspot number for five selected polar paths.

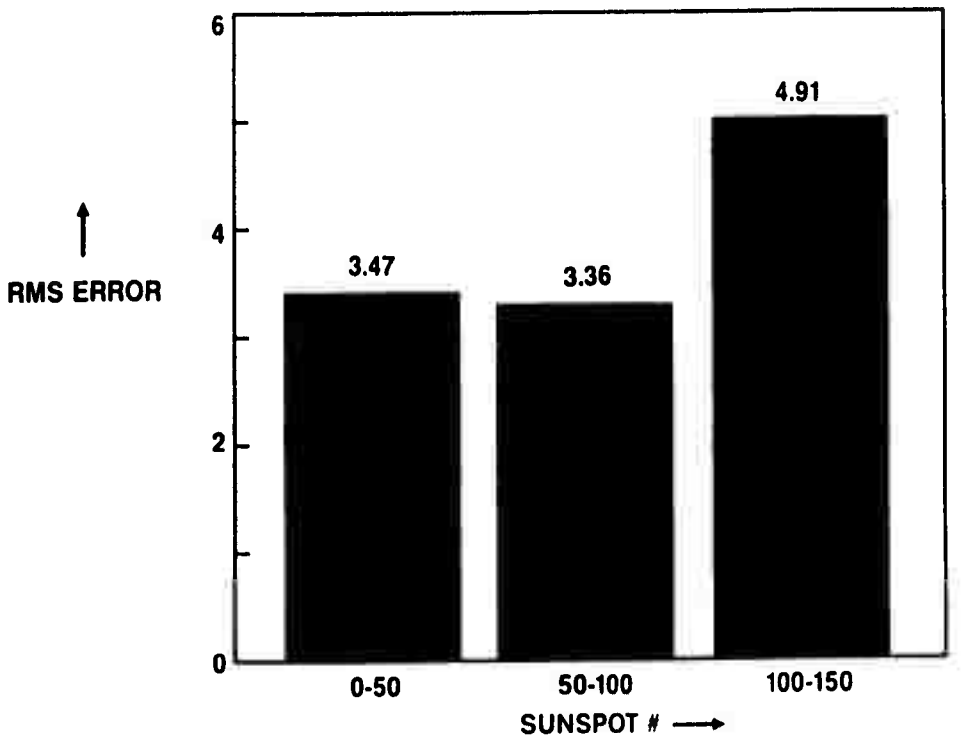

Figure 18. MINIMUF-85 with polar model folded in rms error as a function of sunspot number for five selected polar paths.

Although the size of the polar data sample was small, the results were unambiguous. At least over the north polar paths tested, MINIMUF-3.5(I) makes an average rms error in MUF prediction of 10.92 MHz. While in the polar enhanced versions of MINIMUF, the RMS error is reduced to about 4.0 MHz. It is clear that a considerable improvement in predicting MUF's is attained by including a polar model in the MINIMUF prediction program.

DISCUSSION

This report has presented the development of MINIMUF-85, a simple semi-empirical algorithm for predicting the MUF. It was developed to predict accurate maximum useable frequencies (MUFs) under conditions of anomalously high sunspot numbers, to predict f_oF2 values suitable for ray-tracing applications, and to predict M factor values useable for determining the mirror height of reflection for oblique incidence propagation, and to improve its accuracy for paths into or crossing the polar regions. It includes sunspot number dependence in both the f_oF2 and the M factor calculations. The M factor portion of the algorithm also is modified to include seasonal and diurnal variations.

This section of the report discusses several topics important in the application of MINIMUF-85 including the relationship between the sunspot number and 10.7-cm solar flux, the choice of solar indices for forecasting, the determination of take-off angle from the M-factor, the role of MINIMUF in sounder updating of schemes for determining a pseudo sunspot number, and finally, possible future improvements.

RELATIONSHIP BETWEEN SUNSPOT NUMBER AND 10.7-CM SOLAR FLUX

It has been common practice to use 10.7-cm solar flux as a measure of solar variation in MINIMUF applications. This has been accomplished using the relationship developed by Steward and Leftin (reference 26) between the Ottawa 10.7-cm solar radio noise flux and the Zurich smoothed sunspot number. This relationship is given by

$$\Phi_{12} = 63.7 + 0.728R_{12} + 8.9 \times 10^{-4} R_{12}^{2} \qquad (29)$$

where Φ is the 12-month running mean, Ottawa 10.7-cm solar radio noise flux and R_{12} is the 12-month running mean Zurich sunspot number. It was determined using data from November 1947 to November 1968. They found no systematic differences in the relationship for the rising and declining phases of the solar cycles investigated.

For the years 1947-1966, Joachim (reference 27) presents a relationship between R_{12} and Φ_m, the monthly mean of the daily values of the 10.7-cm solar radio flux at Ottawa. It is given by the expression

$$\Phi_m = R_{12} + 46 + 23e^{-0.05R_{12}} . \tag{30}$$

At values of R_{12} between 10 and 80, this expression gives lower values for Φ_m than equation (29) does for Φ_{12}.

The definition of R_{12} is

$$R_{12} = \frac{1}{12}\left[\sum_{n-5}^{n+5} R_k + \frac{1}{2}\left(R_{n+6} + R_{n-6}\right)\right] \tag{31}$$

in which R_k is the mean of the daily sunspot numbers for a single month k and R_{12} is the smoothed index for the month represented by k = n.

For the years 1947-1963, Gladden (reference 28) presents a relationship between Rz_m, the monthly mean Zurich relative sunspot number, and Φ, the monthly mean daily value of the 10.7-cm solar radio flux at Ottawa. Using all of the data, the form of the relation was:

$$\Phi_m = 0.91\left(Rz_m\right) + 58.8 \tag{32}$$

which had a correlation coefficient of 0.98 and a rms deviation of 11.4.

Since the solar radio emissions in the range of wavelengths from 3-cm to 30-cm show similar variations with a so-called 27-day cycle, Nicolet (reference 29) determined the relationship between the 27-day average value of the Zurich relative sunspot number and the solar radio flux at 10-cm from 1951 until 1962. The results show that, for $R_{27} > 50$, there is a linear relationship between these quantities which, with an error of ±10%, takes into account the variations of the radio flux for values greater than $\Phi_{27} = 100$ units, i.e.,

$$\Phi_{27} = 50 + 0.967\ R_{27} . \tag{33}$$

But for $\Phi_{27} < 100$ or $R_{27} < 50$, the linear variation is given by

$$\Phi_{27} = 68.0 + 0.607\ R_{27}\ . \qquad (34)$$

Thus, the close association of the 10-cm radiation with sunspots cannot be expressed during a whole cycle with the same linear relationship. Figure 19 compares the variation of the monthly mean and 27-day mean Φ provided by equations 32, 33, and 34 with the monthly mean and 27-day mean Zurich sunspot number. The data points in the figure are for the period February 1947 - December 1962. The nonlinear curve is that provided by equations 33 and 34. Note that the relationship provided by equations 33 and 34 appears to give a better fit than that given by equation 32. At sunspot zero equations 30, 32, and 34 should give about the same result for the solar flux as there should be very little difference among R_{12}, Rz_m, and R_{27}. In fact, only equations 30 and 34 give comparable results. Hence, equations 33 and 34 appear to provide a more accurate estimate of the mean monthly solar 10.7-cm flux.

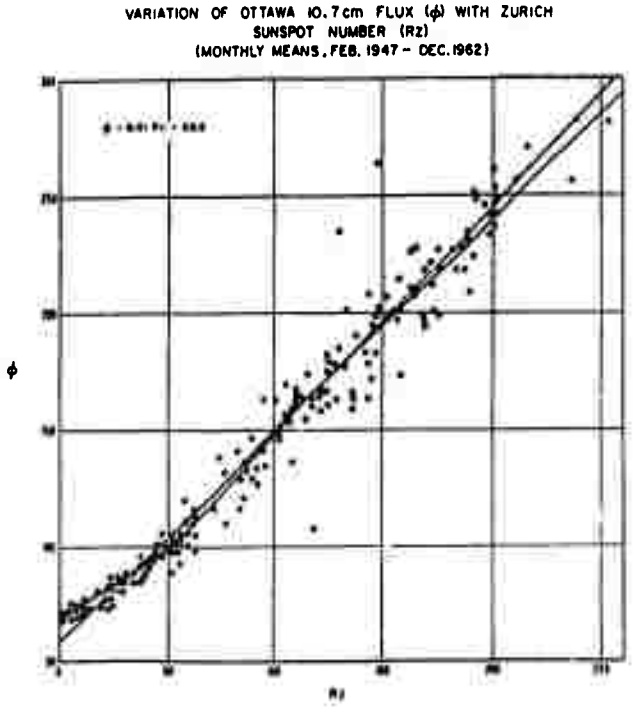

Figure 19. Variation of monthly mean and 27-day mean 10.7-cm flux with monthly mean and 27-day mean Zurich sunspot number.

CHOICE OF SOLAR INDEX FOR FORECASTING

MINIMUF-85, like MINIMUF-3.5 before it, will be used to estimate a near real-time value of MUF. Immediately there arises the question of which solar

index to use. In MINIMUF-85 two indices are used. In the polar model R_{12}, the smoothed Zurich sunspot number is used. In the rest of the model Rz_m, the monthly mean value is used. Evaluation of equation 32 for Φ using R_{12} and equations 33 and 34 for Φ using R_{zm} results in an insignificant difference in Φ for either R going from 0 to 300. The reason for this is that the dispersion of the monthly mean solar flux Φ is large enough to cause either expression to be valid (i.e., if either expression is used to estimate the sunspot number from Φ, either will provide equally valid results). However, if values for both R_{12} and Rz_m are available, they should be used in their respective parts of MINIMUF-85.

The dispersion of the daily values of 10.7-cm solar flux is larger than the dispersion in the 27-day mean values. Figure 20 from reference 29 shows a plot of the daily values for 1958 with a variation reaching ±20 percent from equation 33. The figure indicates how such a solar index may lead to important errors in deducing any empirical correlation with ionospheric parameters. Gladden (reference 28), in the determination of a relationship between the daily values of the solar flux Φ and Rz, found that the rms deviation in the resulting expression for Φ_d was 32.6, whereas, the rms deviation for this expression for the monthly mean Φ_m was only 11.4. The resulting expression given was

$$\Phi_d = 0.84\ Rz_d + 65.1\ . \qquad (35)$$

As PROPHET uses equation 29 to determine the sunspot number from the daily 10.7-cm flux, the results of using these two expressions is compared in table 21. Note that the use of equation 29 with daily flux values always produces lower sunspot numbers than does equation 35.

To further examine the choice of solar indices to be used with MINIMUF-85, we compared the accuracy of using the various choices with measured oblique incidence sounder data taken during Solid Shield exercises conducted by the Naval Research Laboratory which took place between 3 May and 20 May 1981, on the eastern seaboard of the United States (reference 31). The locations of the sounded paths are indicated in figure 21.

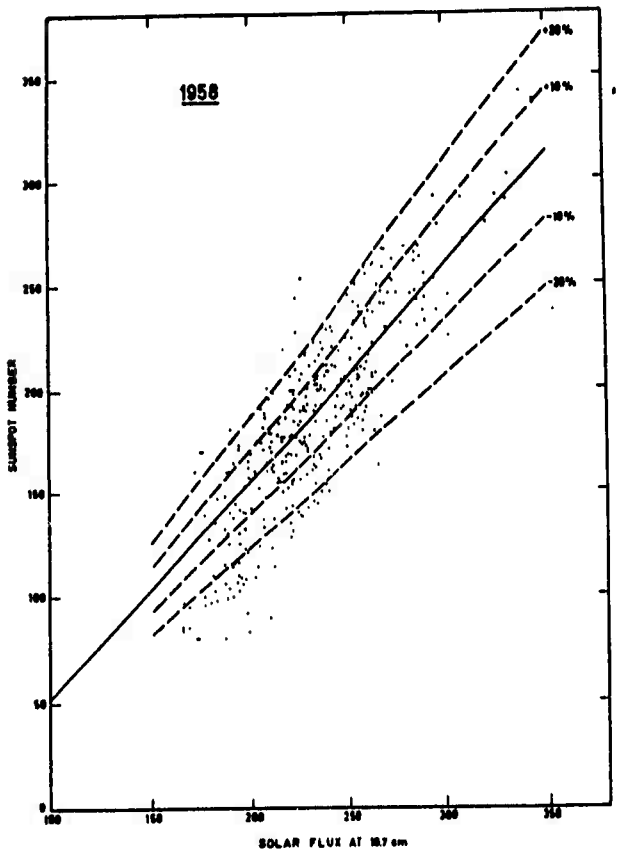

Figure 20. Dispersion of daily values of 10.7-cm solar flux about 27-day mean values for 1958.

Table 21. Comparison of two expressions relating sunspot number R and 10.7-cm daily solar flux.

Φ_{12}	Φ_d	R
63.7	65.1	0
100.1	107.1	50
145.4	149.0	100
192.9	191.1	150
244.9	233.1	200
301.3	275.0	250
362.2	317.0	300

Figure 21. Geometry of the oblique sounder circuits employed by NRL during Solid Shield plotted on a great circle map.

Table 22 and figures 22-25 show the nature of the solar and geophysical conditions during the Solid Shield exercises. Table 22 shows the solar activity background for each of the days during May 1981. It gives the international sunspot number (the continuation of the Zurich sunspot number), the 3- and 5-day running averages of this number, the sunspot number Rz_d derived from the daily 10.7-cm solar flux using equation 35, the sunspot number R_{12} derived from the daily 10.7-cm solar flux using equation 29, the daily 10.7-cm solar flux Φ_d, and the 3- and 5-day running averages of 10.7-cm solar flux. Figure 22 shows the daily variation of the five sunspot numbers given in table 22. Note first the larger variation in R_I, the international sunspot number than in either the running daily averages and those produced by the 10.7-cm solar flux. Second, note that values produced from the 10.7-cm solar flux are higher, although within the published deviations of the relationships, than R_I. Figure 23 shows the daily 10.7-cm solar flux variation given in table 22. Note that the 3-day running average appears between the other curves and only lags the daily curve by 3 days. Figure 24 is a plot of solar flare activity for the month of May 1981. The height of the individual bars in figure 24 represents the relative height of the peak of each solar flare in energy out-

Table 22. Solar activity background for Solid Shield, May 1981.

Day of Month	SUNSPOT NUMBERS	3 and 5 day averages				10.7-cm SOLAR FLUX	3 and 5 day averages		Comment
	R_I			Rz_d	R_{12}	Φ_d			
1	112	103	91	143	142	185.0	177.3	179.9	
2	133	112	103	149	147	190.4	182.7	179.6	
3	156	134	120	164	160	203.0	192.8	185.4	burst
4	152	147	129	181	174	217.5	203.6	193.7	
5	162	157	143	200	189	233.3	217.9	205.8	
6	178	164	156	193	183	227.1	226.0	214.3	
7	171	170	164	196	186	229.8	230.0	222.1	
8	177	175	168	182	175	218.3	225.1	225.2	burst
9	158	169	169	178	171	214.5	220.9	224.6	
10	148	161	166	177	170	213.4	215.4	220.6	burst
11	169	158	165	189	180	223.6	217.2	219.9	burst
12	183	167	167	183	175	218.8	218.6	217.7	
13	149	167	161	181	173	216.7	219.7	217.4	
14	140	157	158	193	184	227.5	221.0	220.0	
15	141	143	156	183	176	219.1	221.1	221.1	
16	127	136	148	177	171	214.0	220.2	219.2	
17	124	131	136	164	160	202.9	212.0	216.0	
18	119	123	130	149	147	189.8	202.2	210.7	
19	100	114	122	139	139	182.2	191.6	201.6	burst
20	77	99	109	132	133	175.8	182.6	192.9	
21	99	92	104	132	133	176.0	178.0	185.3	
22	106	94	100	119	121	165.2	172.3	177.8	burst
23	93	99	95	108	111	155.6	165.6	171.0	
24	96	98	94	120	122	165.5	162.1	167.6	
25	93	94	97	128	129	172.7	164.6	67.0	
26	105	98	99	124	126	169.2	169.1	165.6	
27	79	92	93	128	129	172.3	171.4	167.1	
28	93	92	93	133	133	176.5	172.7	171.2	
29	92	88	92	120	122	166.0	171.6	171.3	
30	83	89	90	113	116	160.1	167.5	168.8	burst
31	92	89	88	103	107	151.8	159.3	165.3	
MEAN	126.0	124.3	126.0	154	151	194.6	195.2	195.7	

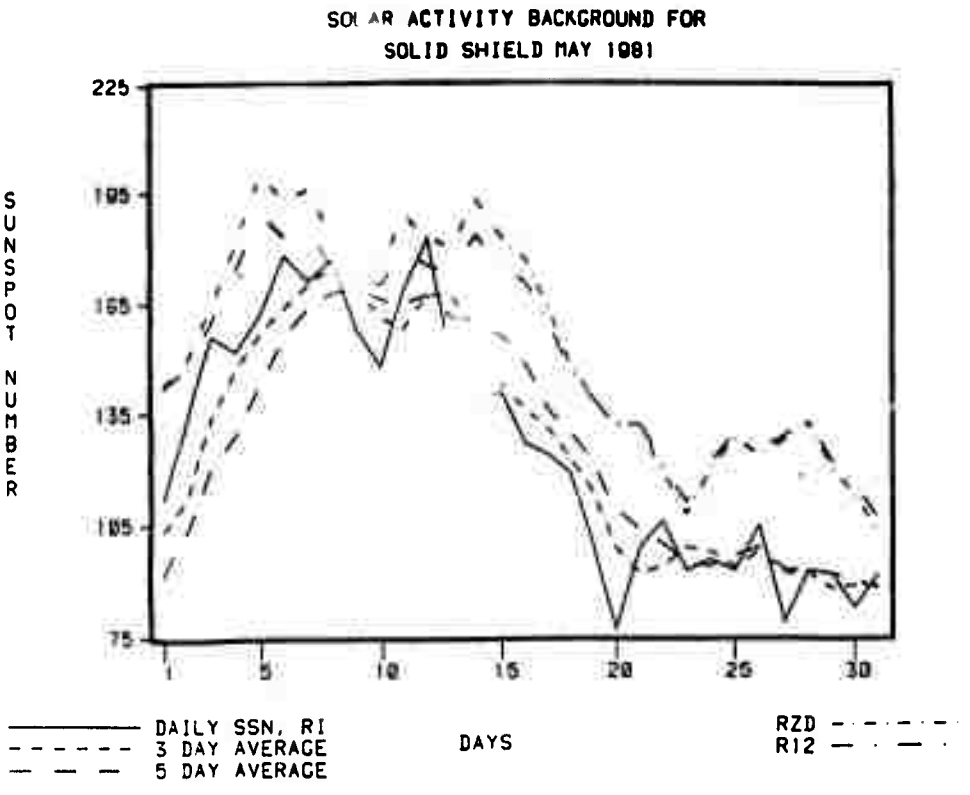

Figure 22. Sunspot variations during May 1981.

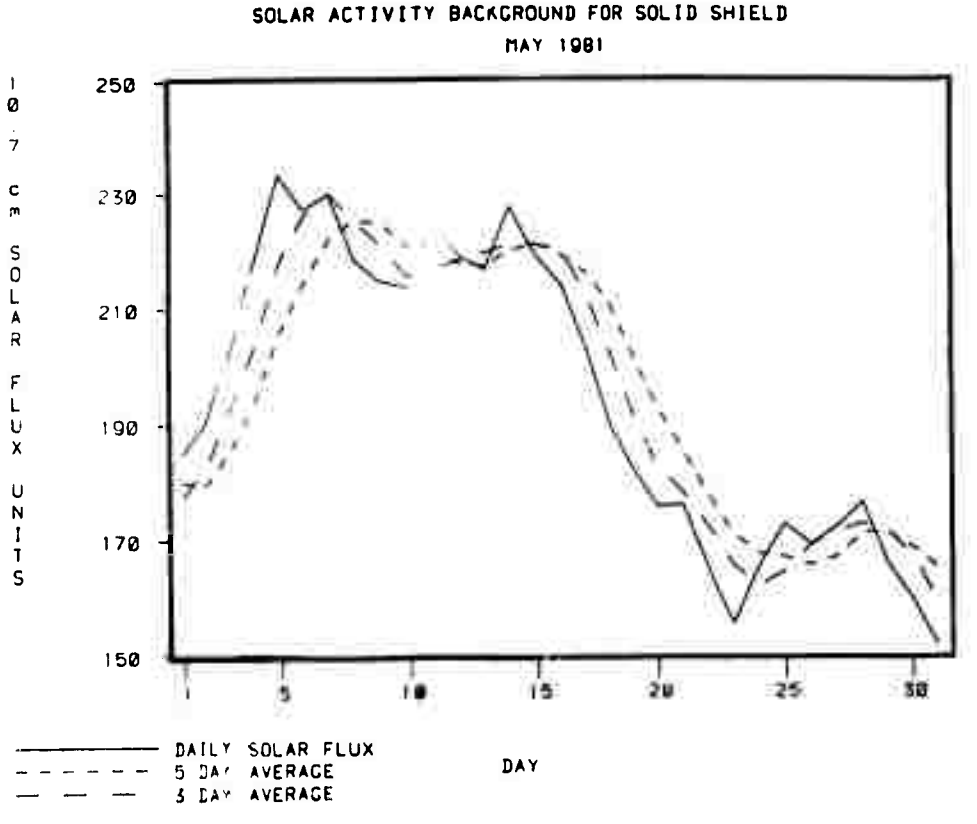

Figure 23 10.7 cm solar flux variations during May 1981.

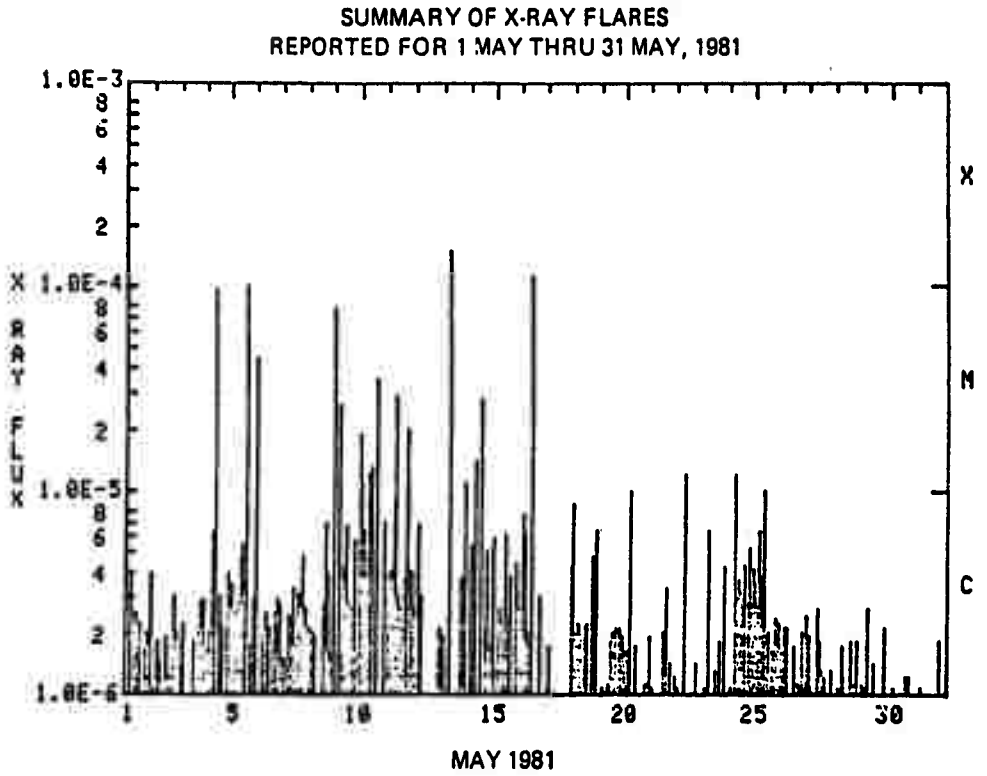

Figure 24. Solar X-ray flare activity for May 1981.

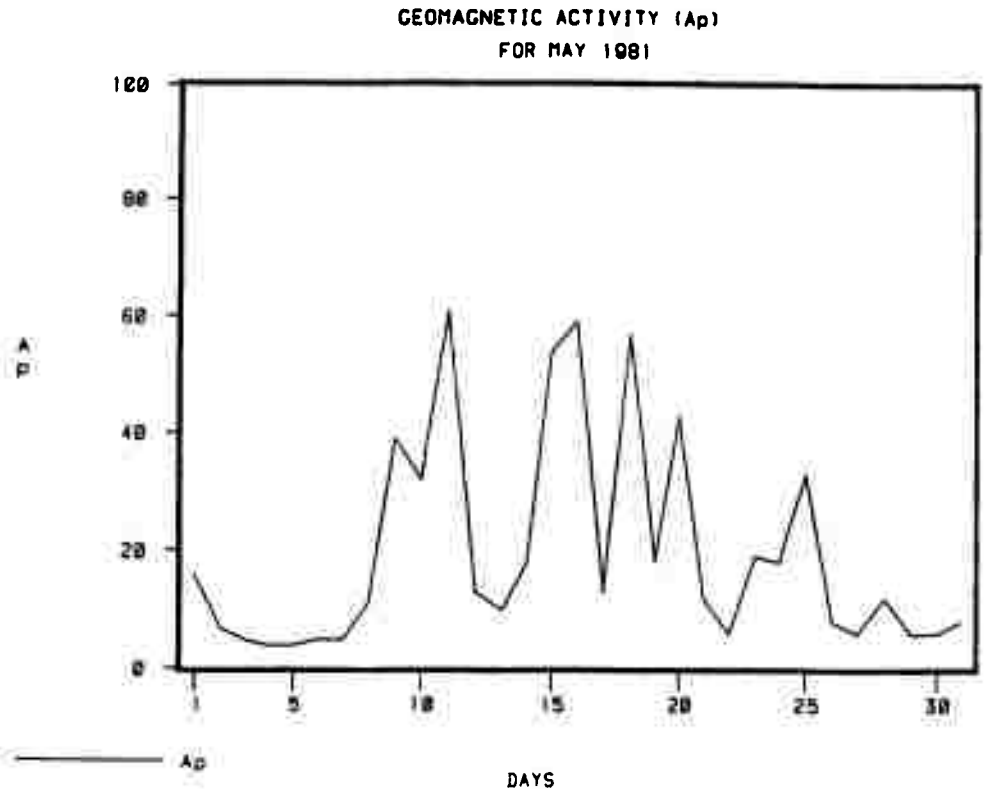

Figure 25. Magnetic activity for May 1981 as represented by the index A_p.

put during the period. The solar activity was high during the full term of the experimental period between 3 and 19 May with the period of highest activity between 7 and 14 May 1981. During the month of May 1981 the earth's magnetic field was also very active. This is shown in figure 25. This activity is indicated by the index A_p. Note that until 9 May 1981 the magnetic activity was very low, but after that date there was a considerable increase.

To limit the amount of comparison against data to an amount handable (i.e., the number of comparisons are proportional to the number of indices being considered) data for 5 and 7 May 1981, Hurlbert-Norfolk path, were used to determine the accuracy of the indices. These two days were chosen because they occur during a period of low geomagnetic activity. Figures 26-29 show the predicted MUF as a function of solar index for each of the two days. Figures 26 and 27 show the effects of the five sunspot indices for 5 May 1981 and 7 May 1981, respectively. On both days the sunspot number Rz produced from equation 35 using daily 10.7-cm solar flux Φ_d gave the highest MUF; the 5-day running average sunspot number gave the lowest values. Figures 28 and 29 show the effect of using different 10.7-cm solar flux values for 5 May 1981, and 7 May 1981, respectively. In each case the largest values were produced by the daily 10.7-cm solar flux Φ_d. Table 23 gives the bias and rms error for each solar index for the two days during the Solid Shield exercise on the Hurlbert-Norfolk path. A positive bias indicates that the model predicts high. The data in the table indicate that the sunspot number R_{zd} produced from the daily solar flux Φ_d using equation 35 has the lowest bias and lowest rms error for the sample examined. The results need to be confirmed using data from other paths and other exercises.

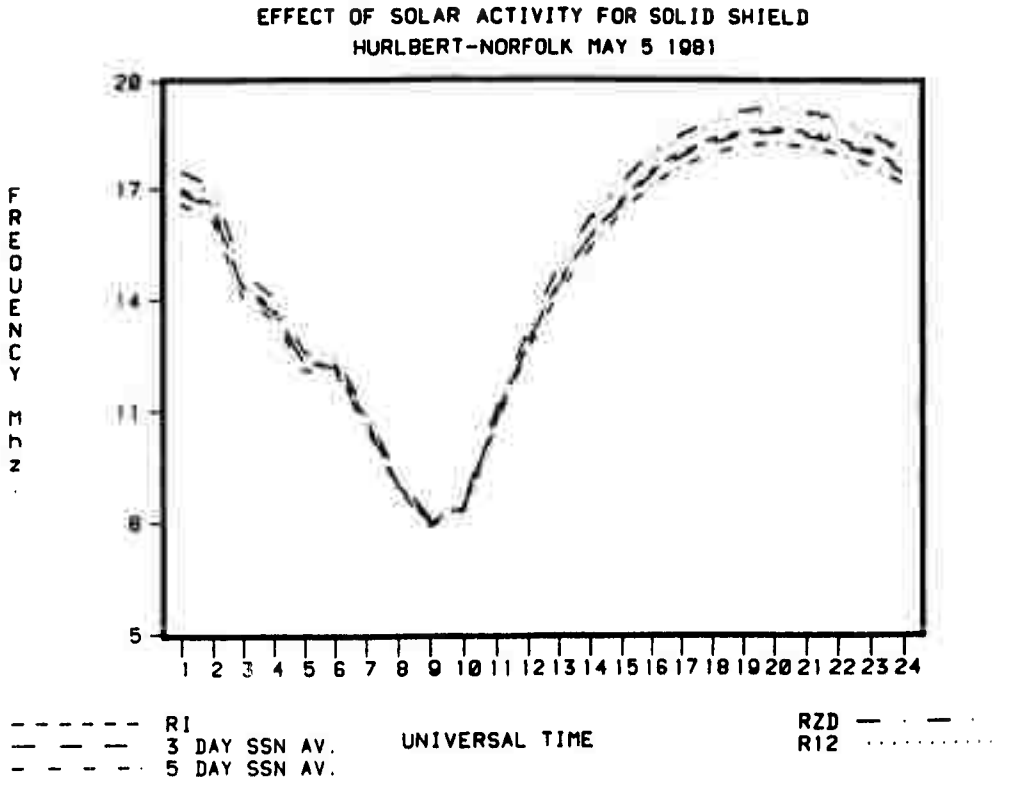

Figure 26. Effect of sunspot number index for Solid Shield, Hurlbert-Norfolk, 5 May 1981.

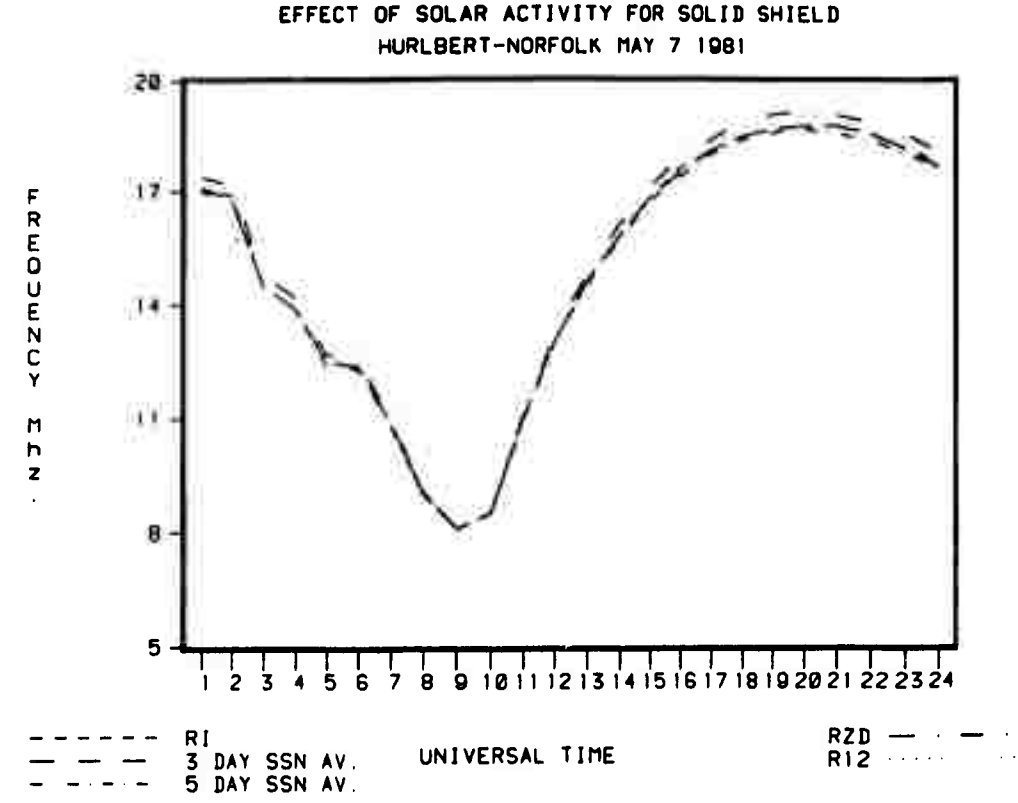

Figure 27. Effect of sunspot number index for Solid Shield, Hurlbert-Norfolk, 7 May 1981.

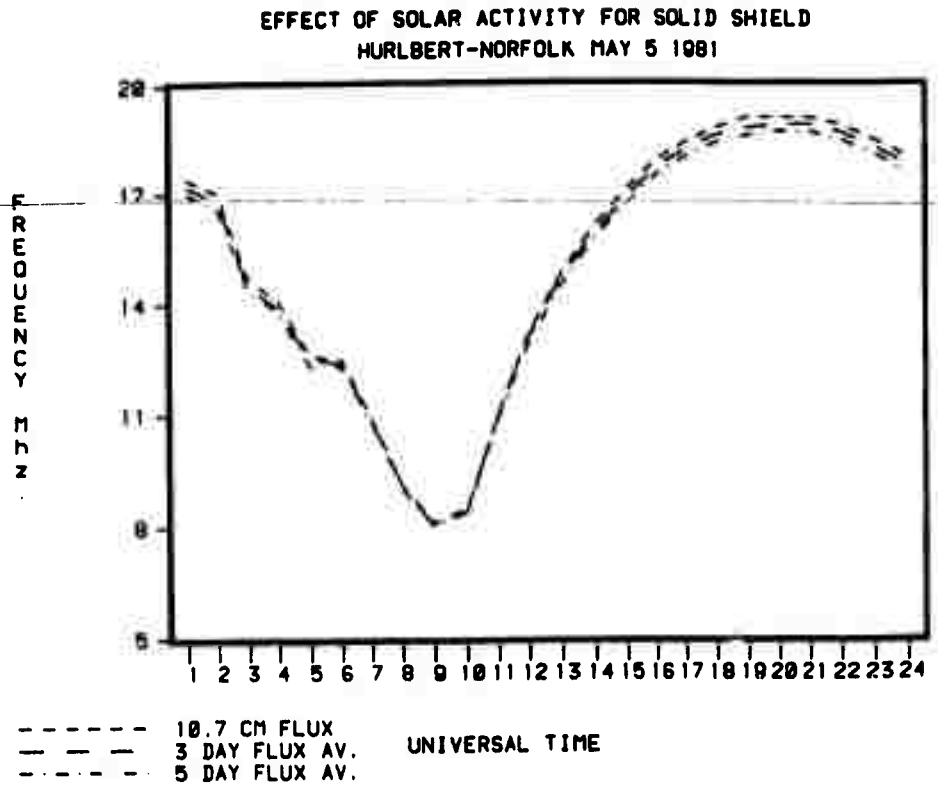

Figure 28. Effect of 10.7-cm solar flux index for Solid Shield, Hurlbert-Norfolk, 5 May 1978.

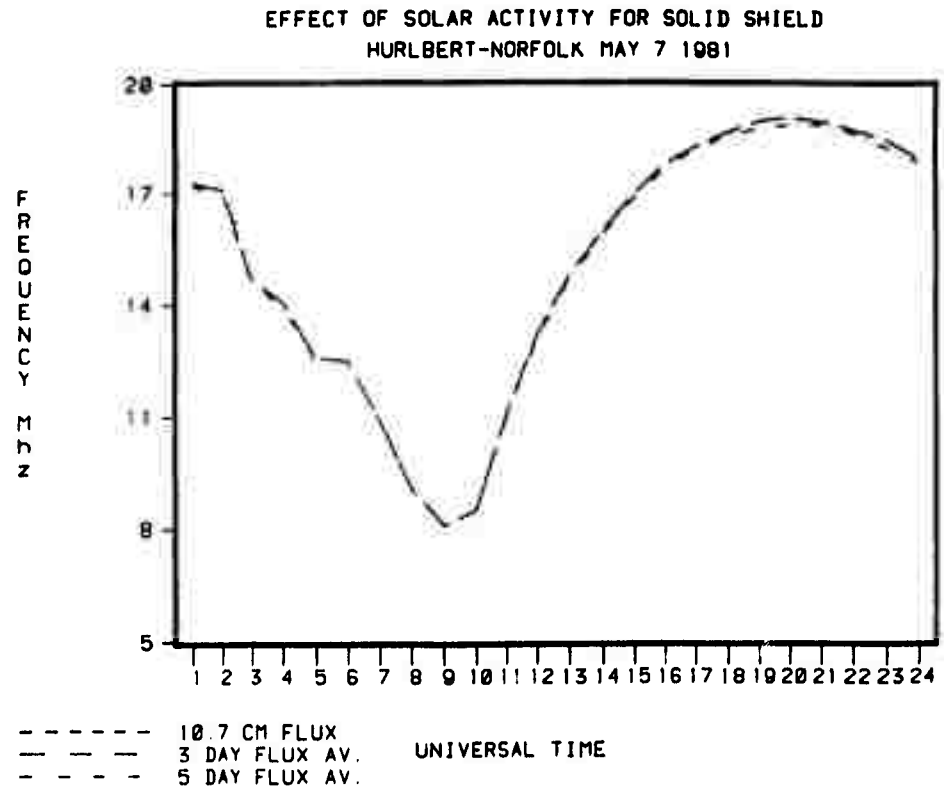

Figure 29. Effect of 10.7-cm solar flux index for Solid Shield, Hurlbert-Norfolk, 7 May 1981.

Table 23. Bias and rms error for each solar index, Solid Shield, Hurlbert-Norfolk.

Index Value	5 May 1981 Bias	5 May 1981 rms error	7 May 1981 Bias	7 May 1981 rms error
R_I	-2.71	3.59	-2.83	3.70
3-day average	-2.78	3.63	-2.84	3.71
5-day average	-3.01	3.78	-2.92	3.76
Rz_d	-2.32	3.37	-2.58	3.55
R_{12}	-2.40	3.42	-2.67	3.60
3-day 10.7 cm solar flux	-2.55	3.49	-2.67	3.60
5-day 10.7 cm solar flux	-2.70	3.58	-2.76	3.65

SOUNDER UPDATING

The day-to-day variation of the MOF and its corresponding predicted MUF about the monthly median MOF and MUF, respectively, are often considerable and may exceed the combined seasonal and solar cycle variation. The monthly median of MUF reflects the main effects of an undisturbed ionosphere. The daily-hourly MUF deviates from the median by 2- to 8-MHz on quiet days and by much larger values during magnetic storms. The causes for these deviations are complicated and cannot be compensated for by simple rules of thumb.

The purpose of sounder updating is to use an ionospheric oblique incidence sounder to provide an input that could be used to compensate for the more systematic part of the deviation of MUF, particularly the daily-hourly variation. The approach used is to obtain a maximum observed frequency (MOF) on a reference path, and use this information to determine an effective or pseudo-sunspot number (references 31, 32, 33, 34, 35, and 36). This pseudo-sunspot number is then used in MINIMUF rather than a daily solar index to predict the MUF on other paths in the same region.

Figure 30 is a drawing which illustrates the approach the Naval Research Laboratory employs to perform model update in support of frequency management. The top illustration in the figure indicates the nature of the diurnal variation of both the measured MOF and the predicted MUF over a given link. There

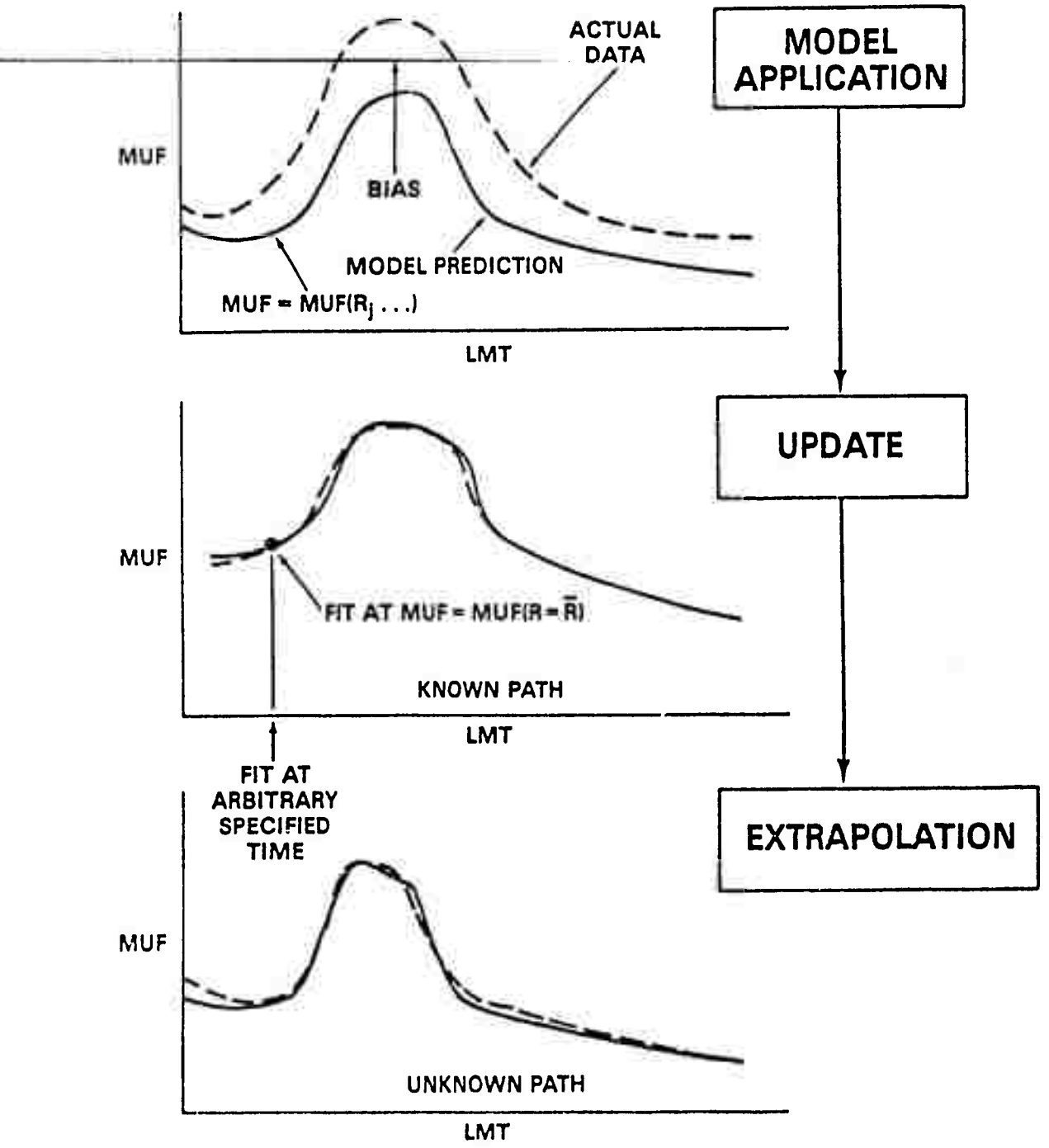

Figure 30. The NRL approach to sounder updating.

is a bias in the prediction due to day-to-day variability. The update process is shown in the middle portion of the figure. A measurement of the MOF is obtained from an oblique sounding over a known circuit and input into the update algorithm. The algorithm then finds the sunspot number that would have produced the input MOF for the specific time of the measurement over the path. This is accomplished by varying the sunspot number from an initial value of zero until the condition that MOF = MUF is satisfied. The success of the fit is tested by determining the rms error over a 24-hour period between the predicted MUFs using the pseudo-sunspot number and the measured MOFs on the same path. In tactical scenarios, a pseudo-sunspot number which was derived from the update procedure is then used to compute MUFs on other unknown paths.

The model update is deemed successful if the rms error of the experimental paths are significantly lower than that yielded by employing the non-updated model. In practice it has been found that updating intervals of three hours is sufficient and that rms errors of 1 MHz in some cases will be obtained. However, values of 2.5 MHz are more common.

To compare the sounder updating technique with that of the non-updated MINIMUF-85 results, the same two days of Solid Shield were run using a pseudo-sunspot number generated for 2200 UT (local noon) for 5 and 7 May 1981 as used in the previous section. The results are presented in table 24. In both cases the pseudo-sunspot number was 250. A slight improvement was obtained over that of non-updating. The sounder updating technique is limited at these high sunspot numbers because of the sunspot number limitation built into MINIMUF-85.

Table 24. Bias and rms error using sounder updated sunspot numbers, Solid Shield, Hurlbert-Norfolk.

	5 May 1981	7 May 1981
pseudo-sunspot number	250	250
bias	-2.16 MHz	-2.39 MHz
rms error	3.28 MHz	3.43 MHz

EFFECTS OF UNDERLYING LAYERS ON M-FACTOR ESTIMATION

In the calculation of MUF in MINIMUF-85, the MUF is determined by the product of the f_oF2 and the so-called M-factor. The range dependence in the M-factor is based on the work of Davies (reference 20) who derived a family curves for the M-factor as a function of range and height of maximum electron density. The range dependence used was obtained by curve-fitting to exact results given by Davies for a parabolic layer of 290 km height and a ratio of semithickness/base height of 0.4. This corresponds to a semithickness/height of maximum electron density of 0.29. The results apply to a single parabolic layer with no underlying layers.

Lockwood has presented a noniterative procedure which enables evaluation of the MUF using a distance factor M(D)F2, with allowance for variations in both the peak height and changes in the underlying plasma (reference 37). The algorithm presented uses values of the ionospheric characteristics f_oF2, f_oE and M(3000)F2. Use is made of the Bradley-Dudeney model of the electron density profile (reference 38), consisting of a combination of linear and parabolic segments to represent the E-, F1-, and F2-regions. Lockwood assumed a fixed value for the ratio Ym F2/hm F2 of .29. He found that using the M(3000)F2- factor scaled according to standard URSI slider resulted in differences between values obtained by using ray-tracing calculations by up to 7.5% for F2 peak heights less than 500 km; this maximum error falling to 3% for h_mF2, the F2 peak height, below 350 km. However, he developed a correction to the M(3000)F2-factor, scaled from the ionogram, based on the ratio of f_oF2 to f_oE, x, that was always accurate to within 0.5%. Using the corrected value for the M(3000)F2-factor in the algorithm for M(D)F2, values are obtained with accuracies to about 6% for any range. The largest errors are for ranges in excess of 4000 km; for ranges less than 4000 km, the algorithm is accurate to within 4%. The algorithm presented was not designed for use at x (f_oF2/f_oE) less than 1.95.

The value of M(D) can be calculated in terms of x, $M(3000)_o$, and D by using

$$M(D) = 1 + \left[\frac{C_D}{C_{3000}}\right][M(3000)_o - 1] \quad (36)$$

where C_D and C_{3000} are given by equations 37 and 38 below for the ranges D and 3000 km, respectively. The parameter C_D is given by

$$C_D = 0.72 - 0.628z - 0.45z^2 - 0.03z^3 + 0.194z^4 + 0.158z^5 + 0.037z^6 \quad (37)$$

where

$$z = 1 - \frac{2D}{D_{max}} . \quad (38)$$

The value of the maximum range D_{max} in kilometers is given by

$$D_{max} = 3940 + s\left[\frac{1}{M(3000)_o} - 0.258\right] \quad (39)$$

with

$$s = 9900 + \frac{15375}{x^2} \quad \frac{106700}{x^5} . \quad (40)$$

Equations 36-40 allow the calculation of the M-factor. This is done in three stages: an estimate of $M(3000)_o$ at a range of 3000 km is determined in terms of $M(3000)_i$ from ionogram data, and then C_D is determined at a range of 3000 km and finally C_D at range D is determined. The value of $M(3000)_o$ is given by

$$M(3000)_o = M(3000)_i - 0.124 + [M(3000)_i^2 - 4]\left[0.0215 + 0.005\sin\left(\frac{7.854}{x} - 1.9635\right)\right] . \quad (41)$$

The value of $M(3000)_i$ is obtained from an ionogram or equivalent than obtained from a numerical map representation of $M(3000)_i$. Alternatively, it can be obtained from the expression given by Bradley and Dudeney (reference 38) for h_mF2 if h_mF2 is available:

$$h_mF2 = \frac{1490}{M(3000)F2 + \Delta M} - 176 \quad (42)$$

where

$$\Delta M = \frac{0.18}{x - 1.4} \quad , \; x > 1.7 \; .$$

For no underlying layers (i.e., x = 100) and h_mF2 = 290 km (the height used currently in MINIMUF-85), the equations become

$$\Delta M = 1.82 \times 10^{-3}$$

$$M(3000)_i = 3.19560$$

$$M(3000)_o = M(3000)_i - 0.02$$

$$M(3000)_o = 3.17562$$

$$s = 9901.54$$

$$D_{max} = 4503.39 \; . \qquad (43)$$

The value of M(D) is found using equations 36-38.

The assumption given by Lockwood for the ratio h_mF2/Y_mF2 of 3.5 implies for the Bradley-Dudency profile used by Lockwood that the parameter h_mF2 can be given by

$$h_mF2 = \frac{\left[h'F, F2 + 104 \left(\frac{0.613}{x-1.33}\right)^{0.86}\right]}{\left[0.71429 + \left(\frac{0.613}{x - 1.33}\right)^{0.86}\right]} \qquad (44)$$

where h'F,F2 is the minimum observed virtual height of reflection from the F-layer or F2- layer whichever may be the case. When x = 100, there is no underlying ionization and h_mF2 becomes

$$h_mF2 = 1.37564[h'F,F2 + 1.31598] \; . \qquad (45)$$

The value for the ratio h_mF2/Y_mF2 of 3.5 also implies that the base of ionization of the layer is given by

$$h_oF2 = 0.71429 \; h_mF2 \; . \qquad (46)$$

If there were no ionization below the F2- layer, h'F,F2 would be approximately equal h_oF2, and h_mF2 would be approximately equal to 1.4 h'F,F2.

Contour maps or numerical coefficient representations of h'F,F2 can be used to infer how $h_m F2$ differs from the value of 290 km used in MINIMUF-85 or even be used to determine M(3000)F2 using equations 42 and 44. Figure 31, based on contour maps of h'F,F2 (reference 39) shows how h'F,F2 varies as a function of time of day, season, and latitude. The F2-layer reflection heights given in reference 39 are the average of observations for the years 1944-1947. Reference 39 also shows the variation of F2-layer height with sunspot number for June at 1200 LT at four receiver sites. There is generally an increase in layer height with increasing sunspot number for northern latitude sites and a decrease with increasing sunspot number at the one southern latitude site. Leftin et al. (reference 40) give numerical maps of h'F,F2 base height as a function of season, sunspot number, location, and time of day.

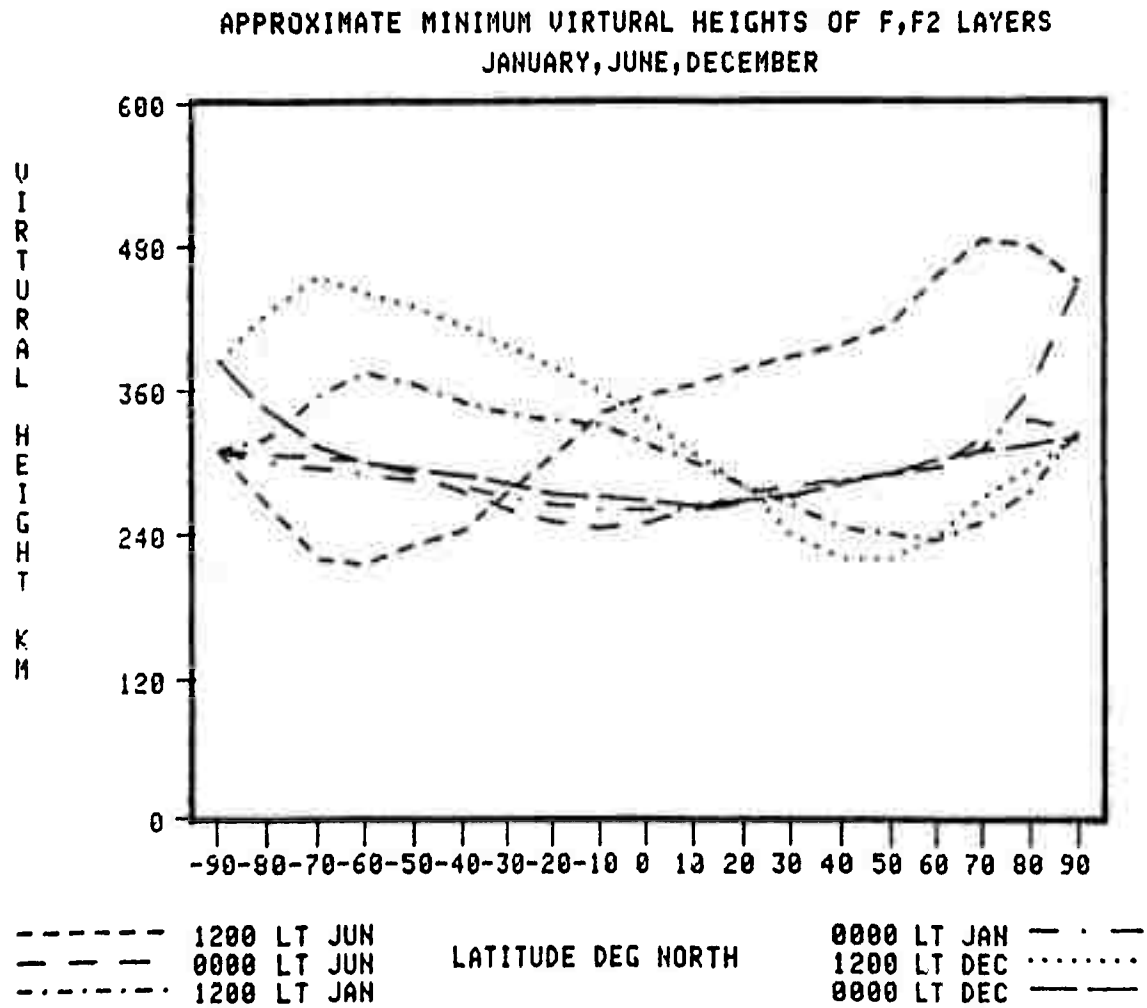

Figure 31. Approximate minimum virtual heights of F,F2- layers, January, June, December.

DETERMINATION OF TAKE-OFF ANGLES

In the evaluation of antenna gains, path loss, and group path delay, the elevation is necessary to determine the take-off angles of the possible modes of propagation. This is done by calculating the so-called mirror-reflection height. This is the height at which an equivalent plane mirror would have to be placed to reflect unrefracted waves with the same elevation angles at the receiver and transmitted as for the real ionosphere.

In PROPHET the take-off angle is determined using figure 4.10 (reference 41). This figure illustrates the relationship between great circle distances in km and radiation or elevation angles in degrees for a variety of propagation modes at fixed heights.

In several of the larger HF propagation prediction procedures, the mirror-reflection height is calculated iteratively (references 5 and 7); alternatively, equations based on some mean reference model ionosphere are employed (reference 42). The advantages of an iterative process are that the effects of variations in the underlying ionospheric regions and of spatial changes can be taken into account and that the evaluation can be continued until the required accuracy can be achieved. For many applications, however, it is undesirable to have an indeterminate calculation time, and the accuracy with which the ionization density profile is known may not justify such a procedure.

Lockwood (reference 43) has developed new algorithms for the prediction of the mirror reflection height h_T. Lockwood (reference 44) has shown that the evaluation times are small yet the accuracy is higher than that of many existing simplified procedures. The algorithms allow for the effects of variations in underlying ionization but neglect the effects of the geomagnetic field and apply for a horizontally stratified ionosphere. A fixed ratio of 3.5 for h_mF2/y_mF2 was assumed in his development. Lockwood used the procedure for determining the M(D)F2 factor described in reference 37 to calculate h_T at a range D and fixed r (f/MUF) by iterating the elevation angle. In this way $h_T(D)$ curves are calculated for various r and for each of the model profiles. Over a large part of the range of r, h_T at a fixed D is only weakly dependent

on r (for r = 0.8 to 0.95 when $h_m F2$ = 500 km, x = 3.33 and for r = 0.7 to 0.95 when $h_m F2$ = 250 km, x = 3.33, except at the shortest ranges). In every case where $r \geq 0.7$, h_T is greatest at all D when r is unity; it is much greater than for the lower r at the smallest and largest distances. Based on these variation patterns, Lockwood developed two representations of the mirror-reflection height: 1) at r = 1.0 for propagation at the MUF or above; 2) at r between 0.75 and 0.95 for propagation at the frequency of optimum transmitting (FOT). Because no formulas are presented for lower ratios of r, the latter is often used at lower values of the ratio.

At all but the shortest ranges, h_T can be described by the linear form when $0.75 < r < 0.95$

$$h_T = sD + C \ . \tag{47}$$

For $M(3000)_i \leq 3.57$

$$s = \left[\frac{1}{M(3000)_i} - 0.24\right]B \ . \tag{48}$$

For $M(3000)_i > 3.57$

$$s = 0.04B \ . \tag{49}$$

The parameter B varies linearly with the inverse of the fourth power of x:

$$B = 0.03 + 14.0/x^4 \ . \tag{50}$$

The parameter C is given by

$$C = 358 + \alpha\left(\frac{1}{M(3000)_i} - 0.35\right) \tag{51}$$

where α is given by

$$\alpha = 1880 - 3200/x^5 \ . \tag{52}$$

Equations 47-52 can be combined into the equation

$$h_T = 358 - (11\text{-}100\ a)\left(18.8 - \frac{320}{x^5}\right) + aD\left(0.03 + \frac{14}{x^4}\right)\text{km} \tag{53}$$

where $a = [1/M(3000)_i - 0.24]$ or 0.04, whichever is the larger.

For no underlying ionization ($x = 100$) and a h_mF2 of 290 km, h_T becomes

$$h_T = 290.61 + 0.0022D \text{ km} . \tag{54}$$

The general form of the $h_T(D)$ curves for $r = 1.0$ cannot be approximated by a single linear relationship as is possible for the $0.75 \leq r \leq 0.95$ curves. In this case the fit is given by

$$h_T = s_1 w + c_1 + \Delta \qquad w \leq 0.95 \tag{55}$$

$$h_T = [h_T]w = 0.95 \qquad w > 0.95$$

where w equals D/D_{max} and

$$\Delta = 23\left(\frac{1}{w} - 1\right) . \tag{56}$$

The intercept c_1 is given by

$$c_1 = 35 + \alpha_1\left[\frac{1}{M(3000)_o} - 0.225\right] \tag{57}$$

where

$$\alpha_1 = 1785 - 4000/x^3 . \tag{58}$$

The slope s_1 varies linearly with $M(3000)_o$ to the power -1.5:

$$s_1 = 230 + B_1\left[M(3000)_o^{-1.5} - 0.14\right] \tag{59}$$

and

$$B_1 = 325 + 6.4 \times 10^4/x^{3.8} \tag{60}$$

Equations 55-60 can be used to evaluate h_T for f = MUF at a given D, in conjunction with values for $M(3000)_o$ and D_{max} obtained in the evaluation of the M(D) factor from the previous section.

For no underlying layer and an $h_m F2$ of 290 km, these equations become

$$h_T = 195.5 + 0.0537\ D + 23\left(\frac{4503.4}{D} - 1\right) . \tag{61}$$

At D = 1000 km, h_T = 329.8 km for f = MUF; and h_T = 292.8 km for $0.75 \leq r \leq 0.95$.

For realistic values of h_T, w used in equations 55 and 56 should have a minimum value given by

$$w_{min} = 0.1 - 0.025\ \frac{500-h_m F2}{310} . \tag{62}$$

The problem with the use of equation 53 for calculating h_T for $0.75 \leq r \leq 0.95$ at short range is that h_T is no longer linear with decreasing range. At short range the h_T variation is similar to that for r = 1.0 (frequencies near the MUF), only not as pronounced. That is as r decreases from 1.0 to 0.6, the increase in h_T with decreasing distance D is proportional to r^3. Further, as x decreases from a value of 10.0 to 2.0, the increase in h_T at short ranges becomes less significant. A correction factor is found to be applied to equation 53 for ranges less than D_{MIN}. This correction is found by finding the range for which equation 55 had a minimum. This minimum range is inserted in equation 55 for r = 1 to determine $h_{T,MIN}$. Then Δh_T is found from $\Delta h_T = h_T - h_{T,MIN}$. D_{MIN} is given by

$$D_{MIN} = D_{MAX}\sqrt{\frac{23}{s_1}} \tag{63}$$

and Δh_T is given by

$$\Delta h_T = 23\ D_{MAX}\left(\frac{1}{D} - \frac{1}{D_{MIN}}\right) + \frac{s_1}{D_{MAX}}\left(D - D_{min}\right) . \tag{64}$$

The restriction of equation 62 still applies. The final correction $\Delta' h_T$ is given by

$$\Delta h' = \frac{r^3}{x}\Delta h_T \quad . \tag{65}$$

The angle of transmission from earth (sometimes called takeoff angle), written in terms of the mirror reflection height h_T and the great-circle distance D from transmitter to receiver is

$$\beta = \tan^{-1}\left[\frac{\cos\left(\frac{D}{2ren}\right) - re/\left(re + h_T\right)}{\sin\left(\frac{D}{2ren}\right)}\right] \tag{66}$$

where n = number of hops and re = radius of the earth.

FUTURE IMPROVEMENTS IN MINIMUF

Before termination of the discussion section of this report, possible additional improvements that might be made to MINIMUF are discussed. There are three areas where improvements might be made. These are in the f_oF2 model, in the M-factor model, and in the Polar region model.

f_oF2 Representation

The representation of f_oF2 in MINIMUF-85 is given by

$$f_oF2^2 = A_o + A_1 \cos^{1/2} \chi_{eff} \tag{67}$$

where A_1 is a function of sunspot number and represents the amplitude variation of f_oF2 (at $\chi_{eff} = 0°$, $A_o + A_1$ = maximum diurnal value of f_oF2 and at $\chi_{eff} = 90°$, A_o = minimum diurnal value of f_oF2^2). If examined the contour plots of f_oF2 given in references 21 and 22 show that the minimum and maximum values of f_oF2 depend on sunspot number, geographic location, and season. By using the f_oF2 data base used to get the representation for A_1 now in MINIMUF-85, it should be possible to obtain A_o, A_1 and $\cos^{\eta}\chi_{eff}$ as a function of sunspot number, season, and geographic location. At each f_oF2 measurement site A_o, A_1, and η would be determined for each season and sunspot number that minimizes the diurnal error in f_oF2. Having determined A_o, A_1, and η at each

site, then the functional form of geographic location, sunspot number, and season dependences of these parameters can be determined.

M-factor Representation

The M-factor representation could be improved by introducing the effects of the underlying layers on M-factor estimation given earlier by equations 36-41. The parameter $M(3000)_i$ can be found from equation 42 using equation 44 for h_mF2. The parameter h'F,F2 required by equation 44 can be determined either from numerical maps of h'F,F2 (reference 39) or from figure 31. To fine tune the model, the resultant MINIMUF model will need to be fit to an oblique sounder data much as the present version was.

Polar Representation

Possible improvements in the polar model include

- development of a polar M-factor model,
- introduction of a seasonal dependence into the folding function to reduce the winter bias error, and
- refinement of the adjustable parameters to further minimize errors. Finally, south Polar MOF data is needed to test the model in that region.

CONCLUSIONS

We have described several changes to the MUF algorithm used in the PROPHET family of prediction programs. The main effect of the changes is to improve the capability of the model during periods of very high solar activity, a situation where the previous model had known deficiencies.

We have also improved the f_oF2 model to provide a much more accurate prediction capability for this parameter. This will improve short distance MUF predictions and give more accurate f_oF2 values for use in other PROPHET outputs, such as ray tracing, where this parameter is required as input.

We have changed the M-factor model to include sunspot numbers, seasonal, and diurnal dependencies. These changes allow more flexibility in using this parameter for other PROPHET output, such as a prediction h_T, which requires the parameter as an input.

Lastly, we have introduced a special f_oF2 for use in the polar regions of the world. This is accomplished by the use of a folding function which folded in the polar f_oF2 model and folded out the MINIMUF-85 f_oF2 model. The folding function is a function of geomagnetic latitude and sunspot numbers. Inclusion of the polar model in MINIMUF-85 reduced the overall bias in the model from 0.16 MHz low to 0.14 MHz low and reduced the rms error from 4.19 MHz to 4.08 MHz. On five Polar paths it changed the bias and rms error, respectively, from 6.85 MHz low and 10.92 MHz to 0.6 MHz low and 4.0 MHz.

REFERENCES

1. National Bureau of Standards Circular 452, Ionospheric Radio Propagation, 25 June 1948.

2. Naval Ocean Systems Center Technical Report 186, MINIMUF-3: a Simplified HF MUF Prediction Algorithm, by R. B. Rose, J. N. Martin, and P. H. Levine, 1 February 1978.

3. Naval Ocean Systems Center Technical Document 201, MINIMUF-3.5, Improved Version of MINIMUF-3, a Simplified h_f MUF Prediction Algorithm, by R. B. Rose and J. N. Martin, 26 October 1978.

4. Naval Ocean Systems Center Technical Report 695, Accuracy of High Frequency Maximum Usable Frequencies (MUF) Prediction, by D. B. Sailors, W. K. Moision, and R. P. Brown, 15 September 1981.

5. Environmental Sciences Services Administration Technical Report TER 1-ITSA-1, Predicting Statistical Performance Indices for High Frequency Telecommunications Systems, by D. L. Lucas and G. W. Haydon, August 1966.

6. Office of Telecommunications Report 76-102, Predicting the Performance of High Frequency Skywave Telecommunication Systems (the Use of the HFMUFES 4 Program), by G. W. Haydon, M. Leftin, and R. Rosich, September 1976.

7. Environmental Sciences Service Administration Technical Report ERL 110-ITS 78, Predicting Long-term Operational Parameters of High Frequency Sky-wave Telecommunications Systems, by A. F. Barghausen, J. W. Finney, L. L. Proctor, and L. D. Schultz, May 1969.

8. Decc Electronics, Inc., Contract No. AF19(628)-3267, First Report, AFCRL-66-381, Oblique-Incidence Ionospheric Investigations, by D. Davidson, May 1966.

9. General Electric Co., Contract AF30(602)-3946, Interim Report 6, RADC-TR-67-618, Expanded Little IDA, Experimental Results, by D. T. Olmsted, J. A. Reeve, and B. Shepelavey, December 1967.

10. Stanford Research Institute, Contract DA-039 AMC-00040(E) Order No., 5384-PM-63-91, Semiannual Report 8, Research-Engineering and Support for Tropical Communications, by E. L. Younker, G. H. Hagn, and H. W. Parker, March 1967.

11. National Bureau of Standards Report 8226, Semi-annual Report to Voice of America, by H. I. Leighton and R. E. Sodergren, July 1963 - March 1964.

12. National Bureau of Standards Report 7276, Semi-annual Report to Voice of America, Part B, by H. I. Leighton and R. E. Sodergren, December 1961 - July 1962.

13. Harnett, D. L. Introduction to Statistical Methods, Addison-Wesley Publishing Co., 1st Edition, pp. 284-333, 1970.

14. Sailors, D. B., "An Improved Version of MINIMUF-3.5," paper presented at the Effects of the Ionosphere on C^3I Systems Symposium, Alexandria, VA, 1-3 May 1984.

15. Vasil'yeva, T. N. and T. S. Kerblay, "Various Types of Dependencies of f_oF2 on Solar Activity," Geomag and Aeronmy, Vol. 5, pp. 669-671, 1964.

16. Vasil'yeva, T. N., "Characteristics of f_oF2 Variations at High Solar Activity," Geomag and Aeronmy vol. 6, pp. 870-872, 1965.

17. Alpert, Y. L., Radio Wave Propagation and the Ionosphere: Vol. 1 The Ionosphere, pp. 311-318, Consultants Bureau, NY 1973.

18. Rose, R. B., "MINIMUF: A Simplified MUF Prediction Program for Microcomputers," QST, vol. 66(12), PP. 36-38, 1982.

19. Devereux, E. L. and D. Wilkinson, "HF Predictions on the Home Computer," Radio Communication, Vol. 59 (3), pp. 246-248, 1983.

20. National Bureau of Standards Monograph 80, Ionospheric Radio Propagation, by K. Davies, April 1, 1965.

21. National Bureau of Standards Technical Note 2, World Maps of F2 Critical Frequencies and Maximum Usable Frequency Factors, by D. H. Zacharisen, April 1959.

22. National Bureau of Standards Technical Note 2-2, Supplementary World Maps of F2 Critical Frequencies and Maximum Usable Frequency Factors, by D. H. Zacharisen, October 1960.

23. Chiu, Y. T., "An Improved Phenomenological Model of Ionospheric Density," J. Atmos. Terr. Phys., vol. 37, pp. 1563-1570, 1975.

24. Yonezawa, T. and Y. Arima, "On the Seasonal and Non-seasonal Annual Variations and the Semi-annual Variation in the Noon and Midnight Electron Densities of the F2 Layer in Middle Latitudes," J. Radio Res. Lab. Japan, vol. 6, pp. 293-309, April 1959.

25. Ching, B. K. and Y. T. Chiu, "A Phenomenological Model of Global Ionospheric Electron Density in the E-, F1-, and F2- regions," J. Atmos. Terr. Phys., vol. 35, pp. 1615-1630, 1973.

26. Stewart, F. G. and M. Leftin, "Relationship between Ottawa 10.7 cm Solar Radio Noise Flux and Zurich Sunspot Number," Telecommunication Journal, vol. 39, pp. 159-169, 1972.

27. Joachim, M., "Study of Correlation of the Three Basic Indices of Ionospheric Propagation: R_{12}, I_{F2} and Φ," Nature, vol. 210, pp. 289-290, 1966.

28. National Bureau of Standards Report 8734, Comparative Study of Solar Indices for Ionospheric Predictions, by S. C. Gladden, 22 January 1965.

29. Pennsylvania State University Ionospheric Research Laboratory Scientific Report 195, Solar Radioflux and Upper-Atmosphere Temperature, by M. Nicolet, 1 October 1963.

30. International Radio Consultative Committee, "Recommendation 371-4," Recommendations and Reports of the CCIR, XVth Plenary Assembly, Geneva, 1982, vol. 6, 38-42.

31. Naval Research Laboratory Memorandum Report 4849, Initial Results from HF Propagation Studies During Solid Shield, by D. R. Uffelman and L. O. Harnish, 30 July 1982.

32. Naval Research Laboratory Memorandum Report 4599, HF Propagation Assessment Studies over Paths in the Atlantic, by D. R. Uffelman, 26 October 1981.

33. Naval Research Laboratory Memorandum Report 4600, HF Systems Test for the Surtass Operation of February 1981, by D. R. Uffelman and L. O. Harnish, 26 October 1981.

34. Naval Research Laboratory Memorandum Report 5246, Real-time Update of Two H. F. Channel Evaluation Models by Oblique Sounding, by D. R. Uffelman and P. A. Hoover, 13 January 1984.

35. Naval Research Laboratory Memorandum Report 5284, H. F. Frequency Management by Frequency Sharing as Assisted by Models Updated in Real-Time, by D. R. Uffelman, L. O. Harnish, and J. M. Goodman, 21 March 1984.

36. Naval Research Laboratory Memorandum Report 5505, An HF Communications Frequency-Management Procedure for Forecasting the Frequency of Optimum Transmission, by M. Daehler, 31 December 1984.

37. Lockwood, M., "Simple M-factor Algorithm for Improved Estimation of the Basic Maximum Usable Frequency of Radio Waves Reflected from the Ionospheric F-region," IEE Proc., vol. 130, Pt. F, No. 4, PP. 296-302, June 1983.

38. Bradley, P. A. and J. R. Dudeney, "A Simple Model of the Vertical Distribution of Electron Concentration in the Ionosphere," J. Atmos. Terr. Phys., vol. 35, pp. 2131-2146, 1973.

39. Army Signal Radio Propagation Agency Tech. Report 9, Analysis and Prediction of Skywave Field Intensities in the High Frequency Band, by P. O. Laitinen and G. W. Haydon, revised October 1962.

40. Environmental Science Services Administration Technical Memorandum IERTM-ITSA 69, Numerical Maps of Monthly Median h'F2, F2 for Solar Cycle Minimum and Maximum, by M. Leftin, S. M. Ostrow, and C. Preston, July 1967.

41. Army Signal Corps Radio Propagation Unit Baltimore Tech. Report No. 6, Calculation of Sky-wave Field Intensities, Maximum Usable Frequencies, and Lowest Useful High Frequencies, under the direction of Chief Signal Officer, revised June 1949.

42. Shimazaki, T., "World-wide Daily Variations in the Height of the Maximum Electron Density of the Ionospheric F2 Layer," J. Radio Res. Labs., Japan, vol. 2, pp. 85-97, 1955.

43. Lockwood, M., "Simplified Estimation of Ray-path Mirroring Height for HF Radiowaves Reflected from the Ionospheric F-region," Proc. IEE, Vol. 131, Pt F., no. 2, pp. 117-124, April 1984.

44. Lockwood, M., "Simplified Evaluation of Propagation Characteristics for HF Radio Waves Reflected from the Ionospheric F2 Layer," paper presented at the Third International Conference on Antennas and Propagation, Norwick, United Kingdom, 12-15 April 1983.

APPENDIX A

BASIC PROGRAM FOR MINIMUF-85

The listing of MINIMUF-85 that follows is written in extended BASIC for the Tektronix 4052A computer. The subroutine Razgc determines the latitude and longitude of a point on a great circle path given the range and bearing from the point. The subroutine Gcraz gives the range and bearing between two points.

INPUT PARAMETERS

Z3 = transmitter latitude, radians $\left(\frac{\pi}{2} \leq Z3 \leq \frac{\pi}{2}\right)$

Z4 = transmitter longitude, radians $(-2\pi \leq Z4 \leq 2\pi)$

Z5 = receiver latitude, radians $\left(\frac{\pi}{2} \leq Z5 \leq \frac{\pi}{2}\right)$

Z6 = receiver longitude, radians $(-2\pi \leq Z6 \leq 2\pi)$

Z0(1) = path length, radians

Z0(2) = azimuth of path, radians

M1 = month

D0 = day of month

H0 = hours, GMT

M0 = minutes, GMT

S9 = monthly median sunspot number

PI = 3.141593

P0 = 1.5707963268

OUTPUT PARAMETER

The output is as follows:

J9 = MUF in MHz.

```
100   ! MNIMUF85 TEST   "MNIMUFTEST"
110   !
120   ! INPUT DATA  DRIVER FOR MINIMUF
130 R1=PI/180
140 P1=2*PI
150 P0=PI/2
160 DIM Z0(8)
170 Z3=75*R1  ! TRANSMITTER LATITUDE
180 Z4=-125*R1  ! TRANSMITTER LONGITUDE WEST POSITIVE
190 Z5=51.95*R1  ! RECEIVER LATITUDE
200 Z6=176.58*R1  !  RECEIVER LONGITUDE WEST POSITIVE
210 M1=1  ! MONTH  1= JAN
220 D0=15  ! DAY
230   !H0=0   HOUR
240 M0=0  !  MINUTE
250 S9=9  !  SMOOTH SUNSPOT NUMBER
260 A=Z5
270 B=Z6
280 C=Z3
290 D=Z4
300 CALL Gcraz
310 Z0(1)=R  !  RANGE BETWEEN TRANSMITTER-RECEIVER
320 Z0(2)=S  !  BEARING ANGLE
330 FOR H0=0 TO 23 STEP 1  !  LOOP FOR 24 HOURS
340    CALL Mnimuf
350    PRINT "LAT=";Z3/R1,"LON=";Z4/R1,"LAT=";Z5/R1,"LON=";Z6/R1
360    PRINT "MONTH=";M1,"DAY=";D0,"HOUR=";H0,"MINUTE=";M0
370    PRINT "SSN=";S9
380    PRINT ""
390    PRINT "MUF=";J9
400 NEXT H0
410 END
420   !
430 SUB Mnimuf
440    DIM Ssn(6),Scn(6)
450    Saa=0.814*S9+22.23
460    Sab=1.3022-0.00156*S9
470    FOR J=1 TO 6
```

```
480       Sar=2*J*PI*M1/12
490       Ssn(J)=SIN(Sar)
500       Scn(J)=COS(Sar)
510    NEXT J
520    Sac=0.9925+0.011*Ssn(1)+0.087*Scn(1)-0.043*Ssn(2)+0.003*Scn(2)
530    Sac=Sac-0.013*Ssn(3)-0.022*Scn(3)+0.003*Ssn(4)+0.005*Ssn(5)
540    Sac=Sac+0.018*Scn(6)
550    I=H0+M0/60
560    J=INT(Z0(1)/0.62784)+1
570    L=1/(2*J)
580    Ak6=1.59*Z0(1)
590    IF Ak6<1 THEN
600       Ak6=1
610    END IF
620    J9=100
630    IF Z0(1)>0.94174 THEN
640       Ak=2*J-1
650    ELSE
660       Ak=J
670    END IF
680    Kkk=1/Ak6
690    IF Kkk<>1 THEN
700       Kkk=0.5
710    END IF
720    FOR D9=1 TO Ak STEP 1
730       IF Z0(1)>0.94174 THEN
740          Ak1=D9*L
750       ELSE
760          Ak1=1/(2*Ak6)+(D9-1)*(0.9999-1/Ak6)
770       END IF
780       C=Ak1*Z0(1)
790       D=Z0(2)
800       A=Z5
810       B=Z6
820       CALL Razgc
830       E=R
840       F=S
850       IF F=>0 THEN 870
860       F=F+P1
870       G=0.0172*(10+(M1-1)*30.4+D0)
```

```
880       Slt=I-F/(R1*15)
890       IF Slt<24 THEN 910
900       Slt=Slt-24
910       IF Slt>0 THEN 930
920       Slt=Slt+24
930       A=E
940       B=F
950       Smg=0.9792*SIN(A)+0.2028*COS(A)*COS(B-1.2043)
960       Sdg=ASN(Smg)
970       IF ABS(Sdg)<0.95993 THEN
980          Sgf=0
990       ELSE
1000          Sgf=0.7578*SQR(1+3*Smg*Smg)*0.5-0.5
1010       END IF
1020       H=0.409*COS(G)
1030       P=3.82*F+12+0.13*(SIN(G)+1.2*SIN(2*G))
1040       IF P<=24 THEN 1070
1050       P=P-24
1060       GO TO 1090
1070       IF P=>0 THEN 1090
1080       P=P+24
1090       Q=2.5*Z0(1)*Kkk MIN P0
1100       Q=SIN(Q)
1110       Q=1+2.5*Q*SQR(Q)
1120       IF COS(E+H)>-0.26 THEN 1170
1130       G=0
1140       S=0
1150       Sad=1
1160       GO TO 1610
1170       S=(-0.26+SIN(H)*SIN(E))/(COS(H)*COS(E)+1.0E-3)
1180       S=S MAX -1 MIN 1
1190       S=12-ASN(S)*7.6394
1200       T=P-S/2
1210       IF T=>0 THEN 1230
1220       T=T+24
1230       U=P+S/2
1240       IF U<=24 THEN 1260
1250       U=U-24
1260       V=ABS(COS(E+H))
1270       W=9.7*V^9.6
```

```
1280        W=W MAX 0.1
1290        X=I
1300        IF U<T AND (I-U)*(T-I)>0 THEN 1440
1310        IF U=>T AND (I-T)*(U-I)<=0 THEN 1440
1320        IF T<=I THEN 1340
1330        X=X+24
1340        Y=PI*(X-T)/S
1350        Z=PI*W/S
1360        F=(T-X)/W
1370        F=F MAX -100 MIN 100
1380        G=V*(SIN(Y)+Z*(EXP(F)-COS(Y)))/(1+Z^2)
1390        P=V*(Z*(EXP(-S/W)+1))*EXP((S-24)/2)/(1+Z^2)
1400        IF G=>P THEN 1420
1410        G=P
1420        Sad=1.11-0.01*Slt
1430        GO TO 1610
1440        IF U<=I THEN 1460
1450        X=X+24
1460        Stt=X-U
1470        Stu=14*Stt/(24-S)
1480        Sag=PI*(Stu+1)/15
1490        Sah=2*Sag
1500        Sai=1.0195-0.06*SIN(Sah)-0.037*COS(Sah)+0.018*SIN(2*Sah)
1510        Saj=-0.003*COS(2*Sah)+0.025*SIN(3*Sah)+0.018*COS(3*Sah)
1520        Sak=0.007*SIN(4*Sah)-0.005*COS(4*Sah)+0.006*SIN(5*Sah)
1530        Sal=0.017*COS(5*Sah)-0.009*SIN(6*Sah)-0.004*COS(6*Sah)
1540        Sad=Sai+Saj+Sak+Sal
1550        Z=PI*W/S
1560        F=(U-X)/2
1570        F=F MAX -100 MIN 100
1580        Y=-S/W
1590        Y=Y MAX -100 MIN 100
1600        G=V*(Z*(EXP(Y)+1))*EXP(F)/(1+Z^2)
1610        Sae=Sab*Sac*Sad
1620        H=SQR(6+Saa*SQR(G))+Sgf
1630        H=H*(1-0.1*EXP((S-24)/3))
1640        H=H*(1+(1-SGN(Z5)*SGN(Z3))*0.1)
1650        H=H*(1-0.1*(1+SGN(ABS(SIN(A))-COS(A))))
1660        CALL Fof2
1670        J9=J9 MIN H
```

```
1680       PRINT "H = ",H
1690    NEXT D9
1700    J9=J9 MAX 2 MIN 50
1710 END SUB
1720 SUB Fof2
1730       !LOCAL Gg,Ff,Ys,Za,Am,Phi,Tmo,Rltm,Rlgm,Plr,Bb,T,U,V,Y,Z,C,W,X
1740    Phi=Slt*PI/12
1750    Tmo=Ml+(D0+I/24)/30-0.5
1760    Rltm=Sdg
1770    Rlgm=COS(A)*SIN(B-1.2043)/COS(Rltm)
1780    Rlgm=Rlgm MAX -1 MIN 1
1790    Rlgm=ASN(Rlgm)
1800    X=(2.2+(0.2+S9/1000)*SIN(Rltm))*COS(Rltm)
1810    Ff=EXP(-(X^6))
1820    Gg=1-Ff
1830    T=PI*Tmo/12
1840    V=SIN(T)
1850    U=COS(T+T)
1860    Y=SIN(Rlgm/2)
1870    Ys=COS(Rlgm/2-PI/20)
1880    Z=SIN(Rlgm)
1890    Za=SQR(ABS(Z))
1900    Am=1+V
1910    IF Sdg<0 THEN 1960
1920    C=-23.5*PI/180
1930    W=EXP(-1.2*(COS(Rltm+C*COS(Phi))-COS(Rltm)))
1940    Plr=(2+1.2*S9/100)*W*(1+0.3*V)
1950    GO TO 2000
1960    B=V*(0.5*Y-0.5*Z-Y^8)-Am*U*(Z/Za)*EXP(-4*Y*Y)
1970    Plr=2.5+2*S9/100+U*(0.5+(1.3+0.2*S9/100)*Ys^4)
1980    Plr=Plr+(1.3+0.5*S9/100)*COS(Phi-PI*(1+B))
1990    Plr=Plr*(1+0.4*(1-V*V))*EXP(-1*V*Ys^4)
2000    T=Gg*H^2/8.12+0.66*Ff*Plr
2010    IF T<0 THEN 2040
2020    Ff2=T^0.5*2.85
2030    H=Ff2*Q*Sae
2040 END SUB
2050 SUB Gcraz
2060    IF ABS(A-C)>1.0E-5 OR ABS(B-D)>1.0E-5 THEN 2100
2070    R=1.0E-6
```

```
2080    S=0
2090    GO TO 2290
2100    IF ABS(A-P0)>1.0E-5 THEN 2140
2110    R=P0-C
2120    S=PI
2130    GO TO 2290
2140    IF ABS(A+P0)>1.0E-5 THEN 2180
2150    R=P0+C
2160    S=0
2170    GO TO 2290
2180    E=SIN(A)
2190    F=COS(A)
2200    G=SIN(C)
2210    H=E*G+F*COS(C)*COS(B-D)
2220    H=H MAX -1 MIN 1
2230    R=ACS(H)
2240    S=(G-E*H)/(F*SIN(R))
2250    S=S MAX -1 MIN 1
2260    S=ACS(S)
2270    IF SIN(B-D)>0 THEN 2290
2280    S=P1-S
2290 END SUB
2300 SUB Razgc
2310    IF C>1.0E-5 THEN 2350
2320    R=A
2330    S=B
2340    GO TO 2610
2350    IF ABS(A-P0)>1.0E-5 THEN 2390
2360    R=P0-C
2370    S=B
2380    GO TO 2610
2390    IF ABS(A+P0)>1.0E-5 THEN 2430
2400    R=C-P0
2410    S=B
2420    GO TO 2610
2430    E=SIN(A)
2440    F=COS(A)
2450    G=COS(C)
2460    H=E*G+F*SIN(C)*COS(D)
2470    H=H MAX -1 MIN 1
```

```
2480     P=ACS(H)
2490     Q=(G-E*H)/(F*SIN(P))
2500     Q=Q MAX -1 MIN 1
2510     Q=ACS(Q)
2520     R=PO-P
2530     IF SIN(D)>0 THEN 2560
2540     S=B+Q
2550     GO TO 2570
2560     S=B-Q
2570     IF S<=P1 THEN 2590
2580     S=S-P1
2590     IF S=>-P1 THEN 2610
2600     S=S+P1
2610 END SUB
```

APPENDIX B

FORTRAN PROGRAM FOR MINIMUF-85

The listing of MINIMUF-85 that follows is written in FORTRAN 77 for the HP 9050 computer. The parameters passed to the subroutine and those returned by it are described in the comments portion of the routine.

```
      subroutine muf85 (tlat, tlon, rlat, rlon, itime, cpnt, ssn,cmuf)
cp
c     subroutine muf85
c
c       update nov 1985
c       an improved version of muf35 which includes ssn,season and
c       diurnal dependence in the M-factor plus an improved FOF2 model
c       call muf85(tlat,tlon,rlat,rlon,itime,ssn,cmuf)
c
c        this routine computes the maximum useable frequency (cmuf) for
c        a given propagation path.  the required input is:
c
c        parameters passed:
c          tlat  - transmitter latitude in radians
c          tlon  - transmitter west lingitude in radians
c          rlat  - receiver latitude in radians
c          rlon  - receiver west longitude in radians
c          itime - six element array containing the month, day
c                  hour, minute, julian day, and year
c          ssn   - sunspot number
c
c        parameters returned:
c          cpnt  - path control point info in radians
c          cmuf  - classical muf in megahertz.
c
c        called by subroutine or function:  mufluf
c
c        subroutines and functions called:  fof2
c                                           path
c                                           razgc
c                                           sygn
c
c        common blocks referenced:          hite
cz
      logical       v, first
      integer       itime(6)
      real          cpnt(8), k5, l0, lmt, k8, k9, m9, mlat,sn(6),cn(6)
c
      common /hite/ h,v,ym
cm
c      common /hite/  h, v, ym
c
c                     h   is the height of the path
c                     v   is a logical variable which decides if the
c                         path length is calculated from 1000 km f
c                         end points and if the multilayered ionospheric
c                         model is to be used.  these will be performed
c                         if v is true.
c                     ym  is the f layer thickness.
c
cz
      data   pi/3.14159265/,twopi/6.2831853/,halfpi/1.57079632/,
     &       dtr/0.017453293/,rtd/57.2957795/,r0/6371./
      data   s8 /250.0/, fm1 /0.728/, fms /0.52998/,
     &       fm2 /0.00356/, fm3 /63.75/, fm4 /0.00178/,
     &       first /.true./
```

```
c
      t5 = float( itime(3) ) + float( itime(4) )/60.0
c
c   convert 10.7 cm flux to sunspot number
c
c     ssn = ( sqrt( fm5 - fm2*( fm3 - flux10 ) ) - fm1 )/fm4
c     ssn = amax1( amin1( ssn, 250.0 ), 0.0 )
c
c   determine number of hops
c   1 hop for path length (= 4000 km ( 0.6278 radians )
c   2 hop otherwise
c
c      a3 is a 6th order fourier series based on month which is part
c          of the new M-factor
c      a2 is a linear function of ssn in the M-factor
c      a1 is a linear function of ssn in the critical frquency
c          expression
c
      do 500 n = 1,6
      qn = float(2*n)
      arg = pi*qn*itime(1)/12.0
      sn(n) = sin(arg)
      cn(n) = cos(arg)
  500 continue
      a3 = .9925+.011*sn(1)+.087*cn(1)-.043*sn(2)
     1    +.003*cn(2)-.013*sn(3)-.022*cn(3)
     2    +.003*sn(4)+.005*sn(5)+.018*cn(6)
      a1 = .814*ssn+22.23
      a2 = 1.3022-.00156*ssn
      call path(tlat,tlon,rlat,rlon,cpnt)
      g1 = cpnt(1)
      azim = cpnt(8)
c
c      control point changes for muf85
c
      if(.not. v)then
         h3=1.59
         ak6 = h3*cpnt(1)
         if(ak6 .lt.1.0)ak6=1.0
         k5 = 1.0/ak6
         if(k5 .ne. 1.0) k5 = .5
         khop = int(cpnt(1)/.62784)+1
         kkhop = khop
         if(cpnt(1) .gt. 0.94174)kkhop = 2*khop-1
      else
c
c      old control point methor for raytrace
c
         khop = 1
         if ( g1 .gt. 0.62784 )  khop = 2
         k5 = 1.0/float( khop )
         kkhop = khop
      end if
c
      cmuf=100.0
      ym = 100.0
```

```
      do 160 k1 = 1,kkhop
c
c    10, w0 = latitude and west longitude of control points
c    mid-point for 1 hop case; points 2000 km from each
c    end for 2 hop case.
c
        if ( khop .eq. 1 )  p1 = g1/2.0
        if ( khop .eq. 2 .and. k1 .eq. 1 )  p1 = 0.31392
        if ( khop .eq. 2 .and. k1 .eq. 2 )  p1 = g1 - 0.31392
c
c    if v is .false., do cntrl pt calculations like in apes
c
        if(v) go to 600
c
c
c       control point method for muf85
c
       if(cpnt(1) .gt. .94174) then
          xk1 = k1
          xhop = khop
          ak1 = xk1/(2.0*xhop)
       else
          ak1 = 1.0/(2.0*ak6)+float(k1-1)*(.9999-1.0/ak6)
       end if
c
       p1 = g1*ak1
c
  600   call razgc( rlat, rlon, p1, azim, 10, w0 )
c
c     lmt = local mean time in hours at the control point
c     mlat = geomagnetic latitude at the control point
c
        if ( w0 .ge. 0.0 )  then
          lmt = w0
        else
          lmt = w0 + twopi
        end if
        lmt = t5 - lmt*rtd/15.0
        if ( lmt .lt. 0.0 )  then
          lmt = lmt + 24.0
        else if ( lmt .ge. 24.0 )  then
          lmt = lmt - 24.0
        end if
        smg = 0.9792*sin( 10 ) + 0.2028*cos( 10 )*cos( w0 - 1.2043 )
        smg = amax1( amin1( smg, 1.0 ), -1.0 )
        mlat = asin( smg )
c
c       gyro frequency for lat ) 55deg
c
        if ( abs( mlat ) .lt. 0.95993 )  then
          gyro = 0.0
        else
          gyro = 0.3789*sqrt( 1.0 + 3.0*smg*smg) - 0.5
        end if
c
c    y1 = 2*pi*date/365.25
```

```
c   y2 = -solar declination
c   k8 = time of local noon
c
        y1=0.0172*( 10.0 + float(itime(1)-1)*30.4 + itime(2) )
        y2=0.409*cos(y1)
c
        k8=3.82*w0+12.0+0.13*(sin(y1)+1.2*sin(2.0*y1))
        if ( k8 .gt. 24.0 )  then
          k8 = k8 - 24.0
        else if ( k8 .le. 0.0 )  then
          k8 = k8 + 24.0
        end if
c
c   m9 = m-factor = muf/f0f2
c
        m9 = amin1( 2.5*g1*k5, halfpi )
        m9 = sin( m9 )
        m9 = 1.0 + 2.5*m9*sqrt( m9 )
c
c   changes to include altitude of the f-layer variations
c   for diurnal,latitude, and solar cycle
c   (if v is .false. bypass all this variation stuff)
c
        if(.not.v) go to 50
51      cchi=sin(10)*sin(-y2)+cos(10)*cos(-y2)*cos((t5-k8)*15.*dtr)
        chi=acos(cchi)
c
c   altitude variations of f-layer
c
        chi1=((chi+0.349)/.873)**2
        x1=(10/0.524)**2
        xmax=3.-(ssn-25.)*5.e-3+1.25*cos((10-0.96)*0.045)
        delx=2.*cos(chi-0.873+.698*cos((10-0.96)*0.045))
     &         +(ssn-25.)*0.01*exp(-chi1)*exp(-x1)
        x11=xmax - delx
c
50     continue
        if ( cos( 10 + y2 ) .gt. -0.26 )  go to 100
c
c   no daylight on path at any time during the day
c
        g0 = 0.0
        k9 = 0.0
        go to 140
100     continue
c
c   k9 = length of daylight
c   t  = time of sunrise
c   t4 = time of sunset
c
        k9 = ( -0.26 + sin(y2)*sin(10) )/( cos(y2)*cos(10) + 1.0e-3 )
        k9 = amax1( amin1 ( k9, 1.0 ), -1.0 )
        k9 = 12.0 - asin( k9 )*7.6394
        t = k8 - k9/2.0
        if ( t .lt. 0.0 )  t = t + 24.0
        t4 = k8 + k9/2.0
```

```
        if ( t4 .gt. 24.0 )  t4 = t4 - 24.0
        c0 = abs( cos( 10 + y2 ) )
        t9=9.7*(amax1(c0,.1))**9.6
        t9 = amax1( t9, 0.1 )
        t6 = t5
        if ( ( t4 .lt. t .and. (t5-t4)*(t-t5) .gt. 0.0 ) .or.
     &       ( t4 .ge. t .and. (t5-t)*(t4-t5) .le. 0.0 ) )  go to 120
c
c   day time at control point
c
        if ( t .gt. t5 )  t6 = t6 + 24.0
c
c      local time conversion
c      t5 is local time, w0 is longitude in radians
c
      z = w0*(180.0/3.14159265)
c
c      local time dependent factor for M-factor
c
      hrlcl  = t5 - z/15.0
      if(hrlcl .ge. 24.0)hrlcl = hrlcl - 24.0
      if(hrlcl .lt. 0.0) hrlcl = hrlcl + 24.0
      a4 = 1.11-.01 * hrlcl
c
        g9 = pi*( t6 - t )/k9
        g8 = pi*t9/k9
        u = ( t - t6 )/t9
        u = amin1( amax1( u, -87.0 ), +87.0 )
        u1 = -k9/t9
        u1 = amin1( amax1( u1, -87.0 ), +87.0 )
        g0=c0*(sin(g9)+g8*(exp(u)-cos(g9)))/(1.0+g8*g8)
        g3 = c0*( g8*( exp( u1 ) + 1.0 ) )
     &       *exp( ( k9 - 24.0 )/2.0 )/( 1.0 + g8*g8 )
        g0 = amax1( g0, g3 )
        if(v) ym = 100.0*(1.0 + 0.2*cos(pi*((t6-t)/k9 - 0.5)))
        go to 140
120     continue
c
c   night time at control point
c
c
c      6th order fourier series night time factor for M-factor,
c         based on hours after sunset,t2
c
        if ( t4 .gt. t5 )  t6 = t6 + 24.0
      t1 = t6 - t4
      t2 = 14.0*t1/(24.0-k9)
      ag = pi *(t2+1.0)/15.0
      ag1 = 2.0*ag
      ag2 = 4.0*ag
      ag3 = 6.0*ag
      ag4 = 8.0*ag
      ag5 = 10.0*ag
      ag6 = 12.0*ag
      a14 = 1.0195 -.06*sin(ag1)-.037*cos(ag1)+.018*sin(ag2)
      a24 = -.003*cos(ag2)+.025*sin(ag3)+.018*cos(ag3)
```

```
      a34 = .007*sin(ag4)-.005*cos(ag4)+.006*sin(ag5)
      a44 = .017*cos(ag5)-.009*sin(ag6)-.004*cos(ag6)
      a4  = a14+a24+a34+a44
c
        g8=pi*t9/k9
        u = ( t4-t6)/2.0
        u = amin1( amax1( u, -75.0 ), +75.0 )
        u1 = -k9/t9
        u1 = amin1( amax1( u1, -75.0 ), +75.0 )
        g0=c0*(g8*(exp(u1)+1.0))*exp(u)/(1.0+g8*g8)
140     continue
        if(.not.v) go to 150
        h = amin1(350.0,amax1(250.,x11*ym))
c   the slope of the mfactor variation
        xm=-1.e-3*amin1(6.0*g1/(khop*.31),6.)
c   the new mfactor
        m9=m9+xm*(h-290)
c
c   g2 = muf at control point
c
150     continue
        g2 = sqrt(6.0 +a1 * sqrt(g0)) + gyro
        g2 = g2*( 1.0 - 0.1*exp( ( k9 - 24.0 )/3.0 ) )
        g2 = g2*( 1.0 + ( 1.0 - sygn( tlat )*sygn( rlat ) )*0.1 )
        g2 = g2*( 1.0 - 0.1*( 1.0 + sygn( abs( sin( 10 ) )
     &        - cos( 10 ) ) ) )
        if ( abs( mlat ) .ge. 0.95993 )  then
c
c      FOF2 corrects for plar region FOF2.  result is G2 if
c         not in polar regiond
c
c
          g2 = m9*fof2( g2, lmt, itime, 10, w0, mlat, ssn )
        else
          g2 = g2*m9
        end if
c
      g2 = g2 * a2*a3*a4
        cmuf = amin1( cmuf, g2 )
160   continue
      cmuf = amin1( amax1( cmuf, 2.0 ), 50.0 )
c
      return
      end
```

```
      function fof2( ff2, lmt, itime, lat, lon, mlat, ssn )
cp
c     function fof2
c
c       x = fof2( ff2, lmt, itime, lat, lon, mlat, ssn )
c
c       this function corrects the f2-layer critical frequency
c       computed by muf35 for polar latitudes using the chiu model.
c
c       reference (to be supplied when available)
c
c       input:
c         ff2     critical frequency from muf35 in mhz - real
c         lmt     local mean time at lat,lon in hours  - real
c         itime   integer array containing month, day,
c                 hour, minute, julian day, and year   - integer
c         lat     geographic latitude in radians       - real
c         lon     geographic west longitude in radians - real
c         mlat    magnetic latitude in radians         - real
c         ssn     sunspot number                       - real
c
c       output:
c         fof2    the f2-layer critical frequency in mhz - real
c
c       called by subroutine or function:  muf35
c
c       subroutines and functions called:  none
c
c       common blocks referenced:          none
cz
      integer         itime(6)
      real            lat, lmt, lon, mlat, mlon
c
      data            pi /3.1415926/
c
      phi = lmt*pi/12.0
      tmo = itime(1) + ( itime(2) + itime(3)/24.0 + itime(4)/1440.0 )/30.0
     &      - 0.5
      cmlat = cos( mlat )
      mlon = cos( lat )*sin( lon - 1.2043 )/cmlat
      mlon = amax1( amin1( mlon, 1.0 ), -1.0 )
      mlon = asin( mlon )
      x = ( 2.2 + ( 0.2 + ssn/1000.0 )*sin( mlat ) )*cmlat
      ff = exp( -( x**6 ) )
      gg = 1.0 - ff
      t = pi*tmo/12.0
      v = sin( t )
      if ( mlat .ge. 0.0 ) then
        w = exp( -1.2*( cos( mlat - 0.41015*cos( phi ) ) - cmlat ) )
        plr = ( 2.0 + 0.012*ssn )*w*( 1.0 + 0.3*v )
      else
        u = cos( t*t )
        y = sin( mlon/2.0 )
        ys = cos( mlon/2.0 - pi/20.0 )
        z = sin( mlon )
        za = sqrt( abs( z ) )
```

```
         am = 1.0 + v
         b = v*( ( y - z )/2.0 - y**8 ) - am*u*( z/za )*exp( -4.0*y*y )
         ys4 = ys**4
         plr = 2.5 + ssn/50.0 + u*( 0.5 + ( 1.3 + 0.002*ssn )*ys4 )
     &             + ( 1.3 + 0.005*ssn )*cos( phi - pi*( 1.0 + b ) )
     &             + ( 1.0 + 0.4*( 1.0 - v*v ) )*exp( -v*ys4 )
       end if
c
       fof2 = 2.85*sqrt( gg*ff2*ff2/8.12 + 0.66*ff*plr )
       return
       end
```

```
      subroutine path (tlat, tlon, rlat, rlon, cpnt)
cp
c       subroutine path
c
c         call path(tlat,tlon,rlat,rlon,cpnt)
c
c         this routine computes the range,azimuth, and control point
c         coordinates for a given propagation path.  the method assumes
c         a spherical earth with a radius of 6371 km.  the required
c         input for this module is:
c              tlat    transmitter latitude in radians
c              tlon    transmitter west longitude in radians
c              rlat    receiver latitude in radians
c              rlon    receiver west longitude in radians
c         this subroutine returns the following information in an 8 word
c         real array (cpnt):
c              cpnt(1) distance between the receiver and transmitter in
c                      radians
c              cpnt(2) latitude of midpoint in radians
c              cnpt(3) west longitude in radians
c              cpnt(4) latitude of point 1000km from the receiver in radians
c              cpnt(5) west longitude of point 1000km from receiver in
c                      radians
c              cpnt(6) latitude of point 1000km from transmitter in radians
c              cpnt(7) west longitude of point 1000km from transmitter
c                      in radians
c              cpnt(8) azimuth from receiver to transmitter in radians
c
c         cpnt(4) through cpnt(7) will not be computed for paths less than
c         1000 km (0.15696 radians) in length.
c
c         subroutines and functions used:  gcraz
c                                          razgc
c
c         common blocks:  none
c
cz
c
      dimension cpnt(8)
c
c   get range and azimuth
c
      call gcraz( rlat, rlon, tlat, tlon, cpnt(1), cpnt(8) )
c
c   get mid-point coordinates
c
      p1 = cpnt(1)/2.0
      call razgc( rlat, rlon, p1, cpnt(8), cpnt(2), cpnt(3) )
c
c   is path length >= 1000 km?
c
      if ( cpnt(1) .lt. 0.15696 )  go to 100
c
c   yes - get coordinates of 1000 km points
c
      p1 = 0.15696
```

```
      call razgc( rlat, rlon, pl, cpnt(8), cpnt(4), cpnt(5) )
      pl = cpnt(1) - 0.15696
      call razgc( rlat, rlon, pl, cpnt(8), cpnt(6), cpnt(7) )
100   continue
      return
      end
```

```
      subroutine razgc( lat1, lon1, range, azim, lat2, lon2 )
cp
c       subroutine razgc
c
c         call razgc(lat1,lon1,range,azim,lat2,lon2)
c
c         this routine computes the latitude and west longitude
c         (lat2, lon2) of a point a specified range from a given
c         point on the earth's surface.  also required for input
c         is the azimuth (azim) to the new point in radians.  this
c         method assumes a spherical earth and recognizes the
c         degenerate cases of the given point being at the north
c         or south pole.  for the degenerate cases, azim should be 0
c         or pi and lon2 is undefined.  however, azim is not checked,
c         and lon2 is arbitrarily set equal to lon1.  this routine
c         recognizes the degenerate case when range is set to zero.
c         all coordinates are in radians.
c
c         subroutines and functions used:  none
c
c         common blocks:  none
c
cz
c
      real         lat1, lon1, lat2, lon2
c
      data  pi/3.14159/,twopi/6.28318/,halfpi/1.570796/
      data  rtd/57.295779/,dtr/0.017453/
c
c   test for degenerate cases
c
      if ( abs( lat1 - halfpi ) .gt. 1.0e-5 )  go to 100
c
c   the given point is the north pole
c
      lat2 = halfpi - range
      lon2 = lon1
      go to 200
100   continue
      if ( abs( lat1 + halfpi ) .gt. 1.0e-5 )  go to 120
c
c   the given point is the south pole
c
      lat2 = range - halfpi
      lon2 = lon1
      go to 200
120   continue
      if ( range .gt. 0.0 )  go to 130
c
c   point 2 coincident with point 1
c
      lat2 = lat1
      lon2 = lon1
      go to 200
130   continue
c
```

```
c   general case
c
      s1 = sin( lat1 )
      c1 = cos( lat1 )
      c2 = cos( range )
      ca = s1*c2 + c1*sin( range )*cos( azim )
      ca = amin1( amax1( ca, -1.0 ), +1.0 )
      a = acos( ca )
c
c   test if destination ends up on the poles
c
      if( abs(a).gt.1.0e-5 ) go to 140
      lat2 = halfpi
      lon2 = lon1
      go to 200
140   continue
      if( abs(a-pi) .gt. 1.0e-5 ) go to 150
      lat2 = -halfpi
      lon2 = lon1
      go to 200
150   continue
c
c   everything seems ok, get destination coordinates
c
      cg = ( c2 - s1*ca )/( c1*sin( a ) )
      cg = amin1( amax1( cg, -1.0 ), +1.0 )
      g = acos( cg )
      lat2 = halfpi - a
      sa = sin( azim )
      if ( sa .ge. 0.0 )  lon2 = amod( lon1 - g, twopi )
      if ( sa .lt. 0.0 )  lon2 = amod( lon1 + g, twopi )
200   continue
      return
      end
```

```
      function sygn ( y )
cp
c       real function sygn
c
c         x=sygn(y)
c
c         this function returns the value of 0 if y is 0, -1. if y is
c         less than zero and a +1. if y is greater than zero.
c
c         subroutines and functions used:  none
c
c         common blocks:  none
c
cz
c
      if  (y)  100, 200, 300
100   sygn = -1.0
      go to 999
200   sygn = 0.0
      go to 999
300   sygn = 1.0
c
999   return
      end
```